
UNIVERSITY OF PAVIA

Department of Physics

Biosanitary physics curriculum

# From radiobiological experiments to treatment planning in patients: a BNCT dosimetry study

***Master Thesis of***

Barbara Marcaccio

***Supervisor***

Prof. Silva Bortolussi

***Co-Supervisors***

Dr. Sara J. González

Dr. Ian Postuma

Pavia, Accademic Year 2020/2021

*Come l'araba Fenice:*
*che vi sia ciascun lo dice,*
*dove sia nessun lo sa*

*METASTASIO, Demetrio*
*(1731), II .3*

# Contents

# Abstract

Boron Neutron Capture Therapy (BNCT) is a highly selective therapy used in oncology that exploits the neutron capture reaction in boron: $^{10}B(n,\alpha)^{7}Li$. The $^{10}B$ is administered to patients via carriers such as Borophenylalanine, capable of enriching the tumour with higher concentrations compared to healthy tissue. The selectivity of the therapy is due to the fact that the products of the neutron capture reaction are highly ionizing particles, releasing all their energy in a limited space (typically 5-9 $\mu$m). It is therefore possible to establish a suitable neutron fluence that compromises the vital functions of the tumour cells while sparing the surrounding healthy tissues.

BNCT has been applied to tumours with a scarce response to traditional therapies such as surgery, conventional radiotherapy and chemotherapy. Several hundred patients have been treated using neutron beams extracted from nuclear reactors in the United States, Japan, Argentina, Taiwan and European countries. The recent availability of accelerators capable of delivering the neutron flux needed for therapy open the way to a significant development of this therapeutic approach. Today, feasibility studies and clinical trials are underway worldwide, especially to treat brain and head and neck cancers.

The BNCT total dose absorbed in tissues comes from a mixed field of radiation with different biological effectiveness. The complexity of this field is reflected in the difficulty of predicting the therapeutic effect of a given dose absorbed by BNCT, using the knowledge of the dose-effect mechanism of conventional radiotherapy with photons. It is therefore necessary to translate BNCT dose into a reference photon dose. The dose calculation models based on reliable radiobiological data are used to predict and understand the clinical outcome. One of the most widely used biological models for establishing photon-equivalent dose is represented by tumour cell cultures irradiated with different doses of neutrons, neutrons in the presence of boron and with a reference radiation (typically $^{60}Co$) as a function of absorbed dose.

The aim of this thesis work is to exhibit the importance of a detailed dosimetric study for *in-vitro* experiments to ensure a reliable treatment plan in the patient. To show this concept, two tumour types were analyzed: osteosarcoma, a bone neoplasm that affects especially pediatric patients, and a head and neck cancer, a typical target of clinical

BNCT worldwide.

The cell survival curves for these two tumours were obtained experimentally in Pavia, using the thermal column of the University TRIGA Mark reactor for neutron irradiation. A detailed study of the administered dose was carried out, comparing two models of calculation: detailed calculation and KERMA approximation. The results show that the assumption of equilibrium of charged particles is not verified and therefore it is not possible to calculate the dose using the KERMA approximation. The only exception is the component of protons emerging from neutron scattering in hydrogen, for which the equilibrium condition is verified. To assess the impact of an overestimation of the administered dose in biological experiments on the in-patient dosimetry, treatment planning was carried out in real clinical cases. From cell survival curves, obtained using dose and KERMA, radiobiological parameters were obtained to serve as the input for the *photon isoeffective dose model*. The dose distribution in the tumour was then compared and the impact of incorrect dosimetry for the biological experiment was quantified. In addition, the impact on the dosimetry using a neutron beam optimized for radiation protection is shown for osteosarcoma, proving that a clinical beam must necessarily meet several criteria that are not only related to clinical efficacy. This part of the work comprises Chapters 2 and 3 of the thesis, while Chapter 1 provides an introduction to BNCT and the computational tools that are used in the following. Chapter 4 deals with the treatment planning of a real case of head and neck cancer, using data from different cell lines, addressing the problem of establishing the best biological model to represent the clinical effect to be described. Finally, Chapter 5 draws conclusions and outlines future work.

# Chapter 1

# Introduction

The term *neoplasia*, from the Greek, or *tumour*, from the Latin, indicates in pathology a mass of tissue that grows in excess and in an uncoordinated manner with respect to normal tissues. The uncontrolled and uncoordinated growth of a group of cells, to the detriment of tissue homeostasis, is determined by alterations in their own genetic heritage and is the basis of a wide class of diseases, classified according to different characteristics. The term *tumour* refers to the macroscopic appearance of most neoplasms, which frequently appear with a prominent mass at the anatomic site of origin. The term *neoplasia*, which literally means *new formation*, indicates its cellular composition more than the external appearance of the mass.

Cancer is the second leading cause of death in the world. Due to its genetic nature, once it manifests itself, the only thing that can be done is to inactivate all the diseased cells to stop their uncontrolled reproduction. It may happen that the abnormal proliferation of mutated cells compromises the normal functioning of the surrounding healthy tissues, endangering the life of those who suffer from this disease. Therefore, it is important that treatment for this type of disease maximizes its effectiveness on malignant cells while preserving healthy ones. Unfortunately, this turns out to be the main difficulty faced by conventional treatments. Cancer surgery, pharmacological therapies and treatments using ionizing radiation have a high impact on healthy tissues; therefore, it is difficult to apply the treatments at the intensity necessary to ensure clinical success without endangering the integrity and the functionality of the organs. Recently, radiation treatments have progressed considerably, reaching a high level of complexity that has allowed improving their effectiveness while safeguarding the patient's quality of life. It is now possible to prolong life expectancy and, in some cases, to cure the disease. Several research projects are ongoing to set-up new therapeutic strategies aimed at protecting the healthy tissues surrounding the tumour, even when this is not localized and, thus, more difficult to eradicate.

The Boron Neutron Capture Therapy (BNCT) is one of alternative or adjuvant treatments that is being developed to this end.
The theoretical concept of using neutron for radiation therapy followed the neutron discovery in 1932. The concept was proposed by the American biophysicist G.L. Locher, whose idea was based on the high cross section that 10-boron has for the capture of low energy neutrons [1]. He hypothesized that concentrating the isotope selectively in the tumour and irradiating it with a beam of thermal neutrons, the produced nuclear reaction would release enough energy to inactivate the proliferation of cancer cells.

## 1.1 Boron Neutron Capture Therapy

Boron Neutron Caption Therapy, BNCT, is a technique that selectively targets cancer cells using a 10-boron formulation followed by irradiation of the patient with a low-energy neutron beam.

It is based on the $^{10}B(n,\alpha)^{7}Li$ reaction, whose cross-section at thermal neutron energies ($\sigma = 3840$ barns at 0.025eV) is the highest among the other interactions of neutrons with the other elements in biological tissue. The capture process leads to the production of an excited $^{11}B^{*}$ nucleus, which decays almost immediately into two highly ionising particles: a $^{7}Li$ ion and an $\alpha$ particle ($^{4}He$ nucleus) [2].

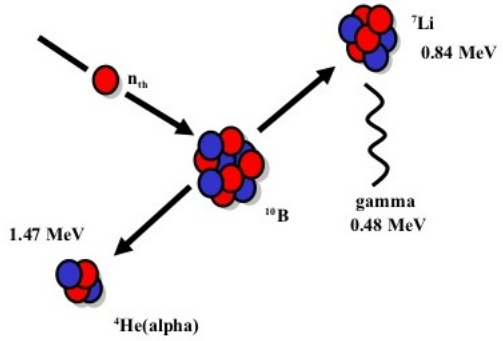


Figure 1.1: Schematic representation of thermal neutron caption reaction.

The reaction products have a high LET (Linear Energy Transfer) value: $150\,\mathrm{keV}\mu\mathrm{m}^{-1}$ for $\alpha$ particles and $175\,\mathrm{keV}\mu\mathrm{m}^{-1}$ for $^{7}Li$ nuclei. This quantity is the amount of energy released per unit length by a particle crossing a material. Therefore, particles with a high LET release more energy per unit length, with a consequent shorter penetration into the material. In fact, the range of $^{7}Li$ particles in biological tissue is about $5\,\mu m$, while the range of $\alpha$ particles is about $9\,\mu m$. Since cell size is of the order of 10 $\mu m$, the entire energy of the reaction products is deposited close to the DNA of tumour cells.

Being densely ionizing radiation, the DNA suffers from non-reparable damages with a high probability to be killed if the cell nucleus is crossed by several charged particles. The chance that one of these particles deposit energy outside the cell where the reaction took place is low, thus the surrounding cells, potentially healthy, are spared. This is the most relevant difference comparing to other forms of external radiotherapy: the intrinsic selectivity of BNCT relies on boron distribution in tissue and not in the conformation of the irradiation beam. In fact, the neutron beam is usually as broad as possible to encompasses the tumour volume and surrounding areas that may contain isolated cells, source of possible metastases or recurrences.

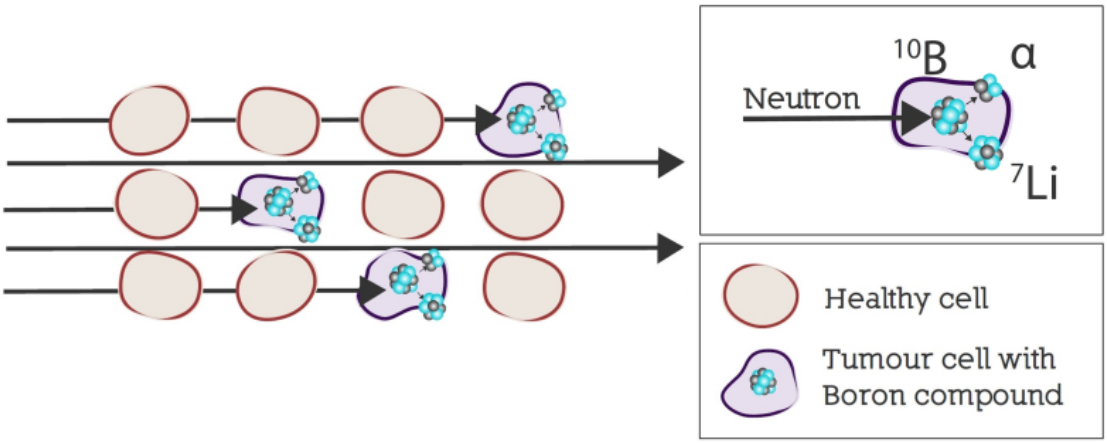


Figure 1.2: Schematic representation of BNCT basic principle.

Another key feature of BNCT, is that the radiation dose is only absorbed during neutron irradiation of the organ, since the reaction products are not radioactive: the rest of the patient's body is preserved from unwanted dose. After neutron irradiation, sodium and chlorine in patients' body are activated, however the dose delivered to tissue by this activation is negligible. This differentiates BNCT from metabolic radiotherapy using radioisotopes, that deposit dose also in distant sites from tumour location.

The described selectivity makes BNCT a possible therapeutic option for some tumours, also those that are disseminated or infiltrated. These cases are often impossible to remove surgically and/or to treat with other types of radiotherapy since the target is not well localised, it is too close to a radiosensitive organ, or difficult to distinguish from the surrounding normal tissues.

The $^{10}B$ is an excellent element for neutron capture therapy, as it is non−toxic, non−radioactive and fairly abundant in nature, approximately 20%. For BNCT to be successful in therapy, it must be transported inside the tumour cells. A good boron

transport agent must have the following characteristics [11].

1. low toxicity;
2. a high capacity to be absorbed by malignant tissues and low penetration in healthy ones;
3. it must be rapidly excreted from healthy tissues and blood and persist in tumour throughout treatment.

Boron drugs currently available that match these requirements are BPA (boronophenylalanine) and BSH (sodium borocaptate) [1]. BPA is a precursor of melanine and in fact it was used for the first time in the treatment of melanomas by Mishima et al. [12, 13]. These boron compounds have been approved for clinical use in different protocols worldwide. Today, BPA is one of the most boron compound used in BNCT trials, sodium *mercaptoundecahydrododecaborate* (BSH) is another one most widely used.

Another key element for BNCT is the neutron beam, which can be obtained either from research nuclear reactors or from particle accelerators. The latter option is becoming increasingly available, and many facilities are being built around the world [17]. Accelerator−Based−BNCT (AB-BNCT) works with a beam of protons or deuterons coupled with a suitable target to obtain neutrons from nuclear reactions such as $^{7}Li(p,n)^{7}Be$ or $^{9}Be(d,n)^{10}B$. One of the advantages of this technology is that it can be installed in hospitals, being smaller and requiring simpler licensing, operation and maintenance [16]. The neutrons produced in the target are then moderated to obtain two types of clinical beams, which differ in their average neutron energy: thermal (25 meV) and epithermal ($\approx 1\,\mathrm{keV}$), depending on the depth of tumours that must be treated. Thermal neutron beams are used to treat only shallow tumours, such as superficial melanoma of the skin, and epithermal neutron beams are used to generate a uniform thermal neutron field deeper in the tissue, to treat deep-seated neoplasms. Figure 1.3 shows a scheme of a BNCT set-up with the accelerator machine, the target, and the Beam Shaping Assembly (BSA) necessary to lower the energy of neutron beam for optimal penetration in tissue and to collimate the neutron beam towards the patient [86].

BNCT was first used in a patient diagnosed with malignant glioma in 1951, using the currently available Brookhaven Graphite Research Reactor [3].
Three series of BNCT treatments followed in 40 patients using low-selective boron compounds, but serious side effects such as radiodermatosis of the scalp and deep ulceration were reported [4]. Slatkin mentioned that the outcome of BNCT was similar to conventional radiotherapy, causing cerebral oedema and intractable shock in patients [5].

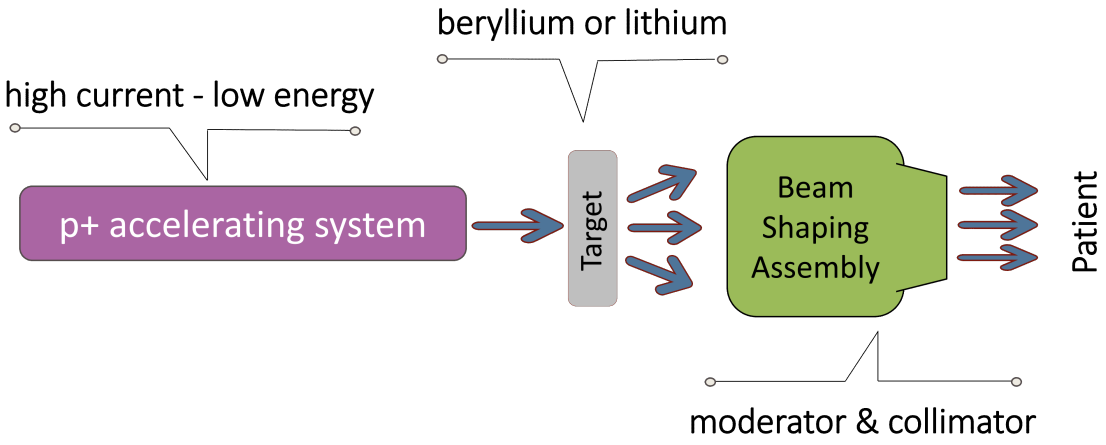


Figure 1.3: Diagram of the general structure of a BNCT accelerator.

Sweet et al. report about 18 patients treated in 1963 at the reactor of the Massachusetts Institute of Technology using disodium decahydrodecarborate, which was considered less toxic, but it was able to deliver more boron to the tumours. [6]. Asbury AK et al. noted severe brain necrosis in patients undergoing BNCT [7]. Due to the side effects of BNCT at this stage, the US stopped the clinical application of BNCT in 1961.
Hiroshi Hatanaka in 1968 reintroduced the clinical application of BNCT in Japan using sodium borocaptate (BSH) by irradiating intracranial tumour surgically exposed and reported impressive results reaching 58% 5 year survival rate [8, 9]. In the following years, Hatanaka and co-workers reconsidered and renewed the clinical application of BNCT in the USA and Europe. In 1987, Mishima applied BNCT in Japan to patients affected by malignant melanoma using boronophenylalanine (BPA), which opened the clinical application of BNCT to the treatment of tumours outside the central nervous system [10]. Slowly but steadily the resurgence of BNCT took place, albeit limited to countries that had research reactors capable of delivering neutron beam of sufficient intensity for patients treatments.
The modern phase of BNCT took off in the 1990s in the USA in Brookhaven [54] and Cambridge [55], then in Europe in Petten [56], Finland [57], Sweden [58], the Czech Republic [59] and Japan [60, 61] and finally in Argentina [62] and Taiwan [63]. BNCT has evolved through 60 years of research and clinical progress. Presently some issues that hindered its application as an established treatment option, such as lack of trials harmonization, the need for nuclear research reactors for clinical irradiation, and disappointment in the evolution of ideal boron carriers [18], are being addressed.

The most important technological advancement for BNCT applicability to a wider patients population is the availability of accelerators as a source of neutrons, as explained above. At the moment, there are several accelerator-based BNCT projects worldwide,

including in Italy (https://fondazionecnao.it). Three of these, in Japan, are currently treating patients, using a 30 MeV proton cyclotron and a beryllium target. The tumours that are being treated are head and neck cancer and glioblastoma multiforme [96].

## 1.2 Dosimetry in BNCT

As for all the radiotherapy treatments, the safety and effectiveness of BNCT is determined by the accuracy with which the dose deposited in the tissues is determined. In BNCT treatment planning, the dose prescription is to the most radiosensitive tissue/organ involved in the irradiation, and the irradiation time is set to achieve this dose. The absorbed dose in the tumour is normally higher, due to the higher boron uptake in the cancer cells.
Calculating the dose in BNCT is not trivial, because the neutron interaction in tissue produces a mixed radiation field. Each radiation component has its own characteristics and, therefore, its own effectiveness in producing biological damage.
The energy deposited by epithermal neutrons in biological tissues is mainly due to scattering in hydrogen nuclei. When scattered, neutrons lose energy causing neutron thermalization with depth. When irradiating patients with epithermal neutrons, the spectrum is harder in the superficial layers of tissue and more thermal in depth, ensuring that the probability of neutron capture in boron is maximised at the position of the tumour. The thermalization process is a cause of dose deposition, because the recoil hydrogen nucleus set in motion by elastic scattering ${}^1H(n,n'){}^1H$ releases its energy in tissue. At thermal energies, the neutron interacts mainly via neutron capture. The soft tissue consists of the elements shown in the Table 1.1.

| Elements | Mass fraction in tissue (%) |
|---|---|
| ${}^{16}O$ | 63 |
| ${}^{12}C$ | 23 |
| ${}^{1}H$ | 10 |
| ${}^{14}N$ | 2.3 |
| ${}^{23}Na$, ${}^{31}P$, ${}^{32}S$, $Cl$ natural, K natural | 1.7 |

Table 1.1: Soft tissue composition from ICRU 46 report [21]. Density 1.06 $\frac{g}{cm^3}$.

The most important capture reactions are:

- ${}^1H(n,\gamma)^2H$;
- ${}^{14}N(n,p)^{14}C$;

- $^{16}O(n,\gamma)^{17}O$;
- $^{17}C(n,\gamma)^{18}C$;
- $^{14}N(n,\gamma)^{15}N$.

Of these reactions, only the first two produce significant energy deposition, as the others either have a low cross section or occur in isotopes with a low fraction in tissue. Capture in hydrogen produces a 2.2 MeV photon, which deposits its energy away from the site where it is produced. Neutron capture in nitrogen produces a 0.583 MeV proton and a 42 keV $^{14}C$ recoil nucleus depositing their energy locally. These radiation components due to scattering and capture, constitute a non-selective source of dose affecting both tumour and healthy cells.
The only selective dose component is due to the alpha and lithium particles, generated by the $^{10}B(n,\alpha)^{7}Li$ reaction. Due to the high cross section and to the Q-value of the reaction, the reaction $^{10}B(n,\alpha)^{7}Li$ constitutes the most relevant dose component even in the presence of small amounts of $^{10}B$. The boron concentration achieved in tissues is of the order of tens of micrograms of $^{10}B$ per gram of tissue (parts per million, or ppm).
Another contribution to the dose is due to the photons present in the neutron beam, the so-called *structural gamma component* usually lowered by shielding materials in the beam shaping assembly. This component sums with the photon produced by neutron capture in hydrogen, constituting a low-LET contribution to the absorbed dose.
The total absorbed dose is the sum of the contributions described below. Each component has a different LET and therefore a different radiobiological effect in the tissue because the mechanisms of energy deposition in matter determine the type of damage suffered by the cells.

In summary, the dose delivered by the BNCT field is decomposed into four primary components (illustrated in Figure 1.4)

- $D_t$ *thermal neutron component*, the dose delivered by neutrons below 0.5 eV, excluding the damage resulting from neutron capture in boron and from the gamma produced in neutron captures. The main reaction contributing to this component is the neutron capture in nitrogen, $^{14}N(n,p)^{14}C$. Scattering occurring at these energies with hydrogen will not produce any dose since the resulting proton energy is below the ionization threshold.
- $D_f$ *fast neutron component*, i.e., the dose delivered by neutrons of more than 0.5 eV (maximum value depending on the beam characteristics, typically of the order of 1 MeV). Fast neutron dose is mostly due to neutron elastic collision with hydrogen.

Reactions with $^{12}C$ and $^{16}O$ (and other elements depending on the tissue [21]) normally count for less than 10% of the dose.

- $D_\gamma$ *gamma component* produced by radiative capture in hydrogen producing prompt gammas of 2.2 MeV. Structural photons coming from the beam are also comprised in this dose component.

- $D_B$ *boron component*, depending on boron concentration present in the tissue. Usually, this is the highest dose component in the tumor.

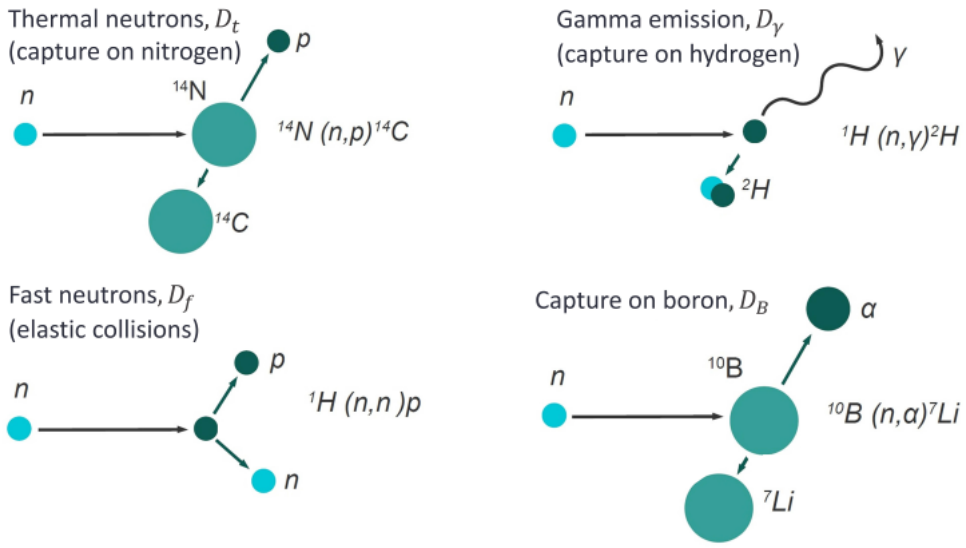


Figure 1.4: The four absorbed dose components that contribute to the BNCT dose and the main reactions that cause them.

As said before, the total radiation dose will be the sum of all the absorbed dose components

$$D = D_t + D_f + D_\gamma + D_B. \tag{1.1}$$

In clinical BNCT it is very important to express the dose due to its mixed field in photon−equivalent units, i.e. the dose of photons causing the same biological effect as the mixed-field dose due to BNCT. In fact, the clinical experience gained in photon-radiotherapy allows a prediction of the treatment outcome as a function of the administered dose. Once the dose is expressed in photon−equivalent units, it is possible to produce a treatment planning which maximizes the therapeutic effect while limiting the dose absorbed by normal tissues below the tolerance limits.

Traditionally, the translation of BNCT dose into *biologically-weighted units* had been obtained by multiplying the absorbed dose component (Gy) by fixed Relative Biological

Effectiveness (RBE) or Compound Biological Effectiveness (CBE) factors. The biological-weighted dose has been expressed in the conventional units Gray-Equivalent (Gy-Eq) [22]. The RBE factor is defined as the ratio between the absorbed dose due to reference photon radiation and the dose of the radiation under study needed to cause the same biological endpoint. The CBE factor is theoretically the same as RBE, but it refers to the dose component of boron. The effects of boron dose component, in fact, also depend on the boron distribution at sub-cellular level obtained with a chosen boron carrier [22]. Both RBE and CBE factors have been considered as dose and dose rate independent and they are calculated at fixed endpoints, for example at 1% of cell survival in *in-vitro* experiments. Thus the total biologically weighted dose $D_w$ (in Gy-Eq) was expressed as:

$$D_w = RBE_t \cdot D_t + RBE_f \cdot D_f + D_\gamma + CBE \cdot D_B. \tag{1.2}$$

The definition presented in equation 1.2 has been used in all BNCT clinical applications so far. While it allows the establishment of safety criteria for the prescription of irradiation times, it wrongly assumes that the biological effect of each component is independent of the biological effect of all the others. This fact, together with the use of dose-independent RBE factors, leads to an overestimation of photon-equivalent dose, inconsistent with observed clinical effects, especially in tumour.

Recently, this model has been revised, with the aim of calculating more realistic photon-equivalent doses using more comprehensive approaches [23, 24]. One of the new models, aimed at solving the two problems mentioned above, is the Photon Isoeffective Dose model proposed by González and Santa Cruz [25].

## 1.3 The Photon Isoeffective Dose in Boron Neutron Capture Therapy

One of the issues with the described RBE-weighted model is that RBE and CBE factors are constant, although they not only depend on the dose, but also on the dose rate. The use of fixed RBE factors derived from each radiation component, considered independent from each other, will always lead to erroneous results, as shown below. For this reason, a more general approach has been proposed. The formalism of this new method includes first-order repair of sublethal lesions by means of the generalized Lea-Catcheside factor in the modified linear-quadratic model and considers synergistic interactions between different radiations (see below).
Before entering into the details of the photon isoeffective dose model, the motivation for the need of paradigm change is shown with an example reported in [25].

The Figure 1.5 exhibits the calculation of the RBE-weighted dose for a given combination of two radiations, A and B. Assume that 3 Gy of radiation A and 12 Gy of the reference radiation R produce the same level of effect, $s_1$. 3 Gy of radiation B and 9 Gy of reference radiation produce $s_2$. Then, the corresponding RBEs for radiation A at level $s_1$ and radiation B at $s_2$ are respectively $r_A^{s_1} = 4$ and $r_B^{s_2} = 3$.

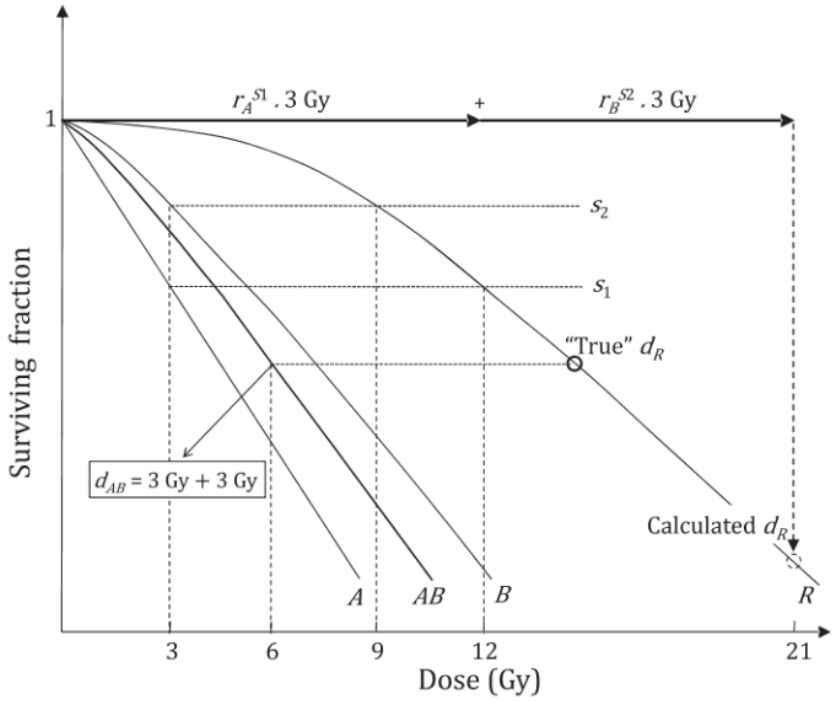


Figure 1.5: *True* vs *Calculated* RBE-weighted doses for a mixed irradiation with 3 Gy of radiation A and 3 Gy of radiation B [25].

The example consists in determining the RBE-weighted dose for the combination of 3 Gy of radiation A and 3 Gy for radiation B. The dose-effect curve for the combination of the two radiations A and B (represented in the Figure 1.5 as AB), corresponds to that obtained using equal proportions of each radiation. Therefore, the desired RBE-weighted dose is the one producing the same level of effect as the 6 Gy combination of radiation A and B.

The RBE-weighted dose for levels of effect $s_1$ and $s_2$ can be calculated using the fixed RBE values established for a pre-defined effect level, i.e. $r_A^s$ and $r_B^s$

$$d'_R = r_A^s \cdot 1\,Gy + r_B^s \cdot 1\,Gy. \tag{1.3}$$

The *Calculated* value, $d_R = 21$Gy is larger than the *True* value for the combination, $d_{AB} = 6$Gy.

This theoretical example shows that working with fixed RBE, determined for one endpoint, leads to dose values which are not accurate.

The cardinal principle of the theory of dual radiation action (TDRA) [26, 27] is that lethal lesions produced to the cell DNA by radiation result either from the direct action of a single event or from the incoherent action of two independent events causing damage entities that together lead to a lethal lesion.

The first case occurs with an average yield proportional to the absorbed dose while the second occurs with the dose squared. To link the average yield per cell of lethal lesions with survival, it is customary to assume that one lesion is enough to inactivate a cell and that the number of lethal lesions distribution is poissonian.

These assumptions lead to the description of cell survival according to the linear quadratic model [28, 29]

$$S(D) = e^{-(\alpha D + \beta D^2)}, \tag{1.4}$$

where alpha is the proportionality constant linking cell lethality to damage per single hit, (linear dependence) growth, and beta is the proportionality constant linking cell lethality to damage per sum of sublethals damages (quadratic dependence).

In equation 1.4 there is a linear term with the dose, representative of those events that cause a break in the DNA double helix, leading to cell death or cell inactivation. Cellular inactivation means that the cell loses its natural ability to reproduce: albeit not dead, it will eventually disappear.

The other term is proportional to the square of the dose, it results from two independent events, each of which is proportional to the dose. Both events break the DNA strand, and only their combination cause the lethal damage.In TDRA, damage entities that do not produce a lethal lesion by themselves are referred to as *sulethal damage*. They must interact to produce a lethal lesion, assuming they coexist in space and in time.

Not necessarily a break in the DNA double helix corresponds to lethal damage to cells. In general, if the cells are normal, the damage can be repaired very easily. However in tumour cells the damage repair mechanisms are less effective.

First-order lesion repair was originally considered in the pioneering works of Lea and Catcheside [28, 29], and was later generalized to consider any dose delivery scheme [26, 30]. The latter led to the generalized Lea-Catcheside time factor, $G(\theta)$, where $\theta$ is the irradiation time.

This factor represents the probability that a sublethal damage will not recombine with another sublethal damage because it has been already repaired. $G$ is a value between 0 and 1: $G{=}1$ when all damage has combined with other damage and $G{<}1$ when no

recombination is taking place, i.e. the cell is managing to repair the damage, corresponding to a higher cell survival.
The $G$ factor is closely linked to the irradiation time: if the cell is irradiated for a time longer than the repair time, then the cell will be able to repair the sublethal damages leading to a higher survival rate; if the cell is irradiated for shorter times, it will not be able to repair the damage caused by the radiation.
Another important aspect is that this model does not take into account the distance between two sublethal damages, but only the temporal aspect; it is a macroscopic model because it does not analyse what happens in the cell nucleus form the spatial point of view.
The simplest model considers that the cell has only one time to repair the sublethal damage. More complex models exist, including one that distinguishes between two types of sublethal damage, those that are more difficult to repair and those that are easier, since not all the sublesions have the same level of complexity. Therefore, there are two characteristic times for repairing sublethal cell damage: a fast and a slow component.
The kinetics of damage repair do not depend on the type of radiation that caused it, i.e. on the LET.
Mathematically it is possible to describe the factor G with the double kinetics of slow ($t_{0s}$) and fast ($t_{0f}$) repair as follows[35]:

$$V_R(\theta, t_{0f}, t_{0s}) = a_{Rf}\, G(\theta, t_{0f}) + a_{Rs}\, G(\theta, t_{0s}), \tag{1.5}$$

where $a_{Rf}$ and $a_{Rs}$ are the proportions of sublesions repaired by the fast and slow kinetics for radiation R (with $a_{Rf} + a_{Rs} = 1$), and

$$G(\theta, t_0) = \frac{2t_0}{\theta}\left(1 - \frac{t_0}{\theta}\left(1 - e^{-\frac{t_0}{\theta}}\right)\right), \tag{1.6}$$

where $t_0$ is the fast or the slow characteristic repair times. Sublethal lesions produced by different radiations that coexist in space and time have a finite probability of interacting and producing an additional effect that cannot be defined by simply adding radiations. This effect is known as *radiation synergism* [31].

Synergism requires the addition of mixed terms in the formalism of the linear quadratic model, due to the possible combination of different radiations. These terms are further modulated by appropriate Lea-Catcheside factors.
Several experiments have demonstrated the synergistic action of high-LET and low-LET radiations [32, 33], when mammalian cells are exposed to sequential doses of different

radiations. Suzuki [34] has derived the corresponding expressions for the simultaneous irradiation with multiple types of radiation: the situation of BNCT.
The formalism to compute BNCT photon isoeffective dose is based on the following assumptions [25]

1. the survival dose-response relationship is adequately described by the Linear Quadratic Model that accounts for dose-rate dependent sublethal lesions repair, the *modified LQ Model*;

2. if synergism is considered, the survival dose-response is adequately described including the additional mixed terms from TDRA, modulated by the $G$ factors for a simultaneous mixed irradiation.

Let $D_1$, $D_2$, $D_3$, $D_4$ be the boron, thermal neutron, fast neutron and photon absorbed dose components of BNCT, and $D_R$ be the dose of the reference radiation $R$. The goal of the photon isoeffective dose formalism is to find $D_R = D_R(D_1, D_2, D_3, D_4)$ that produce the same survival level as a given combination of $D_1, D_2, D_3, D_4$. Typically $R$ is the photon radiation of conventional photon-therapy. Therefore, $D_R$ is the photon dose causing the same effect as the combination of $D_1, D_2, D_3, D_4$ doses delivered in BNCT.

### 1.3.1 Independent Action

If $S_i = S_i(D_i)$ represents the survival probability for the absorbed dose component i, $i = 1, 2, 3, 4$, then $S = S(D_1, D_2, D_3, D_4)$ denote the survival probability for the combination of the four radiation components, and $S_R(D_R)$ denotes the survival probability for the reference radiation. If there is no synergistic effect, the overall probability of survival is the product of the probability of survival due to each radiation component:

$$S(D_1, D_2, D_3, D_4) = \prod_{i=1}^{4} S_i(D_i). \tag{1.7}$$

The photon isoeffective dose $D_R$ must satisfy

$$S_R(D_R) = S(D_1, D_2, D_3, D_4). \tag{1.8}$$

Let suppose that only the low-LET component has a quadratic dependence, i.e. can generate subletal lesions:

$$S_i(D_i) = \begin{cases} e^{-\alpha_i D_i} & i = 1, 2, 3 \\ e^{-\alpha_i D_i + G_i(\theta)\beta_i D_i^2} & i = 4 \end{cases} \tag{1.9}$$

where $\alpha_i$ and $\beta_i$ are the coefficients of the single-fraction linear-quadratic survival model for the corresponding radiations and $G_{i=4}(\theta)$ is generalized Lea-Catcheside time factor for the $\gamma$ component of the BNCT beam. The equation 1.8 becomes

$$-ln(S_R(D_R)) = \sum_{i=1}^{4} \alpha_i D_i + G_{4(\theta)\beta_4 D_4^2}. \tag{1.10}$$

Equation 1.10 can be written as follows:

$$D_R(D_1, .., D_4) = \sum_{i=1}^{4} r_i(D_R) D_i. \tag{1.11}$$

where

$$r_i(D_R) = \begin{cases} \alpha_i \dfrac{D_R}{(-ln(S_R(D_R)))} & i = 1, 2, 3 \\ (\alpha_i + G_i(\theta)\beta D_i) \dfrac{D_R}{(-ln(S_R(D_R)))} & i = 4, \end{cases} \tag{1.12}$$

are the RBE factors as a function of the reference dose $D_R$. They can be also expressed as a function of survival probability $S = S(D_1, ..., D_4)$

$$r_i(S) = \begin{cases} \alpha_i \dfrac{S_R^{-1}(S)}{(-ln(S))} & i = 1, 2, 3 \\ (\alpha_i + G_i(\theta)\beta D_i) \dfrac{S_R^{-1}(S)}{(-ln(S))} & i = 4 \end{cases} \tag{1.13}$$

where $S_R^{-1}(S)$ is the inverse function of the survival probability for the reference radiation.

If the survival of the reference dose is given by the single-fraction linear-quadratic dose expression

$$-ln(S_R(D_R)) = \alpha_R D_R + G_R(\theta)\beta_R D_R^2, \tag{1.14}$$

with $\alpha_R$ e $\beta_R$ as the LQ model parameters $G_R(\theta)$ as the generalized Lea-Catcheside time factor for the reference radiation. Considering equation 1.13 the expression 1.11 can be rewritten as

$$D_R(D_1, .., D_4) = \sum_{i=1}^{3} \left( \frac{\alpha_i}{\alpha_R + G_R(\theta)\beta_R D_R} \right) D_i + \left( \frac{\alpha_4 + G_4(\theta)\beta_4 D_4}{\alpha_R + G_R(\theta)\beta_R D_R} \right) D_4. \tag{1.15}$$

Two aspects have been emphasised here:

1. the factors in brackets multiplying the $D_i$, corresponding to the RBE/CBE factors, are not fixed values, rather, they depend on the $D_R$ dose. This proves why the dose

components cannot be weighted by constant factors such as the classical RBE/CBE.

2. Equation 1.15 is not solved for $D_R$, i.e., an explicit expression of $D_R$ cannot be simply obtained. For some conditions, however, $D_R$ can be analytically expressed, as follows.

When cell survival experiments are carried out with a constant irradiation time, then $G_R(\theta) = G_R$ is constant. If variations of $G_R(\theta)$ during the irradiation can be neglected, or if the irradiation time is shorter that the characteristic repair time, $G_R$ is approximately constant. In this case, the equation 1.15 can be solved for $D_R$ and becomes

$$D_R(D_1,..,D_4) = \frac{1}{2}\frac{\left(\frac{\alpha}{\beta}\right)}{G_R} \times \left( \sqrt{1 + \frac{4G_R}{\alpha\left(\frac{\alpha}{\beta}\right)_R}\left(\sum_{i=1}^{3}\alpha_i D_i + G_4(\theta)\beta_4 D_4^2\right)} - 1 \right). \quad (1.16)$$

The equation above allows the calculation of the photon isoeffective dose for the mixed-LET BNCT radiation field. This expression does not use fixed RBE factors: it depends on the parameters from the linear quadratic model of the BNCT components and reference radiation. These parameters must be determined with experimental measurements.

### 1.3.2 Synergistic Action

If we consider that each $i$-th component produces effects in a synergistic manner (sublethal lesions from different radiations combine to produce a lethal damage), then the yield of sublethal damage per unit dose for each radiation component $i$ is accounted for by $\sqrt{\beta_i}$. For the generic $i$-th radiation, survival is of the type

$$-ln(S_i(D_i)) = \alpha_i D_i + G_i(\theta)\beta_i D_i^2, \quad i = 1,2,3,4, \quad (1.17)$$

where $G_i(\theta)$ is the time factor for radiation $i$.

The appropriate expression obtained from the TDRA model that best describes the synergism between component $i$ and component $j$ is

$$-ln(S_i(D_i,D_j)) = G_{ij}(\theta)\sqrt{\beta_i\beta_j}D_i D_j, \quad i \neq j = 1,2,3,4 \quad (1.18)$$

where $G_{ij}$ is the time factor that accounts for the first-order repair of sublesions produced by radiation $i$ (radiation $j$) that reduces the probability of interaction with sublesions produced by radiation $j$ (radiation $i$) during the irradiation.

Finally, the survival probability for the combination of the four radiations is

$$-ln(S(D_1, D_2, D_3, D_4)) = \sum_{i=1}^{4} \alpha_i D_i + \sum_{i=1}^{4} \sum_{j=1}^{4} G_{ij}(\theta) \sqrt{\beta_i \beta_j} D_i D_j. \tag{1.19}$$

Note that when $i = j$ the quadratic term is included.
Therefore, replacing expressions 1.14 and 1.19 into Eq. 1.8 and solving the equation for $D_R$, the general photon isoeffective dose for BNCT is obtained.

What has just been described is a theoretical framework underpinning the thesis work. In the next chapters the calculation of the parameters for the expression of the isoeffective dose for osteosarcoma and head and neck tumours will be shown. Moreover, the influence of the dose calculation in the radiobiological experiments and of the use of different cell lines on the Treatment Planning in representative patient cases will be evaluated and discussed.

Initially we will show how the parameters for the isoeffective dose depend on the precision with which the dose is calculated in radiobiological experiments. In a second step, we will open the discussion on the in-patient dosimetry evaluation according to the type of cell line that has been chosen as a representative preclinical model. The results will highlight how the radiobiological experiments and the determination of the best treatment plan for the patient are intimately linked.

# Chapter 2

# Calculation of the absorbed dose in cells

This thesis describes *in-vitro* tumour models as a tool to calculate photon-equivalent dosimetry in the patient, using the photon isoeffective model. The parameters for the isoeffective dose are obtained from the fit of the dose-survival curves, which will be explained in details in the following chapters. In order to obtain a consistent fit, the dosimetry needs to be estimated adequately.
Claretta Guidi [39] studied the difference between KERMA approximation and dose in samples of cultivated human skin based on the Reconstructed Human Epidermis Model (RHE). Her results show that Charged Particle Equilibrium (CPE) in RHE volumes for the products of neutron interactions exists, while for electrons due to gamma radiation do not. Thus, a more accurate analysis of the physics of the problem is needed for the latter component. In fact, RHE models have average thickness of 100 microns, ensuring the complete deposition of the energy of the particles produced by neutrons in tissue, but not ensuring the energy balance of the electrons from the gamma radiation that enter and escape the volume.
When the charged particle equilibrium does not exist, the difference between the calculated KERMA and the actual dose absorbed by the samples can be significant. It will be explained in detail in the section 2.1
In this thesis, the samples of interest have thickness of the order of 10 microns, therefore the equilibrium condition assumption may not be correct even for charged particles emerging from neutron interactions (see Introduction for the particle ranges in tissue).

The study of the dose deposited in cells was implemented using a program that simulates particle transport: the MCNP code, version 6.1 [36]. The code permits to simulate the transport of neutrons, photons and all other types of particles and to evaluate the

interactions of particles with matter. The user describes the geometry and the materials of the region of space with which the radiation to be studied interacts, as well as the radiation source with all its characteristics (type of particles, spatial and energy distribution, flight directions). The geometry is constituted by a set of three-dimensional volumes (*cells*) constructed via intersections, unions and complements of three-dimensional regions of space. These cells are treated by MCNP in a Cartesian reference system: the surfaces delimiting the cells are represented by equations whose parameters are defined by the user. Thanks to the information of the input file, MCNP is able to recreate the transport of the radiation using the cross sections of the materials embedded in its libraries.
In order to calculate quantities such as current, particle flux and released energy, MCNP uses estimators called *tallies*. The nuclear and atomic data libraries available for the code are continuous functions of energy. For neutrons, more than 500 interaction tables are available for about 100 isotopes and elements; for some isotopes multiple tables are available that take into account the temperature dependence of the data. Tables of neutron interactions include, in addition to cross sections, information on the average number of neutrons produced per fission, the average energy released per interaction, and the angular and energy distribution of neutrons scattered in all reactions where absorption does not occur as a function of the energy of the incident neutron.
With regard to photons, MCNP considers coherent and incoherent scattering, photoelectric absorption with the possibility of fluorescence emission, Compton scattering and pair production. The code covers around 2000 reactions involving over 400 target nuclei in both the stable and excited states.

## 2.1 Dosimetry concepts

Before describing the MCNP simulations, some basic concepts on dosimetry are here introduced. Crossing the media, ionizing radiations deposit their energy. The quantification of that deposited energy is the objective of radiation dosimetry. Specific quantities have been defined to this end, some of which are summarized below.
Fixed a generic point P of the space, we consider a sphere with centre P, finite radius r and maximum cross section $dA$, and let $dN$ be the number of particles crossing the sphere in a time interval $dt$, we define the *particle fluence* quantity as

$$\Phi = \frac{dN}{dA}. \tag{2.1}$$

The unit of measurement of particle fluence is particles/cm$^2$.

In order to estimate the energy flowing through the considered surface S, if R is the expectation value of the total energy transported by the $N$ particles, the *energy fluence* can be defined, analogously to the particle fluence, as

$$\Psi = \frac{dR}{dA}. \tag{2.2}$$

The unit of measurement of energy fluence is $J/cm^2$.

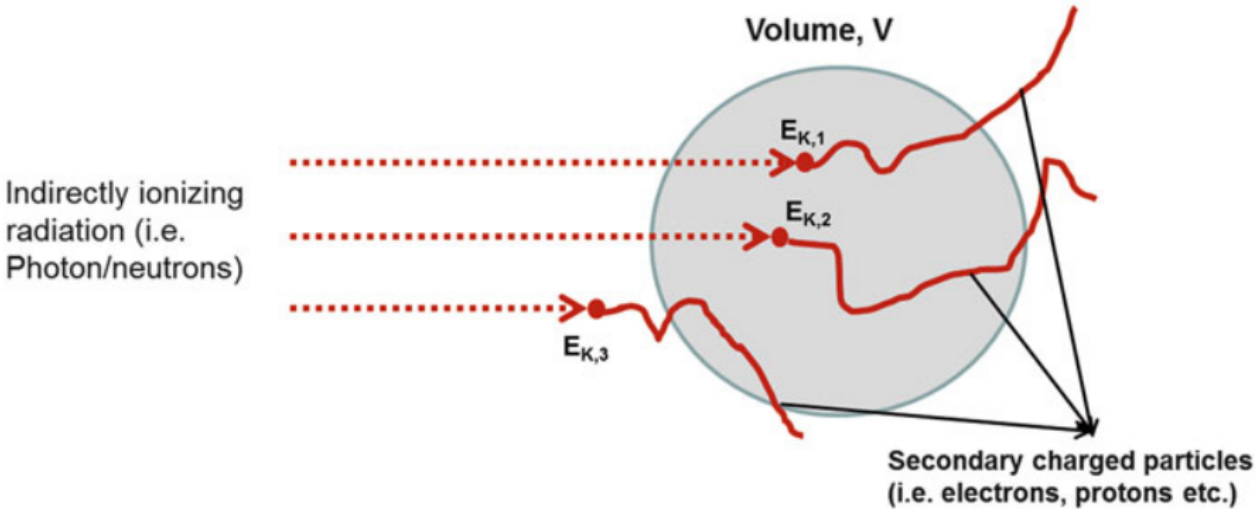


Figure 2.1: Neutral radiation entering and leaving the volume V [81].

The energy transferred into a volume V by non-directly ionising radiation (neutron and photon) is defined as, by referring to the Figure 2.1,

$$\varepsilon_{tr} = (R_{in})_n - (R_{out})_n^{nonr} + \Sigma Q \tag{2.3}$$

where $(R_{in})_n$ is the energy associated with neutral particles entering the considered volume V, $(R_{out})_n^{nonr}$ is the energy associated with neutral particles leaving V, excluding the one that photons produced in radiative dissipation phenomena undergone by charged particles set in motion in the volume V, $\Sigma Q$ is the energy resulting from the transformations of mass at rest into energy, and vice versa, occurring in V (Q is positive if mass converts into energy, negative if energy is converted into mass).
According to its definition, it can be observed that the *transferred energy* is the kinetic energy transferred by the neutral radiation to the charged particles in the specified volume V. Through the transferred energy, the *KERMA* K is defined around a point P as:

$$K = \frac{d\varepsilon_{tr}}{dm}. \tag{2.4}$$

The unit of KERMA is the Gray, $1\,Gy = 1\,J/kg$.

The kinetic energy of electrons can be dissipated through collision losses and radiation losses; in collision losses the energy causes excitation and ionisation while in radiation losses bremsstrahlung photons are emitted. For this reason, KERMA is divided into two components:

$$K = K_c + K_r. \tag{2.5}$$

1. $K_c$ refers to the kinetic energy that charged particles spend in collisions leading to a local release of energy around the point where the charged particle was set in motion;

2. $K_r$ refers to the kinetic energy spent in radiative losses with emission of photons; in this case the photons carry energy to points far from where the charged particle received it. When the primary neutral particles are neutrons, the secondary charged particles set in motion are heavy particles (for example p or $\alpha$); in this case, the radiative losses are negligible, therefore $K_r$ is also negligible, and the KERMA is practically all collision.

The collision KERMA can be defined by another quantity, called *net transferred energy*, which in volume V is given by

$$\begin{aligned} \varepsilon_{tr}^{n} &= (R_{in})_n - (R_{out})_n + \Sigma Q & (2.6)\\ &= (R_{in})_n - (R_{out})_n^{nonr} - (R_{out})_n^{rad} + \Sigma Q & (2.7)\\ &= \varepsilon_{tr} - (R_{out})_n. & (2.8) \end{aligned}$$

The KERMA can be then expressed as the product of a quantity describing the characteristics of the radiation field, and an interaction coefficient, which depends on the properties of the radiation and the medium in which the interaction occurs. The latter factor is the *energy transfer coefficient*, the fraction of the incident energy that is transferred to the charged particles as kinetic energy, per unit path. Through this coefficient it is possible to calculate the KERMA from the energy fluence as:

$$K = \Psi \left( \frac{\mu_{tr}}{\rho} \right)_{E,Z}. \tag{2.9}$$

If at point P the photons are not monoenergetic, but have a spectral distribution $\Psi'(E)$, then the KERMA at P can be obtained by integrating over the whole energy range

$$K = \int_{E=0}^{E_{max}} \Psi'(E) \left( \frac{\mu_{tr}}{\rho} \right)_{E,Z} dE. \tag{2.10}$$

Although the relationship between KERMA and radiometric quantities is essentially the same for photons and neutrons, traditionally the conversion factors are expressed differently for the two types of radiation. A relationship is then defined between KERMA and energy fluence for photons, and between KERMA and particle fluence for neutrons. For monoenergetic neutrons, KERMA is given by:

$$K = \Psi \left( \frac{\mu_{tr}}{\rho} \right)_{E,A} = \Phi E \left( \frac{\mu_{tr}}{\rho} \right)_{E,A} = \Phi (F_n)_{E,A} \tag{2.11}$$

where $\Phi$ is the neutron fluence and $(F_n)_{E,A}$ is the KERMA factor for neutrons, tabulated as a function of the neutron energy E and the atomic number Z of the irradiated element.
For neutrons whose fluence is distributed according to the spectrum in energy $\Phi'(E)$, the KERMA is:

$$K = \int_{E=0}^{E_{max}} \Phi'(E)(F_n)_{E,A} dE. \tag{2.12}$$

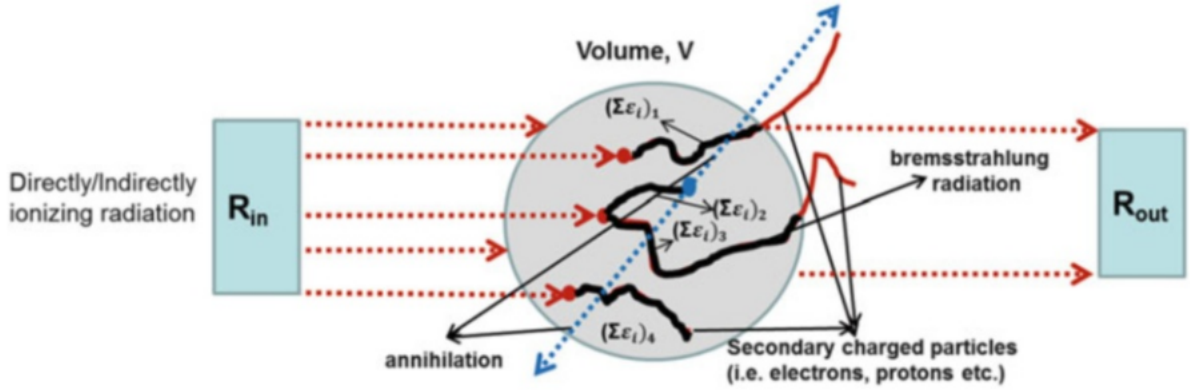


Figure 2.2: Neutral radiation and charged particle radiation entering and leaving the volume V [81].

Finally, the *absorbed dose* can be defined by the *imparted energy*. Referring to Figure 2.2, the energy imparted by ionising radiation to a medium of mass m in a finite volume V is defined as:

$$\varepsilon = (R_{in})_n - (R_{out})_n + (R_{in})_c - (R_{out})_c + \Sigma Q \tag{2.13}$$

where $(R_{in})_n$ and $(R_{out})_n$ represent the energy associated with the neutral particles entering and leaving the volume V, respectively; $(R_{in})_c$ and $(R_{out})_c$ the energy associated with the charged particles entering and leaving the same volume, and $\Sigma Q$ is the sum of the transformations of energy to mass and mass to energy that occur in V.
The absorbed dose at each point P belonging to V is the magnitude:

$$D = \frac{d\varepsilon}{dm}. \tag{2.14}$$

The unit of the dose is the same as for KERMA, i.e. Gray.

Absorbed dose is a fundamental quantity in radiation physics, but it is the most difficult to calculate, because it is closely linked to the secondary radiation and the point at which the energy is actually absorbed.
However, there are particular situations in which it is possible to establish relationships of equality between the dose and the KERMA, the calculation of which is less problematic. This case is verified if **radiation equilibrium** or the **equilibrium of charged particles** are fulfilled.
There is radiation equilibrium in a volume V if the following conditions are satisfied:

$$(R_{in})_n = (R_{out})_n \quad e \quad (R_{in})_c = (R_{out})_c. \tag{2.15}$$

Thus, the energy brought into V by charged and neutral particles entering V is balanced by the energy brought out of V by charged and neutral particles.

It follows from the definition of imparted energy that

$$\varepsilon = (R_{in})_n - (R_{out})_n + (R_{in})_c - (R_{out})_c + \Sigma Q = \Sigma Q. \tag{2.16}$$

Therefore the absorbed dose is

$$D = \frac{d\varepsilon}{dm} = \frac{\Sigma Q}{dm}. \tag{2.17}$$

When radiation equilibrium conditions are not realised, the simpler conditions of charged particle equilibrium (CPE) may still exist. There is an equilibrium of charged particles in the volume V if the energy brought in by charged particles is equal to the energy brought out of V by charged particles, i.e. the following equality is verified:

$$(R_{in})_c = (R_{out})_c. \tag{2.18}$$

Recalling the definition of imparted energy

$$\varepsilon = (R_{in})_n - (R_{out})_n + (R_{in})_c - (R_{out})_c + \Sigma Q = (R_{in})_n - (R_{out})_n + \Sigma Q \equiv \varepsilon_{tr}. \tag{2.19}$$

Therefore

$$D \overset{CPE}{=} K_c. \tag{2.20}$$

## 2.2 How to calculate KERMA and dose in MCNP

MCNP provides different ways of obtaining KERMA and dose in cells.
The $F_4$ tally is an estimator of the track length of the flux in a specific cell and is measured in particles/cm$^2$ per unit of source particle.

$$F_4 = \int_V \int_t \int_E \phi(\vec{r}, E, t) dE dt \frac{dV}{dt} \tag{2.21}$$

where $\phi(\vec{r}, E, t)$ is the particles flux.

The MCNP code estimates this integral by summing the quantity $WT_l/V$ for each particle track in the desired cell, $W$ being the weight of the particle, $T_l$ the length of the track in cm and V the volume of the cell in cm$^3$.
Through the FM multiplication card it is possible to modify the tally, obtaining a quantity of the form

$$FM = C \int \phi(E) R(E) dE, \tag{2.22}$$

where $R(E)$ is the response function found in the MCNP libraries and C is an arbitrary normalization constant.
Without going into too much detail, coupling the tally $F_4$ with the card FM

$$F_{n4} : \text{particle}$$
$$FM_{n4}\ (C\ M\ R),$$

it is possible to obtain the reaction rate per gram of a specific reaction identified by $R$ and involving the element specified in M. C is a normalization constant, given in this case by

$$C = m_B \frac{N_A}{A} \cdot \theta \cdot 10^{-24}, \tag{2.23}$$

where $m_B$ is the weight fraction of the element B in the material where the reactions take place, $N_A$ is the Avogadro number ($6.0221 \cdot 10^{23}$) and $A$ is the mass number of the element B. The factor $10^{-24}$ converts barn to $cm^2$, necessary because the libraries of cross sections are tabulated in barn while fluence is calculated in cm$^{-2}$, $\theta$ is the normalisation for the true intensity of the source (particles/s), necessary because the tallies are always normalized per unit of source particle.
When all the reaction products deposit all their energy in that particular cell, the absorbed dose rate in Gy/s can be obtained by multiplying the reaction rate by the Q-value of the reaction and by the conversion factor to transform $\frac{MeV}{g}$ into $\frac{J}{kg}$:

$$C = m_B \frac{N_A}{A} \cdot \theta \cdot 10^{-24} \cdot Q \cdot (1.6 \cdot 10^{-10}). \tag{2.24}$$

Another way to obtain KERMA is by coupling the tally $F_4$ with the cards DE/DF where, a list of KERMA factors as a function of energy can be specified. The code calculates the fluence and multiplies the KERMA factor by the energy of the particles.

MCNP provides a special tally type for dose calculation: the tally $F_6$ is a track length estimator of the average energy deposited in a cell per unit mass:

$$F_6 = \frac{\rho_a}{\rho_g} \int_V \int_t \int_E H(E)\phi(\vec{r}, E, t) dE dt \frac{dV}{dt}, \tag{2.25}$$

with $H(E)$ heating response, $\rho_a$ density atoms and $\rho_g$ density in grams. To estimate this integral, MCNP evaluates the quantity

$$W \cdot T_l \cdot \sigma_T(E) H(E) \cdot \frac{\rho_a}{m}, \tag{2.26}$$

where $\sigma_T(E)$ is the microscopic cross section. The code returns a result in $\frac{MeV}{g}$.
$+F_6$ is a collision heating tally that returns the energy deposition due to all particles transported in the problem.

## 2.3 Simulations

For the calculation of the dose due to neutron irradiation, the TRIGA Mark II reactor model was used [38].

The KCODE function, specifically designed in MCNP to reproduce fission, was used to calculate the neutron source in the rector core, which had been previously validated [43] and recently updated considering the fuel burnup and the new position of the fuel elements in the core.

Figure 2.4 shows on the left three flasks of 75 $cm^2$ (T-75) prepared with cell cultures to be irradiated at the thermal column of the TRIGA Mark II reactor; on the right the MCNP geometry with the three stacked flasks in the irradiation position. The colors represent the different materials: white is air, pink is bismuth and gray is graphite.
For the cell culture, 0.5 cm of culture medium was simulated, whose composition was reproduced considering the osteosarcoma cells protocol: HAM'S F10 and high glucose DMEM supplemented with 10 % fetal bovine serum (FBS) and 40 $mg/ml$ gentamicin. The cells were represented by a uniform 10 $\mu$m layer of cell nucleus material as reported

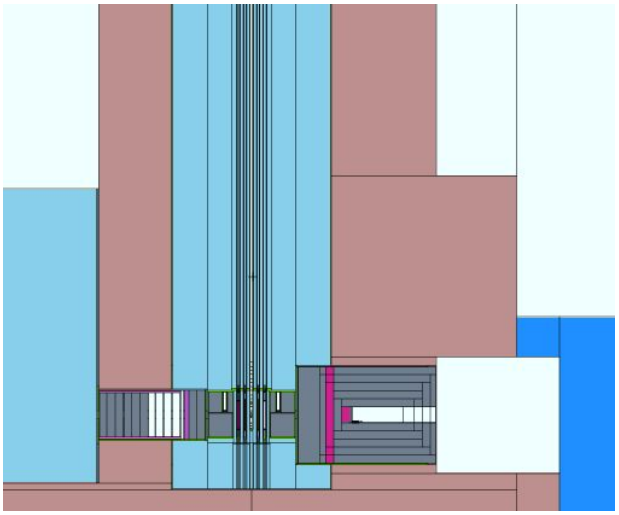

Figure 2.3: Left: MCNP model of the Triga Mark II reactor in Pavia (XZ plane). The thermal column is visible at the bottom right. Grey is graphite, pale blue is water, white is air, dove-grey is concrete.

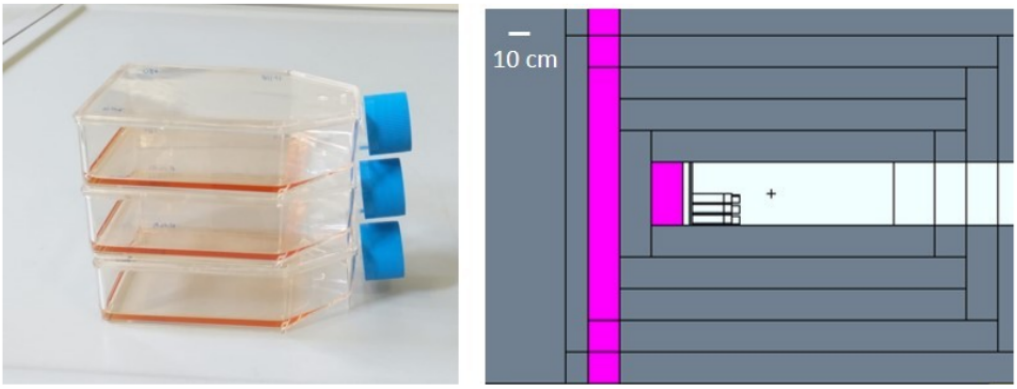


Figure 2.4: Left: T-75 flasks prepared for the irradiation in the thermal column of the reactor. Right: MCNP model of the irradiation set-up at the facility, side view. Grey is graphite, white is water, fuchsia color is bismuth.

by ICRU 46 [21], with a representative $^{10}B$ concentration of 30 ppm . This concentration value serves for the sole purpose of considering the influence of boron in neutron transport, but the final dose is calculated with the actual boron concentration measured for each experiment.
The simulations were carried out with 2 or 3 flasks stacked one on top of the other (depending on the irradiation set-up). The dose slightly changes since hydrogen contained in the plastic and in the culture medium on the top generates photons releasing dose on the cell layers of the lower flasks.
The model is provided with a feature that allows to improve efficiency in calculations: *variance reduction*. Variance reduction techniques transform the calculation into non-analog simulations, where particles considered more contributory for the tally are followed more than others. A proper normalisation is then applied by the code to avoid any bias in the final results. A weight is associated to each transported particle, representing the number or the fraction of real particles that would be present in the analog situation. The weight windows, defined for each geometry cell, allow to split heavy particles into more non-analog, lower-weight particles and to condense several low weight particles into fewer higher-weight particles. This allows keeping the total weight and the multiplicity of particles under control, optimizing the convergence and the calculation time. For more details, see MCNP manual [36].

MCNP performs the coupled transport of neutrons, photons and electrons. Its features allow the inclusion of secondary particles from neutron capture in boron and from neutron scattering. However it does not allow the transport of the protons emerging from neutron capture in nitrogen [36]. Anyway, the use of the complete reactor simulation to obtain the dose in the cell layer would be poorly efficient, even with the variance reduction techniques mentioned above. In fact, the tally must converge in a small volume ($0.838\,\mathrm{cm}^3$), located quite far away from the neutron source (around 135 cm from the centre of the reactor core), see Figure 2.5.

For this reason, to obtain statistically significant results in an acceptable computation time, we used a track-by-track source, previously generated and validated. This type of source records the information of the particles crossing a surface, for a subsequent run which only considers a reduced geometry. This limits the phase-space, reduces the computation time and provides a reliable distribution of particles. In this case, a neutron and photon source was obtained in surfaces enclosing the irradiation position as shown in Fig. 2.6. This source was used to calculate the reaction rates of neutron interactions and to transport photon and electrons.

Considering the complexity of the BNCT mixed field, the problem of dose calculation in cells was divided into two parts:

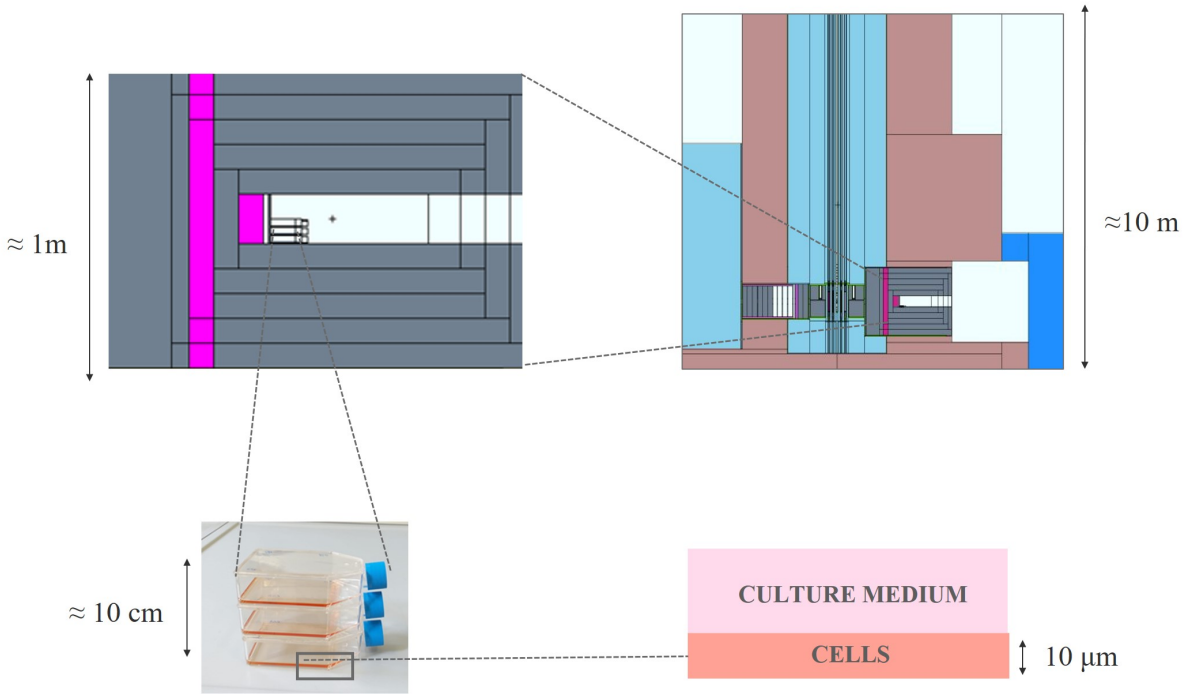


Figure 2.5: Spatial scales of simulation. Top right: the reactor. Top left: the three flasks located in the thermal column of the TRIGA Mark II reactor (Pavia, Italy). Bottom left: an enlargement of the three flasks. Bottom right: an enlargement of the cell layer with the culture medium.

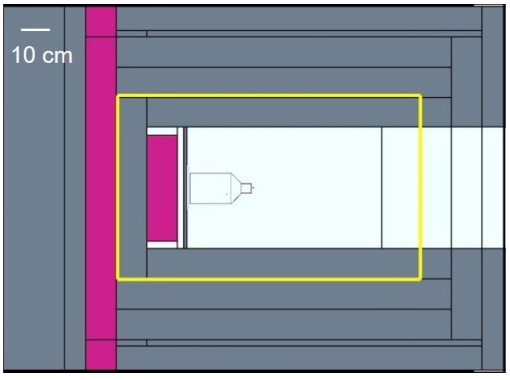


Figure 2.6: Top view of the flask positioned in the irradiation position in the thermal column of the TRIGA Mark II reactor at the University of Pavia (Italy). The yellow lines indicate the position of the track-by-track surface source.

1. **the dose component due to charged particles** from the capture reaction in boron and nitrogen and through neutron scattering in hydrogen nuclei;

2. **the dose from photons** produced in neutron capture materials or from the fission reaction in the reactor core.

To calculate the dose in the most accurate way, the secondary particles produced by the interaction of neutrons with cells must be transported separately. This requires two separate runs: the first one to calculate the reaction rates per unit of source neutrons, considering all the possible interactions; the second one to calculate the dose deposited per unit of secondary particles emitted, considering for the geometry only the flask.
For electrons due to photon interaction the calculation is more difficult because gamma rays are generated all over space. Therefore, for this component, the coupled photon-electron transport is necessary.

KERMA can be calculated with the methods described above with a dedicated run with the track-by-track source, because it does not require a detailed transport of all the secondary particles.

## 2.4 Dose delivered by charged particles from neutron interactions

In Claretta Guidi's thesis, a study was carried out to verify the reliability of dose calculation under CPE conditions in RHE samples [39]. Her results showed that CPE can be assumed for the charged particles generated by neutron interaction in nitrogen and hydrogen, but not for electrons generated by photons. Here, the same conditions are tested for cells (whose volume is one order of magnitude lower) studying also the contribution due to protons set in motion by neutron scattering.

Figure 2.7 illustrates the strategies used to calculate KERMA and absorbed dose. The dose calculation part is described below.

In order to calculate the energy deposition without assuming CPE, each emitted particle must be transported separately, which is impossible to do with a single simulation because the transport of secondary particles in the reactor geometry would be too expensive in terms of both time and calculation. Moreover, MCNP does not allow the coupled n-p transport for capture in nitrogen. Secondary particles due to the interaction with boron and nitrogen were thus generated isotropically in the cell culture and transported using

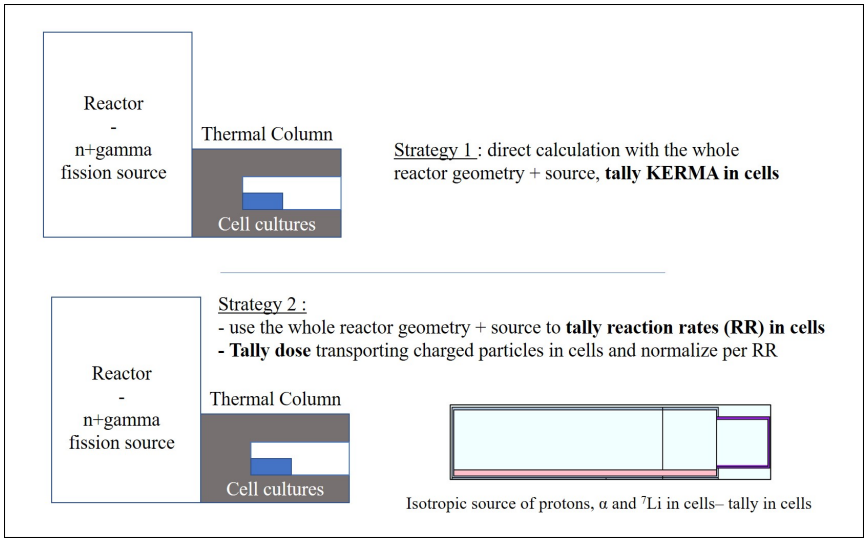


Figure 2.7: Strategies for calculating the dose due to secondary charged particles from neutron capture in nitrogen and boron. Strategy 1: Assumption of CPE. Strategy 2: Detailed transport.

the mode a (alpha particles) p (photons) h (protons) # (heavy charged particles: $^{7}Li$). Several input files were prepared to calculate the contribution to the total dose due to

- proton from 583 KeV and $^{14}C$ from 42 keV due to the reaction $^{14}N(n,p)^{14}C$
- alpha particle from $^{10}B(n,\alpha)^{7}Li$
- recoil ion $^{7}Li$ from $^{10}B(n,\alpha)^{7}Li$

For neutron capture in nitrogen, a uniform and isotropic 583 keV monoenergetic proton source was created, setting the mode h and p the dose was estimated using the $+F_6$ tally in the cell of interest. As the $^{14}C$ recoil nuclei deposit almost all their energy locally so their contribution was calculated dividing their energy (42 keV) by the mass.
The dose component due to alpha particles was calculated by generating a uniform isotropic source with the correct energy deposition, taking into account that the reaction $^{10}B(n,\alpha)^{7}Li$ occurs with two branches. The defined source emits alpha particles isotropically with two different energies: 1.78 MeV in 6 % of the cases and 1.47 MeV in 94 %. The required tallies are $F_6 : a$, and $+F_6$.
For the dose due to the lithium ions the same strategy as for the alpha particles has been used, thus the source emits $^{7}Li$ with two different energies: 1.01 MeV in 6 % of the cases and 0.84 MeV in 94 %. The required tally are $F_6 : \#$ and $+F_6$, with modes a, p, h, #.
MCNP has a default energy value below which the particle is not transported anymore and its residual energy is deposited locally. The card *cut:particle* modifies the energy cutoff; in this case the cutoff has been lowered for charged particles. For protons the default cutoff energy is 1 MeV, for alpha particles 4 MeV and for heavy ions 5 MeV. The

lowest cutoff energies allowed by the code have been set as 1 keV, the lowest possible energy for charged-particle transport. MCNP switches to nuclear models for calculations below the energy for which nuclear data are present in the libraries.

Results of dose deposited in cells by charged particles have been then compared with KERMA.

## 2.5 Dose component from photons

The photon dose contributions in BNCT irradiation are due to:

- 2.2 MeV gamma generated by the reaction $^1H(n,\gamma)^2H$ in cells, culture medium and hydrogen of the flasks materials;
- prompt photons resulting from the interaction of neutrons with surrounding materials;
- gamma rays produced in fission reactions;
- 478 keV photons derived from the $^{10}B(n,\gamma)^7Li$ reaction in 94 % of cases.

The $F_8$ tally for neutrons always assumes a local deposition of the energy of the non-transported secondary particles produced in the cell of interest, except for the energy of the photon. If photons are transported through the mode:n,p, their contribution to the dose can be evaluated with tally $F_6$. However, by doing so, all energy transferred to the secondary electrons is included by assuming a local deposition. Therefore F6:p may overestimate the actual dose deposited in the volume of interest, especially when the volume is small compared to the range of secondary particles in the specific material. In the cell tally is likely that the electrons leave the volume where they were generated depositing part of their energy elsewhere. Only under conditions of electronic equilibrium in the volume considered the $F_6$ tally return a realistic value. In fact, in this case, the energy deposited outside is compensated by energy deposited in the tally volume by electrons coming from outside. Under the conditions of electronic equilibrium one can calculate the dose due to all the photons of the problem by means of the tallies $F_6$:p and $F_4$ with the DE/DF-cards.
Note that the $F_6$:n tally includes all energy deposition due to secondary particles produced in the neutron interaction but not the once due to photons, which is calculated with $F_6$:p. Therefore the sum of these two tallies must be equal to $+F_6$.
CPE assumption is not obvious for the secondary electrons produced in the interaction of photons with the materials surrounding the cell samples. It is therefore appropriate to use a different tally to be able to transport the secondary electrons, as already shown in [39].

The tally $*F_8$ gives the energy deposited in MeV by photons and electrons in the cell of interest, obtaining the quantity $\mathrm{W} \cdot \mathrm{E}$ where W is the particle weight and E the kinetic energy in the cell.
When a particle crosses a surface entering the cell, or is created inside it, the quantity $\mathrm{W_i} \cdot \mathrm{E_i}$. is added. Including electrons and photons in the problem, mode p e, the $*F_8$:e, tally provides the correct contribution of gamma to the total dose in a specific volume taking into account the contribution due to secondary electrons.
With non-analogue transport this tally does not work, producing an unreliable result. Also for this, the simulation of electrons is quite difficult, especially in the case of complex systems such as small tally volumes away from the primary particle source. Unlike neutral particles, which interact through isolated collisions, electrons lose energy through several collisions along their path, thus requiring a long calculation time.
As other Monte Carlo codes, MCNP uses condensed history transport for the simulation of electrons, consisting in grouping the effects of many individual collisions into one energy-step so that multiple scattering approximations are valid. Collisions can be in fact described by multiple scattering theories such as the Goudsmit-Saunderson theory for angular deflections and the Landau/Blunck-Leisegang theory for straggling energy dispersion. The energy steps comprising multiple scattering effects must be long enough to include several interactions but at the same time short enough to ensure a small energy loss with respect to the kinetic energy of the electron. MCNP calculates major steps and a default number of substep. Energy loss and straggling are calculated at the beginning of each major step, while angular deflection and production of secondary particles are determined at the end of each substep.
The details of this strategy can be found in MCNP manual and were reported in Chapter 3 of [39] when the issue of electron dose was addressed for the RHE samples. In that case, it was evidenced that the default number of substeps was not adequate to represent the dose deposited in tissue. In fact, the MCNP developers recommend that the number of substeps is at lest 10 in the volume of interest. In fact, in a very small region, there may not be enough substeps to obtain an accurate simulation of the electron trajectory and the deposited energy may not be properly calculated.

Moreover, the Single-Event mode was explored, suppressing the condensed history below 100 keV and transporting electrons one by one.
The results of the preliminary calculations showed that the best condition in terms of accuracy of results and calculation time were to keep condensed history but adjusting the substeps number.
In Table 85 of the MCNP output file, the quantity ESTEP range is reported as a function of the electron energy. This represents the step size in $\frac{g}{cm^2}$. Therefore, given the density

of the material in $\frac{g}{cm^3}$, $\rho$, the length of a step in cm is given by

$$\frac{e - step\ range}{\rho \cdot m'}. \tag{2.27}$$

To obtain a total number of substeps N in the shortest linear dimension $SS$, in cm, the minimum value of $m'$ required results

$$m' = \frac{e - steprange}{\rho} \cdot \frac{N}{SS} \tag{2.28}$$

The same reasoning can be done for heavier charged particles, but since they have a higher stopping power in the same material than electrons, they have a shorter substep path length. Therefore the rule of having at least 10 substeps even in small regions of the geometry is respected, the calculation has been made and is reported further on.
To obtain 10 substeps ($N = 10$) in the volume representing the cell layer, some preliminary considerations were made. First, the spectrum of the electrons present in cells was calculated using the $F_4$ tally coupled to the E-card, which divides the total flux into different energy bins. The aim was to obtain information on the average energy of the electrons which can influence the substeps to be set for the simulation. The weighted average electron energy was calculated according to

$$\overline{E}_e = \frac{\sum_{k=1}^{m} \overline{\Delta E}_k \phi_k}{\sum_{k=1}^{m} \phi_k} \tag{2.29}$$

with k being the index of the energy bin, $\overline{\Delta E}_k$ the average energy of the k-th bin in MeV and $\phi_k$ the particle flux relative to the k-th bin in $\frac{particles}{cm^3}$. It is obtained

$$\overline{E}_e = (1.255 \pm 0.003) MeV. \tag{2.30}$$

The ESTEP range was obtained from Table 85 of the MCNP output file by selecting the value closest to $\overline{E}_e$. Using the equation 2.28 the value of the ESTEP was calculated to obtain 10 sub-steps taking into account that

- $\rho = 1.05 \frac{g}{cm^3}$,
- $SS = 10 \mu m$,
- $N = 10$.

Obtaining the corresponding value of the parameter

$$m' \simeq 543.$$

The Table 2.1 shows the results of the tally $^*F_8$, for the photon dose component, comparing two cases: the calculation with the default ESTEP value and the one where it is modified to obtain at least 10 substeps. The third column shows the percentage variation among the two cases. In the first flask, the difference is 2.1 % while in second the difference is slightly higher (5.9 %). As in the case of RHE, it was proved that increasing further the number of substeps does not change the results of the tally, as the correct dose deposition has been already reached with this value.

Even if the effect of the ESTEP does not cause a relevant change in the overall dose calculation, because it is only one of the dose components, it is appropriate to set the ESTEP in order to have a more precise estimate of dosimetry.

| $^*F_8$ tally results (Gy/kW) | | | |
|---|---|---|---|
| I flask | default e-step | $(9.4 \pm 0.1) \cdot 10^{-3}$ | 2.1 % |
| | modified e-step | $(9.2 \pm 0.1) \cdot 10^{-3}$ | |
| II flask | default e-step | $(1.01 \pm 0.01) \cdot 10^{-2}$ | 5.9 % |
| | modified e-step | $(9.5 \pm 0.1) \cdot 10^{-3}$ | |

Table 2.1: Results of tally $F_8$ in cases where the ESTEP is left as default and modified for the first and second flask. Results are for the irradiation time of 10 minutes. The third column reports the difference between the default and the modified ESTEP calculations.

Table 2.2 shows the values of the photons dose obtained with the default ESTEP and with the modified one. Dose is obtained dividing $*F_8$ tally by the cell layer mass (0.09 g). The Table reports the average dose of the two stacked flasks. In fact, the dose used for cell-survival curves is always the average between the different irradiated flasks, as the survival results are not related to one particular flask. Between the two values there is a difference of about 4%.

| Photon Dose component | |
|---|---|
| default ESTEP | 0.00976±0.00008 Gy/kW |
| modified ESTEP | 0.00935±0.00008 Gy/kW |

Table 2.2: Photon dose component (average of 2 stacked flasks) when ESTEP is default and when it is modified to obtain 10 substeps in the volume of interest.

The considerations just made for electrons can also be applied to charged particles. The corresponding step ranges were also extrapolated from Table 85 of the MCNP output file of the dose transport from protons, alpha particles and lithium.
In this case an energy of 600 keV was taken for protons, while for charged particles, alpha and lithium, the average energy of the two reaction branches was calculated.

$$\overline{E}_{\alpha} = (P_1 E_1 + P_2 E_2)_{\alpha} = (0.94 \cdot 1.47 + 0.06 \cdot 1.78) MeV = 1.49 MeV \tag{2.31}$$

$$\overline{E}_{^7Li} = (P_1 E_1 + P_2 E_2)_{^7Li} = (0.94 \cdot 0.94 + 0.06 \cdot 1.01) MeV = 0.85 MeV. \tag{2.32}$$

Assuming that there are 10 substeps from the equation 2.28, the following values are obtained

$$m'_p \simeq 1.15$$

$$m'_{\alpha} \simeq 0.62$$

$$m'_{^7Li} \simeq 0.022.$$

Being all the obtained values lower that the default value 3, there are at least 10 substeps, as suggested by the developers [40], therefore the default value has been used.

## 2.6 Evaluation of the dose due to neutron scattering in hydrogen

The most difficult component to estimate in this type of evaluation is the hydrogen scattering component. In fact, traditionally, the calculation is made by coupling $F_4$ tally with an FM card, which modifies the flux with the scattering cross section and a heating function. This function gives the average energy deposited in the material for each scattering. This corresponds to a KERMA calculation. Protons from the elastic scattering of neutrons in hydrogen are generated not only in cells, but also in the culture medium, in the flask and in the caps. For this reason it is likely that the conditions of charged particle equilibrium is satisfied, however some considerations were made to prove this hypothesis.

To assess the correct dose it is necessary to transport the generated protons and to calculate the deposited dose by $F_6$ tally. Also in this case, the transport of protons in all the reactor geometry would be too expensive in terms of calculation time, after calculation of the energy distribution of the scattered protons.

To calculate the proton spectrum in the parts of the set-up containing hydrogen, a file input was created where the scattering in hydrogen was turned on. To this end the card PHYS:N, containing neutron physics options, was used. This data card has different entries

***PHYS:N emax emcnf iunr j j j coilf Cutn Ngam j j i_int_model***

***i_ els_ model,***

where

- ***emax*** represent the upper limit for neutron energy (default energy is 100 MeV);

- ***emcnf*** is the analog energy limit (default value is 0 MeV);

- ***iunr*** controls unresolved resonance range probability table treatment when data tables are available.
  If iunr= 0, treatment is on (DEFAULT).
  If iunr= 1, treatment is off;

- ***j***, ***j***, ***j*** are unused but if a number appears is a fatal error;

- ***coilf=n.m*** is the parameter dealing with light and heavy ion recoil and NCIA control, n is an integer and m is a specified fractional value.
  If $0 < m \leq 1$ and $n = 0, 1, 2 \text{ or } 4$, then m is the number of light ions (protons, deuterons, tritons, 3 He, and alphas) per incident neutron to be created at each neutron elastic scatter event with light nuclei H, D, T, $^3He$, and $^4He$. Heavy ions are also created if they are specified on the MODE card.
  If $n = 3$ or $n = 5$, then $m = 0$ and light-ion recoil is turned off.
  For $n = 2$ or $n = 3$, NCIA is active only when the production of NCIA ions is not modeled with the nuclear data Tables.
  For $n = 4$ or $n = 5, NCIA$ is active and the nuclear data Tables for production of NCIA ions are not used.
  Therefore, the following description for coilf entries are valid If coilf = 0 then light-ion recoil is off; NCIA is off. (DEFAULT)
  If 0.001 < coilf < 1.001 then light-ion recoil makes coilf ions from elastic scatter.
  If 1.001 < coilf < 2.001 then light-ion recoil makes coilf-1 ions from elastic scatter; NCIA ions from neutron capture.
  If coilf = 3 then light-ion recoil is off; NCIA ions from neutron capture.
  If 3.001 < coilf < 4.001 then light-ion recoil makes coilf-3 ions from elastic scatter; NCIA ions from neutron capture.
  If coilf= 5 then light-ion recoil is off; NCIA ions from neutron capture;

- ***Cutn*** is the controls table-based physics cutoff and memory reduction;

- ***Ngam*** is the controls secondary photon production;

- ***j***, ***j*** are unused but if a number appears is a fatal error;

- ***i_int_model*** is the control treatment of nuclear interactions;

- ***i_els_model*** is the control treatment of nuclear elastic scattering.

If the optional neutron capture ion algorithm (NCIA) is activated by the 7-th entry on the PHYS:N card, it performs neutron capture in $^3He$, $^6Li$, and $^{10}B$ to produce protons, tritons, deuterons, and/or alphas and lithium according to the following reaction

$$^3He(n,h)t,\ n(^3He,d)d$$

$$n(^6Li,t)\alpha$$

$$n(^{10}B,\alpha)^7Li.$$

The energies of light ions are often very low, especially when dealing with thermal neutron capture. Therefore, to allow the transport of these secondaries, the cutoff energy must be lowered using the card CUT:<pl> [36].
The default value of the coilf is set to 1, in order to enable the transport of the proton generated by each hydrogen scattering.
In this way, only scattered protons are generated, because the physics of the reaction $^{14}N(n,p)^{14}C$ is not implemented in MCNP, with no risk of double counting the protons.
The track-by-track source was used to calculate the proton spectra in the cells, culture medium, flask and cap. The mode n, h was set, therefore the protons were also transported. The proton cutoff energy was lowered to 1 eV via the card cut:h j 1e-6, even if MCNP cannot transport protons with energies below 1 keV. The tally $F_4$ was used to request the proton flux on the cells on the medium on the flask and on the cap in an energy range of 0 to 17 MeV in 11 logarithmic bins. The spectrum obtained below 1 keV resulted 0, as expected. This prevented the implementation of the strategy described above. In fact, neutron spectrum in cells is for 99.8% below 1 keV, as shown in Figure 2.8. The average energy of this spectrum is 0.4 keV, which would lead to proton maximum energy of 0.4 keV, and average energy of half this value. According to the Nist database [82], a proton with an energy of 1 keV has a range of $9.045 \cdot 10^{-7}$ g/cm$^2$ or $8.6143 \cdot 10^{-7}$ cm $= 8.6143 \cdot 10^{-3}\,\mu$m. Protons of 0.4 keV have range in tissue considerably lower than the thickness of cell layer. This consideration justifies the hypothesis of equilibrium and the approximation of dose with KERMA for this component. Moreover, protons coming form culture medium and flask may compensate those leaving the cells.

To deepen the insight into ths issue, a theoretical spectrum was also built to calculate the dose deposition, assigning the same probability as the neutron spectrum in every energy bin, because for as many neutrons interacting on hydrogen, as many scattering protons will be generated, but halving the bin energy. This was used to generate the

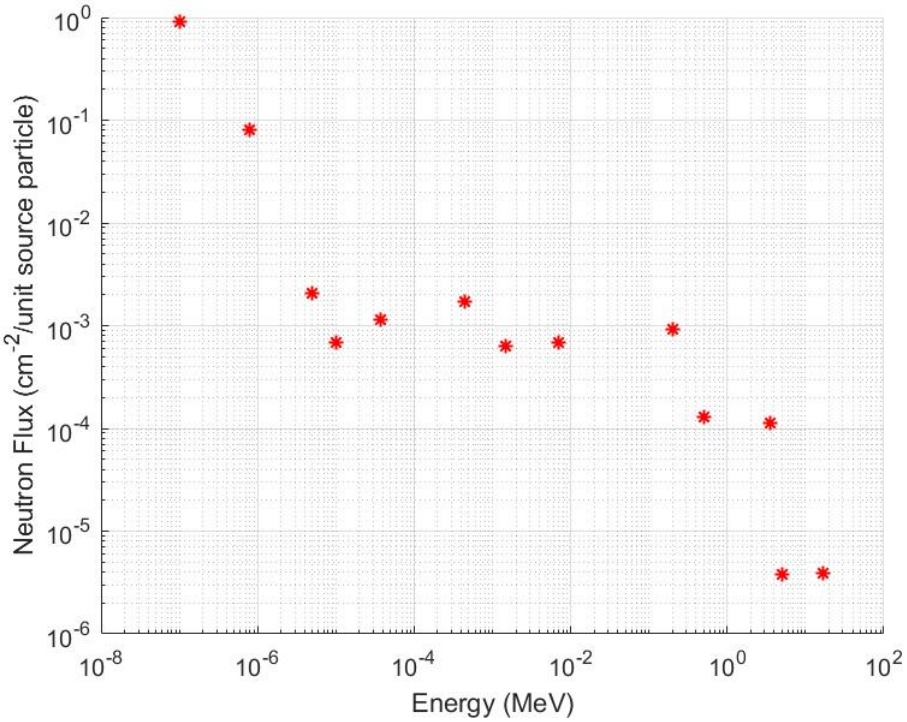


Figure 2.8: The neutron spectra in the cells in a semilogaritmic scale.

proton source isotropically distributed in the hydrogenated materials for dose calculation in cells. In this case, dose due to protons below 1 keV was calculated by KERMA and the rest was calculated by transport. For protons with energies above 1 keV, once the theoretical proton spectrum was obtained, a run was made in which only the flask was simulated and the protons were transported according to the energy distribution found.

The source specification was obtained using cell rejection to sample uniformly the source within a cell comprising the entire flask, accepting the sample point if within the cell of interest, otherwise rejecting it and producing another sample. MCNP cells representing the cells, the culture medium, the flask and the cap were used for rejection. When the acceptance rate is too low the problem is terminated due to inefficiency, so it is necessary to lower the efficiency threshold. In this case, since the efficiency of the source is lower than the default (0.01 MeV), the EFF card was set to 0.00001 MeV.
The ERG card in the source specification has been defined a function of the rejection cells:

$$\mathrm{ERG} = \mathrm{FCELL} = \mathrm{D_x}.$$

In this way, the proton energy is sampled in the correct spectrum, according to the cell in which the proton has been sampled.

Considering only the contribution of protons set in motion in the cells above 1 keV, this method evidences a difference between KERMA and dose of 16.15 %. Adding the other components, this difference is in fact completely compensated by higher energy protons coming from the medium and the flask. The protons coming from the cap do not contribute at all. This proves that KERMA approximation is acceptable for proton scattering.

It should be emphasised that the scattering dose component is the lowest in this irradiation position, because scattering is dominant at epithermal/fast energies. In the thermal column the thermal component is 2 and 4 orders of magnitude higher than epithermal and fast components, respectively.

## 2.7 Results

KERMA and absorbed dose in cells obtained from computational simulations are given in Table 2.3. The values are given per unit of neutron emitted from the source and for a boron concentration of 1 ppm.The values obtained show that KERMA overestimates the all component of absorbed dose except those for the elastic scattering that equals the value. Therefore, the condition of charged particle equilibrium cannot be assumed [64].

| Component | KERMA $(Gy\,n^{-1}) \cdot 10^{-19}$ | Absorbed dose $(Gy\,n^{-1}) \cdot 10^{-19}$ | Relative difference (%) |
|---|---|---|---|
| $^{10}B(n,\alpha)^{7}Li$ | 0.747±0.001 | 0.667±0.001 | 12 |
| $^{14}N(n,p)^{14}C$ | 1.576±0.016 | 1.127±0.001 | 40 |
| $^{1}H(n,n')^{1}H$ | 0.297±0.004 | 0.297±0.004 | 0 |
| Photons | 2.749±0.008 | 2.327±0.004 | 18 |

Table 2.3: Results of MCNP simulation for the cell irradiation set-up. All the component are reported per source neutron and the boron one for 1 ppm. The last column represent the percentage of relative difference for each radiation component.

## 2.8 Photon irradiation

Gamma irradiation was performed at the Policlinico San Matteo in Pavia (Italy) using a Cobalt-60 unit.

For each dose assessed, the flasks were exposed to a homogeneous gamma field of 32 x 32 $cm^2$. The distance between the surface and the source (SSD) was set at 78.5 cm and the dose rate to 0.81 Gy $min^{-1}$ [44].

An average layer of 0.5 cm thickness provided the monolayer of cells with electronic equilibrium, so that in these irradiation sessions it was not necessary to carry out computational

studies to estimate adequate absorbed dose values for the survival assay.

This chapter has explained how the dosimetry calculation was performed. The results obtained were used to construct dose-response curves for two types of tumors: osteosarcoma (Chapter 3) and head and neck cancers (Chapter 4). The purpose of the next steps is to evaluate the effect of the difference found between KERMA and absorbed dose calculated in radiobiological experiments in patient treatment planning.

# Chapter 3

# BNCT of Osteosarcoma

Osteosarcoma is a rare malignant tumour that arises from bone cells: osteoblasts (cells that build bone) and osteoclasts (cells that act as scavengers of dead bone and help the bone maintain its natural shape). It is an aggressive neoplasm, and its incidence is higher in children and adolescents [46].
Osteosarcoma can affect any segment of bone, although almost all cases involve the long bones (humerus, radius, ulna, femur, tibia and fibula). In other locations the neoplasm is more often diagnosed in adults or the elderly.
There are different forms of osteosarcoma, recognisable by their degree of malignancy (low, intermediate, high). In almost eight out of ten cases, the disease has a high degree of malignancy. Due to the speed of replication of the neoplastic cells, the disease can also cause metastases, which are present at an early stage in 15% of cases. Nevertheless, micrometastases, i.e. small aggregates of neoplastic cells that are invisible to diagnostic tests, are certainly present in more than 80 % of patients.
Osteosarcoma frequently appears as a second tumour in patients already treated with radiotherapy for other childhood malignancies.
Currently, this type of tumour is treated with preoperative chemotherapy (neo-adjuvant), followed by surgery removing all the detectable diseased cells, including metastases. Finally, further postoperative chemotherapy (adjuvant) is administered [47].
These procedures are effective in 70% of patients with a localised tumour, but if metastases are present the long-term survival rate is lower than 20% [48].
While neo-adjuvant chemotherapy allows for more pronounced tumour margins facilitating surgery, adjuvant chemotherapy is critical in the control of micrometastases [49, 50].
In the last decades a new surgical technique called *limb salvage* has been developed with the aim to avoid limb amputation and to preserve the functional and aesthetic status of patients without decreasing the survival rate [51].
Osteosarcoma is considered a radioresistant tumour, however it has been noted that a

high photon dose in a single fraction can be effective. Therefore, radiotherapy has been used for local treatment of unresectable tumours or as palliative treatment.
Due to the low tolerance of the surrounding tissues it is difficult to deliver high doses of photons in a single fraction; recently patients have been treated with charged particles, such as protons or carbon ions, capable to administer a more precise dose distribution in accordance with the tumour volume. In other cases they have been treated with intraoperative radiotherapy and even extracorporeal [52, 53].
BNCT can play an important role in this treatment scenario, as it is a therapy capable of selectively destroying cancer cells, thus a larger area could be irradiated hitting the isolated cells, infiltrated in the healthy tissue, which are considered a source of recurrence or micrometastases. The possibility to perform a less aggressive surgery and to treat the surrounding tissues with BNCT would guarantee a better quality of life for patients while maintaining a high tumour control probability. For this reason, the feasibility of BNCT for osteosarcoma has been studied in Pavia since many years, also considering that irradiation of limbs with neutrons is relatively easy, both for patient positioning and for the substantial sparing of important organs located in the abdomen and in the thorax. To calculate dosimetry, it is essential to know the boron concentration in the healthy tissues and in tumour. Extensive pre-clinical research have been conducted in Pavia, as described in [94]. As the in-vitro model, the rat osteosarcoma cell line UMR-106 has been used both for boron uptake studies and for dose-survival curves.

## 3.1 Experimental set up

The rat osteosarcoma cell line (UMR-106) was treated in Pavia according to the following protocol: the cell culture was incubated for 4 hours with BPA-enriched medium and washed with PBS after the contact time. For irradiation, cells were supplied with fresh medium, BPA-free, so the dose of boron depends solely on the boron atoms internalised by the cells. Flasks of cells treated in the same way as those subjected to neutron irradiation were used to measure boron in the cells by means of neutron autoradiography as described in [45]. In this way, biological variability in cell behaviour on different days and under different environmental conditions can be included in the dose calculation. With a clonogenic assay [44], cell survival is measured as a function of dose. The latter is modified by increasing the reactor power, thus increasing the neutron fluence. The irradiation time is 10 min and it is kept constant over all the irradiation experiments. The motivation of fixing the irradiation time is that cells stay outside the incubator and in non-ideal conditions for a short time. Moreover, the fact that cells are irradiated in fresh medium, generates a washout of boron from cells for longer times [95].

Clonogenic assay was chosen because the effect to be measured as a function of the dose is the ability of the cells to generate a new tumour after irradiation. Cells that are detected alive in a mortality test could still undergo programmed death or failure to reproduce. Clongenicity is therefore the most meaningful test for assessing the ability of BNCT to control the tumour. Rat osteosarcoma cells UMR-106 are an immortalised cell line.
Immortalised cell lines are cells derived from tumours or genetically modified cells through oncogenic transformation that has enabled them to grow indefinitely. They are used experimentally to clone individual cells or to study and modify their behaviour.
On 8 February 1951 George Gey of Johns Hopkins University isolated cells from a biopsy of a cervical tumour and placed them in a petri dish with culture medium to keep them alive. All the cells tested until that moment had led to unsatisfactory observations. Unexpectedly, these cells from a patient named Henrietta Lacks adapted very well to their new environment.
This outcome created the first immortalised cell line, nicknamed HeLa, capable of renewing itself indefinitely in artificial culture [68].
Immortal cell lines offer various advantages such as being convenient, easy to use and providing an unlimited supply of material. Moreover, the effect of being a pure population of cells allows to have consistent samples and repeatable results [66, 67].

## 3.2 Determination of cell survival curves

The aim of this work is to study the treatment planning of a patient, using photon-equivalent units calculated with different models. Models are fed with the parameters obtained fitting the cell survival curves from *in vitro* experiments.
The survival curves were built for three cases: photon irradiation, irradiation with neutrons (beam only) and neutron irradiation after BPA treatment (BNCT).
The dose components were obtained by MCNP simulations, as explained in chapter 2, considering the boron concentration measured in the samples for each experiment, the reactor power and the irradiation time per second, from the following equation:

$$D = (d_B \cdot B + d_p + d_s + d_\gamma) \cdot P(kW) \cdot t_{irr}, \tag{3.1}$$

where

- $d_B$ $(Gy/s)$ is the dose rate per unit kW and for ppm of boron due to $^{10}B(n,\alpha)^7Li$ reaction;

- $B$ $(ppm)$ is the boron concentration in the cells;

- $d_p$ $(Gy/s)$ is the dose rate per unit kW due to 583 keV protons and 42 keV recoil $^{14}C$ from $^{14}N(n,p)^{14}C$ reaction;

- $d_s$ $(Gy/s)$ is the dose rate per unit kW due to hydrogen recoil nuclei from $^{1}H(n,n')^{1}H$ reaction;

- $d_\gamma$ $(Gy/s)$ is the dose rate per unit keV due to all photon in the problem;

- $P$ $(kW)$ is the rector power;

- $t_{irr}$ $(s)$ is the irradiation time, fixed at 600 s.

There are two important considerations when calculating the dose

1. **Dose vs KERMA**
   Table 3.1 shows the KERMA values with the actual reactor power and boron concentration for the rat osteosarcoma cell line, both in the presence of boron (BNCT) and in its absence (beam only). Table 3.2 shows the same for absorbed dose.
   Different data sets are obtained which will give rise to two different curves, see Figure 3.1.

| ***KERMA*** | | | | |
|---|---|---|---|---|
| | **BNCT** | | **BEAM ONLY** | |
| P(kW) | Boron (ppm) | KERMA (Gy) | Boron (ppm) | KERMA (Gy) |
| 1 | 30.5 | 0.13±0.01 | 0 | 0.022±0.002 |
| 7.5 | 34.1 | 1.0±0.1 | 0 | 0.16±0.01 |
| 30 | 18.5 | 2.5±0.2 | 0 | 0.65±0.05 |
| 60 | 12.0 | 6.2±0.5 | 0 | 1.3±0.1 |
| 100 | | | 0 | 2.2±0.2 |
| 150 | | | 0 | 3.2±0.3 |
| 200 | | | 0 | 4.3±0.3 |
| 250 | | | 0 | 5.4±0.4 |

Table 3.1: Dose for BNCT and beam only for the KERMA approximation.

2. **Calculate the concentration of boron in cells treated with BPA vs taking a fixed value of boron concentration**
   In the previous point, the boron dose was calculated considering the measured boron concentration in each experiment. The measurement is important as the concentration varies greatly depending on the conditions, from 12 ppm to 42 ppm [64], thus influencing the boron component of the dose.
   This procedure was introduced in Pavia and the measurement is done the same day

| *Absorbed dose* | | | | |
|---|---|---|---|---|
| | **BNCT** | | **BEAM ONLY** | |
| P(kW) | Boron (ppm) | Dose (Gy) | Boron (ppm) | Dose (Gy) |
| 1 | 30.5 | 0.11±0.01 | 0 | 0.0176±0.0002 |
| 7.5 | 34.1 | 0.90±0.06 | 0 | 0.132±0.002 |
| 30 | 18.5 | 2.2±0.1 | 0 | 0.529±0.007 |
| 60 | 12.0 | 5.4±0.3 | 0 | 1.06±0.01 |
| 100 | | | 0 | 1.75±0.02 |
| 150 | | | 0 | 2.65±0.03 |
| 200 | | | 0 | 3.53±0.05 |
| 250 | | | 0 | 4.41±0.06 |

Table 3.2: Absorbed dose for BNCT and beam only.

of the cells irradiation, in cells treated in the same way as the irradiated cultures. Lacking a measurement procedure giving the actual boron concentration at the moment of irradiation, boron dose would be estimated using historical biodistribution data, for example assuming for each experiment a boron concentration in the cells of about half the treatment concentration. This has been observed on average for many cell lines in Pavia, for 4 hours of BPA contact time. Therefore, boron concentration in cells would be 40 ppm for a treatment with 80 ppm in medium.

### 3.2.1 Results

Figure 3.1 shows the experimental cell survival, plotted as a function of the KERMA (left) and of the absorbed dose (right). Curves were fitted according to the model described in the paragraph 1.3.
The fit was obtained from the equation 1.19 taking into account the Lea-Catcheside time factor, assuming that the kinetic repair follows a biexponential decay with two characteristic repair times, one slow and one fast, and considering first order sublethal damage (SLD) and synergism between the different radiation components.

| | | SLD repair (%) | |
|---|---|---|---|
| | Characteristic repair times | Low LET | High LET |
| $t_{0f}$ | $24/ln2\ (min)$ | 0.53 | 0.2 |
| $t_{0s}$ | $14/ln2\ (hours)$ | 0.47 | 0.8 |

Table 3.3: Parameters used for the calculation of the Lea-Catcheside time factors $G$ in the survival models.

It is assumed that the survival probability for reference radiation $R$ (San Matteo

Polyclinic gamma beam) is given by single fraction modified LQ dose expression

$$-ln(S_R(D_R)) = \alpha_R D_R + \beta_R G_R(\theta) D_R^2. \tag{3.2}$$

The alpha and beta parameters of the gamma component of the BNCT dose can be assumed to be equal to those of the reference radiation. Since the energy spectra of the reference gamma radiation, i.e. photons arising from the decay of cobalt-60 at around 1 MeV, and those of the reactor beam at around 2 MeV are almost the same, it can be assumed that

$$\alpha_R = \alpha_\gamma, \tag{3.3}$$

$$\beta_R = \beta_\gamma. \tag{3.4}$$

Six parameters remain to be estimated in the equation 1.19, namely alpha and beta of boron, slow and fast neutrons.

Fast neutrons in BNCT beams have energies that are mostly less than about 1 MeV. For this neutron energy group, elastic recoils with hydrogen is the most important contribution to the charged particle slowing down spectrum, with energies comparable to those of protons produced by nitrogen thermal neutron capture. Therefore a similar responses of biological systems are expected when exposed to radiations with comparable lineal energy spectra. Thus the alpha and beta parameters of fast neutrons will be the same as those of slow neutrons because they will always produce the same lethal damage due to the protons

$$\alpha_{nt} = \alpha_{nf} = \alpha_n$$

$$\beta_{nt} = \beta_{nf} = \beta_n.$$

Finally, the boron effect is is due to high-LET radiation; consequently, the quadratic term of this component is considered negligible and set equal to zero

$$\beta_B = 0.$$

Under these assumptions, the 8 free parameters have been reduced to 3

- $\alpha_B$,
- $\alpha_n$,
- $\beta_n$.

These parameters are obtained using a MATLAB [65] program that fits the experimental data using the least squares method.

The graphs obtained are shown in Figure 3.1, representing cell survival data and fit

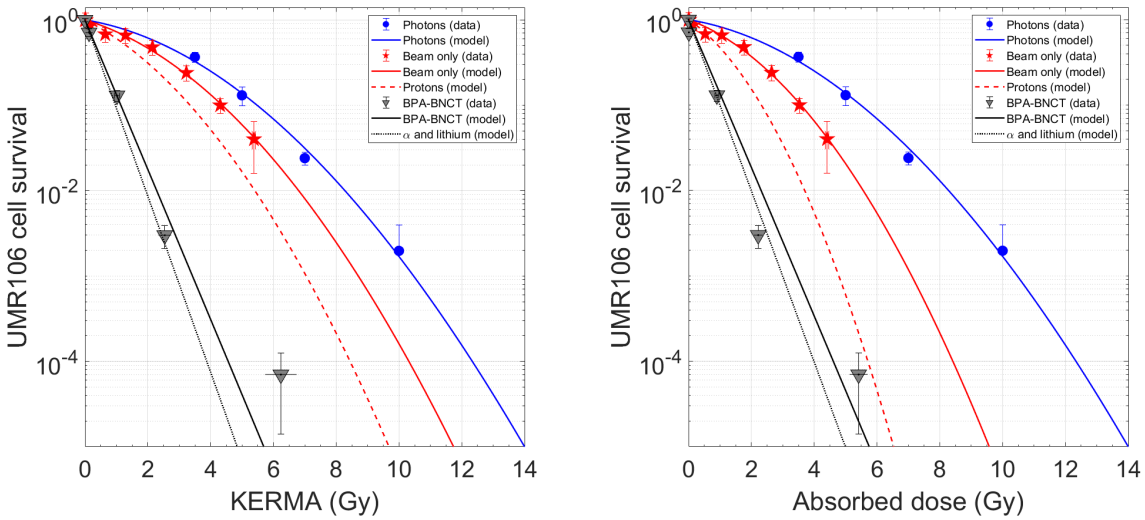


Figure 3.1: Left: survival curve as a function of the KERMA, assuming CPE condition. Right: survival curve as a function of the absorbed dose.

results for reference photon radiation, Beam only and BNCT. The isolated contributions of *protons* $+^{14}C$ and the $\alpha$ *particle* $+^{7}Li$ are also shown.

On the left side of the Figure 3.1, the cell survival curve is represented as a function of the KERMA values under equilibrium conditions of charged particles. On the right, it is shown the curve of cell survival as a function of absorbed dose, derived from accurate calculations, without assuming CPE conditions and considering the boron concentration measured on the day of the experiment.

Tables 3.4 and 3.5 show the radiobiological parameters of the mathematical model that describes the cell survival as a function of the absorbed dose and the KERMA, respectively, for reference radiation according to equation 3.2 and for BNCT according to equation 1.19.

| **Absorbed dose** | | |
|---|---|---|
| | Parameters of survival models | |
| | Alpha ($Gy^{-1}$) | Beta ($Gy^{-1}$) |
| $^{60}Co$ source Reference radiation | $0.14 \pm 0.05$ | $0.05 \pm 0.01$ |
| Beam gamma photon | $0.14 \pm 0.05$ | $0.05 \pm 0.01$ |
| Neutrons | $0.6 \pm 0.03$ | $0.2 \pm 0.1$ |
| Boron (BPA) | $2.3 \pm 0.2$ | 0 |

Table 3.4: Radiobiological parameters of the survival models for the photon reference radiation and for BNCT based on the corrected dosimetry of the *in-vitro* experiments for the osteosarcoma cell line. Values are presented with ±1SD.

The RBE and CBE are calculated for a cell survival of 1 %, for absorbed dose and

| KERMA | | |
|---|---|---|
| | Parameters of survival models | |
| | Alpha ($Gy^{-1}$) | Beta ($Gy^{-1}$) |
| $^{60}Co$ source Reference radiation | $0.14 \pm 0.05$ | $0.05 \pm 0.01$ |
| Beam gamma photon | $0.14 \pm 0.05$ | $0.05 \pm 0.01$ |
| Neutrons | 0.4±0.2 | 0.0808±0.0007 |
| Boron (BPA) | 2.4±0.1 | 0 |

Table 3.5: Radiobiological parameters of the survival models for the photon reference radiation and for BNCT based on KERMA of the *in-vitro* experiments for the osteosarcoma cell line. Values are presented with ±1SD

KERMA. The component of protons+$^{14}C$ curve is used to calculate the neutron RBE and the component of $\alpha +^{7} Li$ curve is used to calculate the CBE. To this end, the parameters of the fit corresponding to these components are used to calculate dose necessary to obtain 1% of survival and compared to the corresponding photon dose. The obtained results are shown in table 3.6.

The $CBE_{1\%}$ factor remains the same for KERMA and absorbed dose while the mean $RBE_{1\%}$ values differ by more than 30%. RBE quantifies the differences in biological effectiveness of different qualities of radiation. Since 30% to 50% of the dose to normal tissues is due to intermediate LET protons, the difference in the $RBE_{1\%}$ may significantly change prospectively a treatment prescription, or retrospectively the analysis of radiotoxic effects observed after BNCT.

| | **KERMA** | **Absorbed dose** |
|---|---|---|
| $RBE_{1\%}$ | 1.5±0.2 | 2.2±0.4 |
| $CBE_{1\%}$ | 4.4±0.4 | 4.4±0.4 |

Table 3.6: RBE and CBE factor for a 1 % survival for absorbed dose and KERMA.

In Figure 3.2 the cell survival curve is represented as a function of the absorbed dose obtained from detailed dosimetry calculations where a value of 40 ppm is taken into account for the boron concentration in the cells treated with BPA. If the high dose values are correct, the high survival rates measured for those values are unexpectedly high. In particular, it is surprising that for 14 Gy of photons the survival would be much lower than for 14 Gy dur to BNCT. As there is no evidence of error in the survival measurement, it is evident that dosis is not accurate. In fact, measurements show that boron concentration is different for each dose value; this highlights the importance of measuring boron in the irradiation experiments.

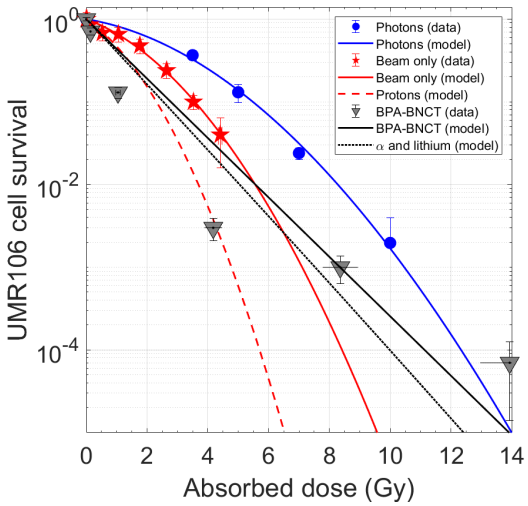


Figure 3.2: Survival curve function of the absorbed dose considering constant boron concentration of 40 ppm.

## 3.3 Treatment planning

The medical images of a patient can be converted into a Monte Carlo model for simulation of the radiation transport and the calculation of the dose distribution in the patient. The most accurate model is ideally obtained by converting the smallest geometric unity of the medical image available into a voxel. The dose is thus calculated in these small volumes. Using a Monte Carlo simulation, the administred dose can be calculated in each voxel.
The clinical case examined in this work is a 17 year old male patient. The patient presents a parosteal osteosarcoma arising from the posterior aspect of the distal metaphysis of the femur and extending to the popliteal fossa (tumour volume approximately 50 $cm^3$). The mass is well demarcated on imaging and the appearance of the newly formed tissue has both blastic and lytic characteristics [92]. This clinical case reported in the cited reference, was employed to study in details the effects of a detailed dosimetry in radiobiological experiments, that was not available at the time of the publication
The medical images were used as input to NCTPlan [84], to create a voxelized model of the limb in the MCNP syntax. NCTPlan is a Treatmente Planning System coupled to MCNP for transport calculations code for applications in BNCT [113] , developed in collaboration by the CNEA (Comisión Nacional de Energía Atómica, an Argentinean agency for research and development in the field of nuclear energy) and the medical research centres at Harvard University and MIT (USA).
Based on the MCNP code with a graphic interface to reconstruct the patient's geometry in voxels starting from medical images, the patient's anatomy is reconstructed. A voxel-model is a three-dimensional matrix of contiguous parallelepipeds, each of which is considered to have a uniform material composition (*voxel*: vox "volume", el "element").

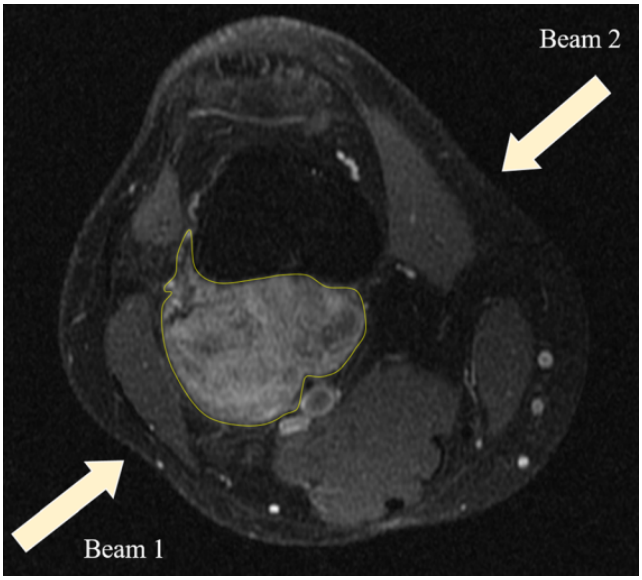


Figure 3.3: MRI image of the osteosarcoma tested with the selected beam configuration.

The construction of the voxel model consists of superimposing a three-dimensional rectilinear grating on such an image of the patient and determining the frequency distribution of the different tissue types in each voxel. Only a limited number of tissue types are used and the materials are defined by Hounsfield units, a scale used to quantitatively describe the transparency of a material with respect to the passage of X-rays. The dose is calculated in each voxel. The user changes the orientation of the voxel model with respect to the source plane, but the program makes sure to change the orientation of the source plane in the input while leaving the position of the patient model unchanged. The user must also provide information about the angular distribution and spectrum of neutrons and photons in the beam. The input for MCNP is created by adding the indications for the desired tally.

The particularity of the chosen clinical case is that the tumour is large and deep-seated. The most efficient irradiation configuration was obtained using two opposite parallel fields as shown in Figure 3.3. Irradiating one portal at a time, it is possible to better preserve the healthy tissue and also reach the deepest part of the tumour. The aim of the first calculations was to demonstrate the suitability of an accelerator-based neutron beam to treat this tumour. The beam was mostly epithermal, to ensure good penetration. The skin is the organ with the highest risk and is therefore the most limiting.

Many studies have been done on the skin, particularly melanoma [88], and it has been found that the maximum dose it can receive is 22 Gy_Eq.
In this thesis, the beam described in [92] was used, and the two sets of parameters obtained with KERMA and Absorbed dose (Table 3.4 and 3.5) were applied in the photon isoeffective dose model for dose translation into photon-equivalent units. Moreover, the

dosimetry in patient was obtained also using an optimized beam, that has been selected as the most performing in clinical cases as well as the safest from the point of view of radioprotection and out-of-field dose [86].
Dealing with a limb, the tissues involved are bone, soft tissue, tumour and skin. The latter is the most limiting tissue, because the concentration of boron it absorbs is 1.5 times higher than in blood. Therefore, the prescription was set to deliver a maximum dose of 22 Gy_Eq to the skin, calculated using the formalism of fixed RBE and CBE factors reported in [13, 93]. The dose released into the tumour was calculated with both the traditional formalism of fixed RBE (*biological weighted dose*), and with the photon isoeffective dose model. As explained in the Introduction, the photon equivalent dose formalism calculates biological weighting factors at fixed endpoints, such as 1% survival in *in-vitro* experiments, the isoeffective dose model exploits the entire dose-dependent cell survival curve.
Boron concentration in tumour was taken as 60 ppm, as measured in experimental rat models bearing osteosarcoma. Boron concentration was set to 15 ppm in soft tissue (experimental results) while skin was assumed to absorb 22.5 ppm, as BPA concentrates a factor 1.5 comparing to normal tissues [62].
The study of dosimetry in the patient was carried out with Python software [83], in particular NumPy[91]. The last is a fundamental package for scientific computing in Python. It is a Python library that provides a multidimensional array object, various derived objects (such as masked arrays and matrices), and an assortment of routines for fast operations on arrays, including mathematical operations, logic, shape manipulation, sorting, selection, I/O, discrete Fourier transforms, basic linear algebra, basic statistical operations, random simulation, and much more .
The first step is to load the functions that will be used.
The project IT_STARTS (an Innovative Toolkit to Simulate neuTron cApture theRapy irradiaTion and doSimetry), funded by INFN, develops a tool to calculate the dose with different models, superpose the photon isoeffective dose curves to the anatomy and build the Dose Volume Histograms (DVH) for the Region of Interest (ROI). The output of the treatment planning simulation was not analyzed with NCTPlan, but with this new analysis tool, built to integrate a new Treatment Planning System under development at INFN and CNEA. This represents a further advancement comparing to the past work published in [92]. To calculate the dose in ROIs, it is necessary to select the various masks of the tissues of interest. In the case of osteosarcoma, there are three masks: the tumour, or Gross Tumour Volume (GTV), the soft tissue between the tumour and the skin, and the skin. First, the medical images are loaded. An image is created with 125 pixels in z and 256 in x and y and the three bodies representing the knee tissues are

defined. These newly created masks are necessary to calculate the dose exclusively in the corresponding volume. Figures 3.4 show, starting from the left, the images with the three bodies overlapped to the medical images: the body that represents the whole anatomy, the tumour and finally the tissue under the skin.

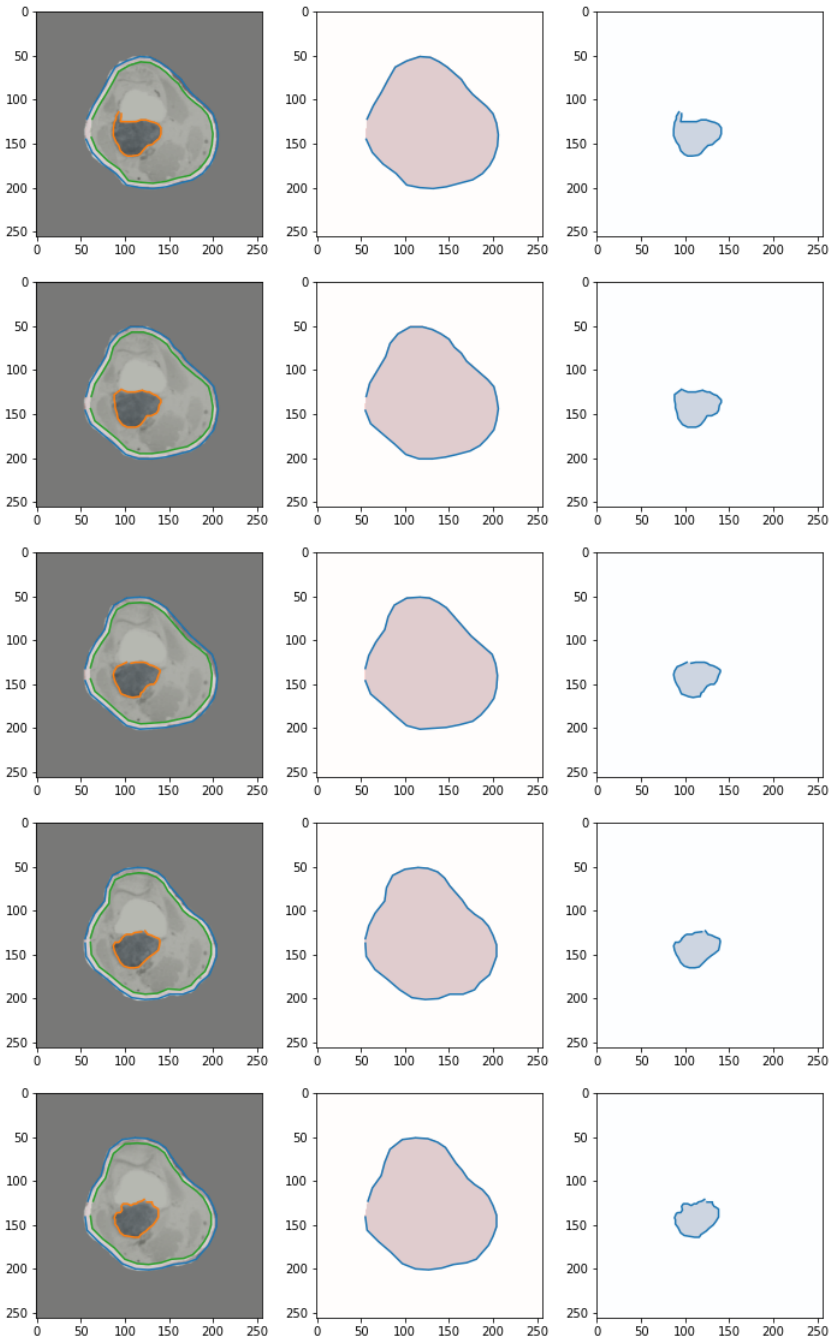

Figure 3.4: Five representative slices of the medical imaging of patient. Form left to right: the ROIs superimposed to the anatomy, the ROI of the tissue under the skin and the ROI of the tumour.

An input file for MCNP calculation was created with NCTPlan in which the volume of interest was voxelized using the lattice structure. The dose tally of the 4 components: boron, thermal and fast neutrons and photons were requested within each voxel. The output files were loaded into Numpy, the dose components of the two beams were added together,in this way the same weight is given to both beams: 50%-50%. The biological weighted dose with RBE/CBE factors and the photon isoeffective dose were calculated in the tumour via functions previously defined. It is not possible to calculate the isoeffective dose due to the lack of suiTable parameters for the skin model. For this reason, the experience gained in the clinical BNCT based on a prescription dose using the standard model and RBE/CBE factors was used as reference. The concentration of boron absorbed by the skin was set to 22.5 ppm and the RBE/CBE factors to 2.5,2.5,2.5,1 for thermal and fast neutron, boron and photons respectively as described in [92].
The boron concentration for the tumour has been set at 60 ppm, i.e. four times the boron concentration in healthy tissue (15 ppm), as measured in an experimental model of rat bearing osteosarcoma. The RBE/CBE factors for KERMA and absorbed dose are as in Table 3.6.
For the calculation of the photon isoeffective dose the radiobiological parameters obtained in section 3.2 were used (Tables 3.5 and 3.4, for KERMA and absorbed dose respectively).

Using the masks defined above, it is possible to calculate the dose released in tumour and skin. The weighted dose and the isoeffective dose were plotted in tumour for each z-direction of the beam fixed in a Cartesian plane where the two axes represent the x and y coordinates of the points.

Figures 3.5 represent, for three representative images, the biological weighted dose rate in the tumour (left) and in skin (right). For simplicity, only RBE/CBE dose is shown.

To prescribe the irradiation time, the maximum dose rate of biological weighted dose released to the skin was calculated. The required irradiation time is:

$$t_{irr} = \frac{22\,(Gy - E)}{Dose\ rate_{max}\,(Gy/min)}. \tag{3.5}$$

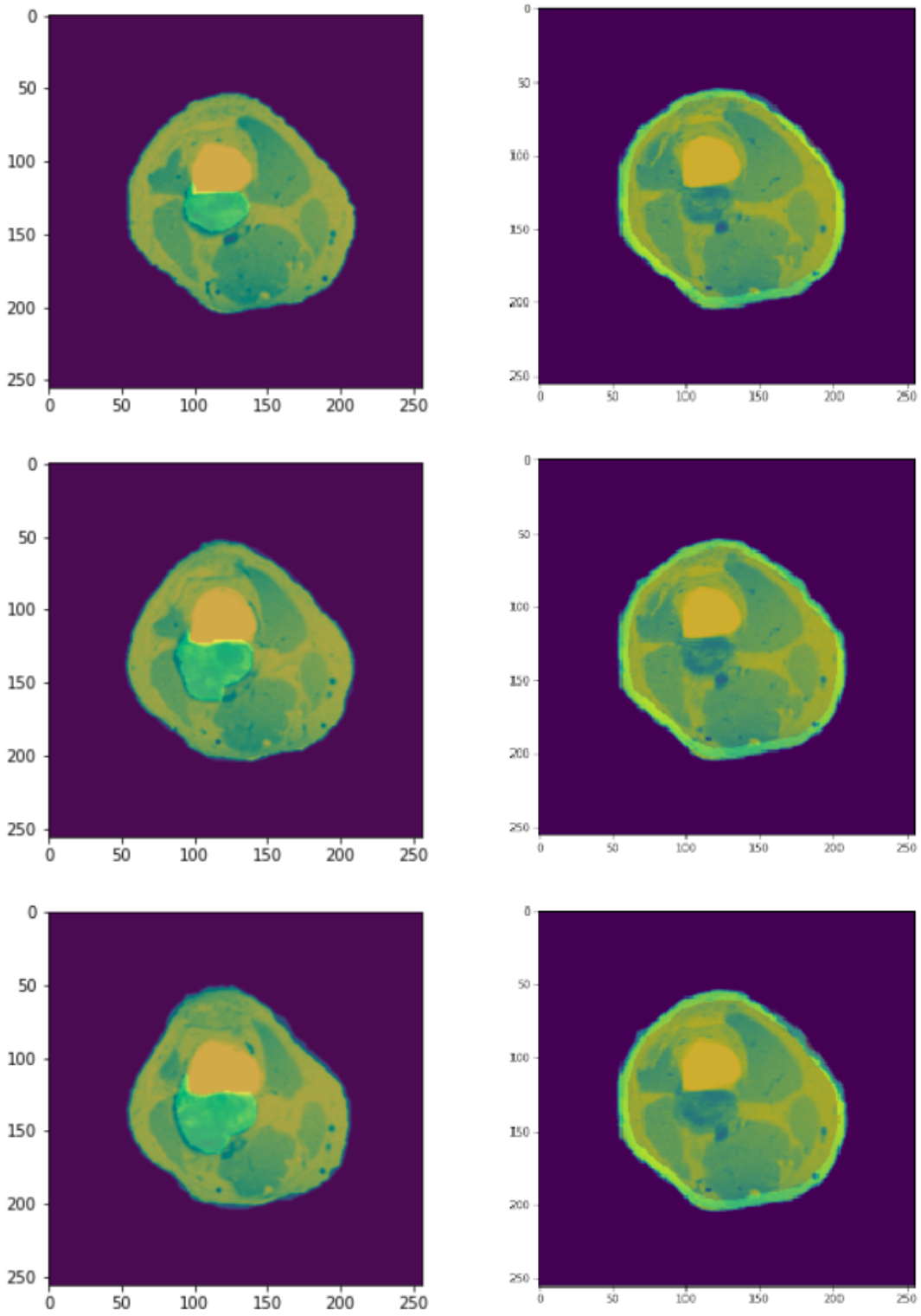


Figure 3.5: Left: weighted dose with RBE/CBE factors on tumour superimpose on the medical image of the patient. Right: weighted dose with RBE/CBE factors on skin superimpose on the medical image of the patient.

### 3.3.1 Simulation using an optimized neutron beam

In designing the beam for neutron therapy, the principal aim is to create a uniform distribution of thermal neutrons in the treated volume. This volume includes a margin around the tumour in the event that cancer cells have contaminated the surrounding healthy tissue.
Neutrons of energy greater than thermal slow down through elastic scattering interactions as they pass through hydrogen, which is contained in tissues. The result is an accumulation or broadening of the thermal neutron beam distribution.
Since boron is selectively targeted to the tumour, the need for complex adaptation of the spatial profile of the beam is less stringent than in other therapies. Boron selectivity also allows to treat a volume considerably larger than in other radiotherapy types, as the absorbed dose in normal tissue is lower than in tumour.
Collimating the neutron beam is necessary to preserve healthy peripheral organs or tissues, which may have some radiosensitivity or have absorbed some of the boron administered. This also applies to critical organs both inside and outside the treated volume. Therefore a careful selection of beam characteristics is extremely important. In treatment planning, beam position, aperture size and beam filtering options are simulated to optimise the dose to the tumour.
As explained in [85], some of the characteristics necessary in a BNCT facilities are

- High intensity to deliver the required dose in reasonable treatment times, which also means that the advantage of tumour-to-normal tissues concentration ratio can be exploited at most. Other beam parameters must be optimized, such as collimation and low contamination in thermal and fast energy. The beams optimal characteristics were described in the IAEA TecDoc-1223[114], used for many years as the guideline to design clinical BNCT beams.

- The neutron beam purity and energy spectrum should achieve a therapeutic ratio greater than unity of at least 9 cm in-depth, with the typical boron concentration ratios obtained.

- Well-collimated beams, with an accessible portion of the beamline near the patient, and a wide beam diameter are desirable. This will optimize tumor dose while preserving the rest of the body.

The beam used for simulations published in [92] was optimized for the treatment of the deep-seated tumour. However, for the reasons mentioned above, a clinical beam must comply with other constraints dealing with safety and radioprotection. Further optimization of that beam towards the implementation of an accelerator-based clinical

facility has been described in [86]. This beam has proved a *therapeutic potential* compatible with the FIR-1 beam (used to treat patients in Finland) and the best *suitability* concerning the sparing of peripheral organs. This beam also proved to guarantee safety requirements about air and materials induced activation [115]. The availability of the new beam design prompted the treatment planning simulation of the same clinical case to explore the differences of a more realistic beam compared with a beam that was only optimized for its dosimetric performance in the tumour.

### 3.3.2 Dose Volume Histograms

In order to graphically summarise the simulated distribution of dose delivered within a patient's volume of interest, a cumulative dose-volume frequency distribution plot is used: dose volume histogram, DVH. DVHs are useful tools for comparing alternative treatment plans for a patient. They show dose uniformity in the target volume and possible hot spots in adjacent organs or normal tissues. However, because of the loss of positional information in the target volume, it should not be the sole criterion for evaluating a treatment plan. Dosimetry can be used as the input to estimate the probability of tumour control (TCP) and the probability of normal tissue complication (NTCP).

In the Table 3.7 the values of the maximum and minimum dose rates calculated both as KERMA and absorbed dose with the two formalisms are reported for the previous beam.
Figures 3.9 shows for the old beam the DVH in the skin obtained by setting 22 Gy as the maximum dose that the skin can receive. Figure 3.6 shows the DVHs of the old beam of the dose delivered to the tumour for the two formalisms: top image with RBE factors and bottom image with isoeffective dose for both KERMA (right) and absorbed dose (left). Figures 3.7 and 3.8 describe the overlap of the DVH for the skin and the tumour with the two formalisms.

For the new beam we only calculated the isoeffective dose model using the parameters obtained with the absorbed dose, i.e the most accurate setting available. Table 3.8 reports the photon iso-effective dose obtained with the absorbed dose parameters. The DVHs shown in the Figures 3.9 and 3.10 are obtained with the new beam. The first Figure represents DVH in the skin calculated as a function of the weighted dose. The second one depicts the DVH in the tumour as a function of absorbed dose calculated with the photon isoeffective dose formalism again for KERMA and absorbed dose. The last one is the overlap of the two graphs previously described.

| | **Old beam** | |
|---|---|---|
| | ***Absorbed dose*** | ***KERMA*** |
| *Skin* | $Dose\,rate_{max} = 0.33\,Gy/min$ | |
| *Tumour* | ***Weighted dose*** | ***Weighted dose*** |
| | Dose $_{\max}$=113.23 Gy_Eq | $\text{Dose}_{\max}$=95.72 Gy_Eq |
| | Dose $_{\min}$=84.67 Gy_Eq | $\text{Dose}_{\min}$= 71.67 Gy_Eq |
| | ***Iso-effective dose*** | ***Iso-effective dose*** |
| | Dose $_{\max}$=30.33 $\text{Gy}_{iso}$ | $\text{Dose}_{\max}$=30.70 $\text{Gy}_{iso}$ |
| | Dose $_{\min}$=25.96 $\text{Gy}_{iso}$ | $\text{Dose}_{\min}$=26.28 $\text{Gy}_{iso}$ |
| $t_{irr}$ | $44.73\,min$ | |

Table 3.7: Dose rate maximum and minimum for weighted dose and iso-effective dose calculated as KERMA and absorbed dose in the skin and tumour for the old beam.

| | **New beam** |
|---|---|
| | ***Absorbed dose*** |
| *Skin* | $Dose\,rate_{max} = 0.49\,Gy/min$ |
| *Tumour* | ***Iso-effective dose*** |
| | Dose $_{\max}$=28.13 $\text{Gy}_{iso}$ |
| | Dose $_{\min}$=23.90 $\text{Gy}_{iso}$ |
| $t_{irr}$ | $65.04\,min$ |

Table 3.8: Dose rate maximum and minimum for weighted dose and iso-effective dose calculated as KERMA and absorbed dose in the skin and tumour for the new beam.

| | *New beam* |
|---|---|
| | ***Absorbed dose*** |
| *Skin* | $Dose\,rate_{max} = 0.49 Gy/min$ |
| | **Isoeffective dose** |
| Tomour | $Dose_{max} = 28.13\,Gy_{iso}$ |
| | $Dose_{min} = 23.90\,Gy_{iso}$ |
| $t_{irr}$ | 65.04 min |

Table 3.9: Dose-volume histogram in skin calculated with RBE-weighted dose for the old beam. In the left DVH as a function on dose rate and in the right of the dose.

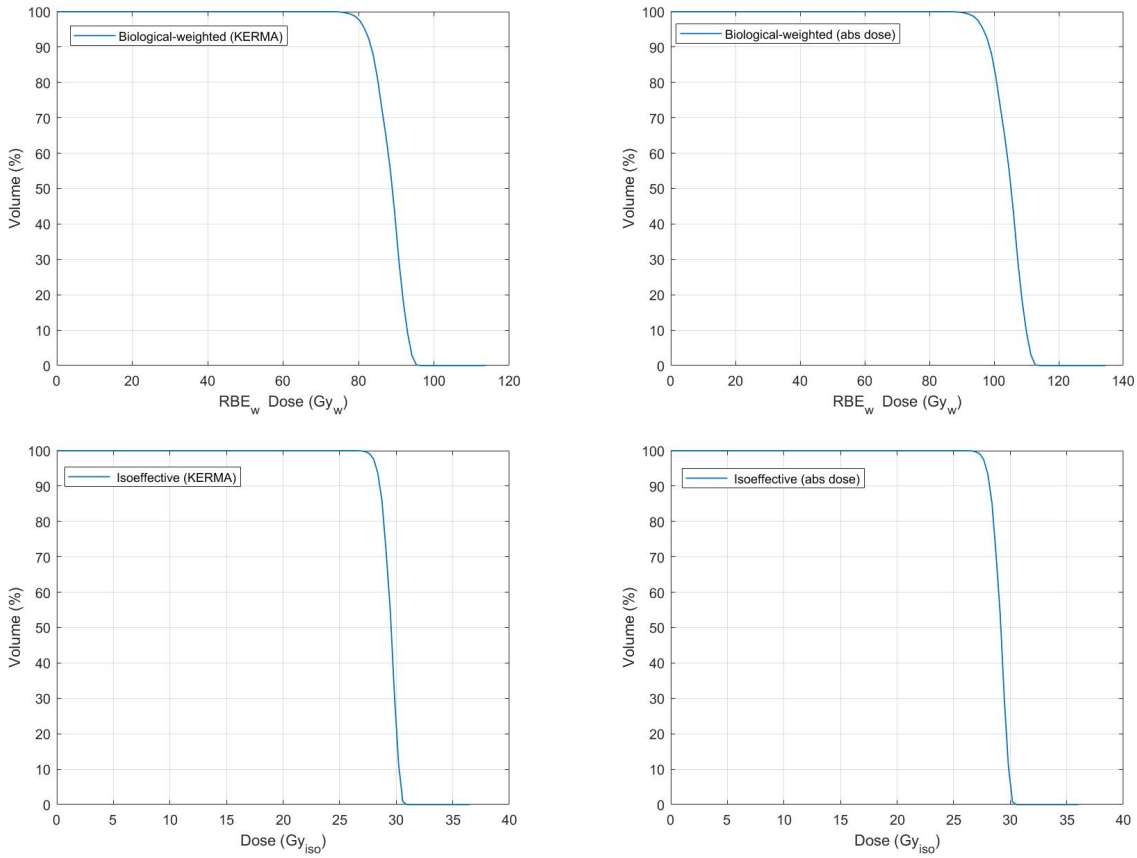


Figure 3.6: Dose-volume histogram for 60 ppm in tumor with the old beam. In the top RBE-weighted dose and in the botton photon isoeffective dose. In the left the results for KERMA-based and in the right for aborbed dose.

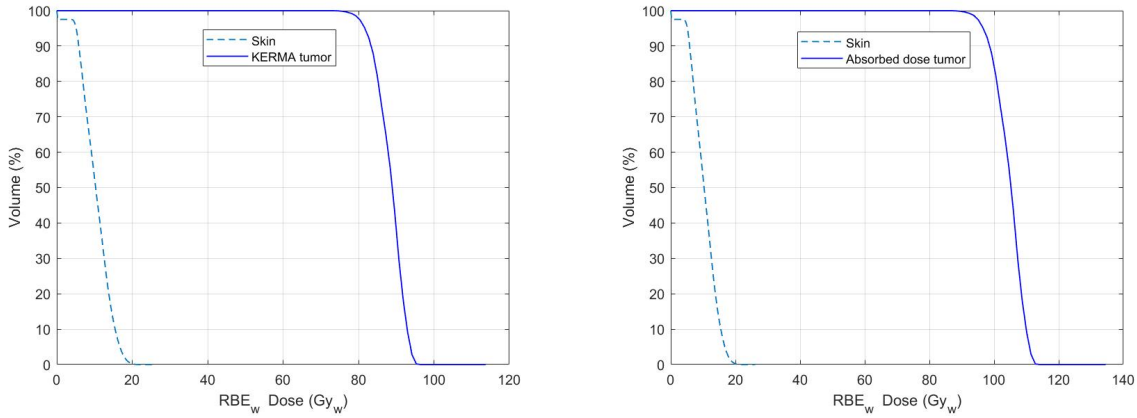


Figure 3.7: Dose-volume histogram for 60 ppm in tumor and skin with the RBE-weighted dose In the left the results for KERMA-based and in the right for aborbed dose.

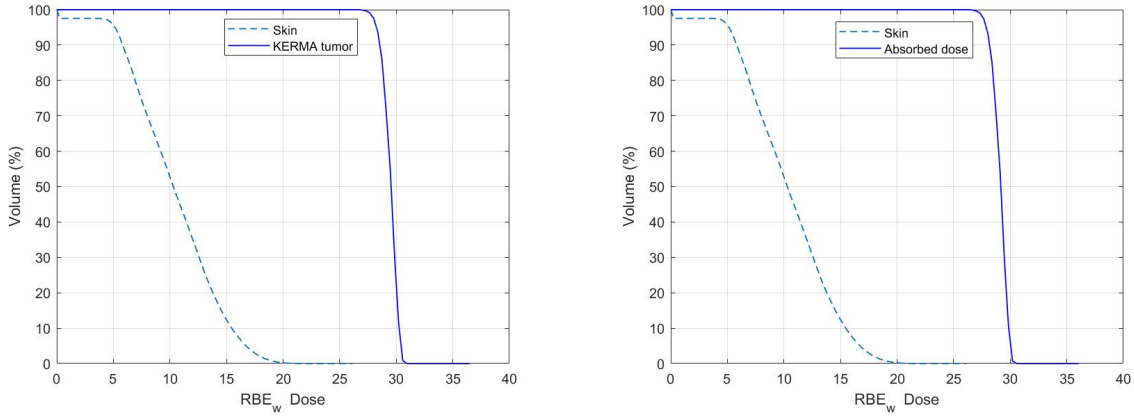


Figure 3.8: Dose-volume histogram for 60 ppm in tumor and skin with the photon iso effective dose In the left the results for KERMA-based and in the right for aborbed dose.

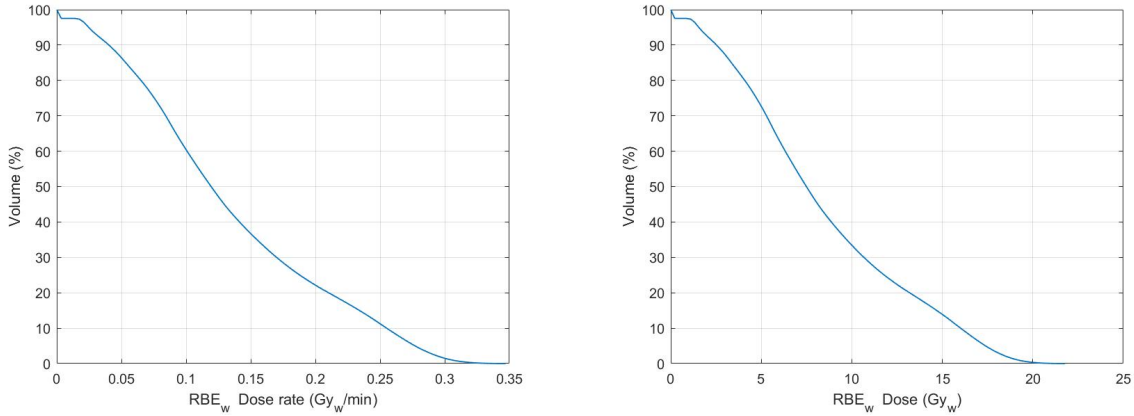


Figure 3.9: Dose-volume histogram in skin calculated with RBE-weighted dose for the new beeam. In the left DVH as a function on dose rate and in the right of the dose.

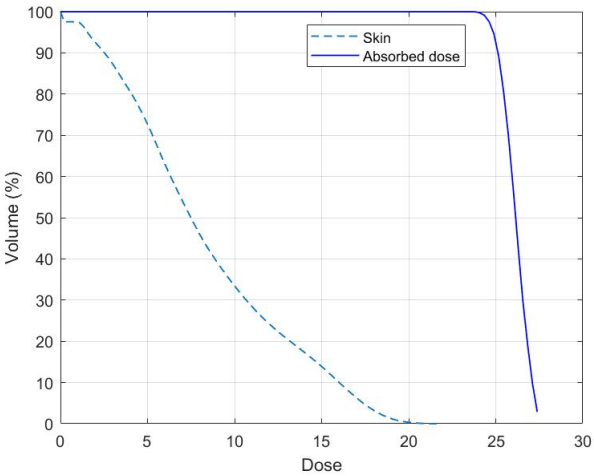


Figure 3.10: Dose-volume histogram for 60 ppm in tumor and skin with the photon iso effective dose.

A difference between the dose calculated using the parameters of the fit in the cases of KERMA and absorbed dose can be seen in Table 3.7. Albeit the difference between KERMA and dose in cells is not negligible, the isoeffective dose values are comparable. This is due to the fact that osteosarcoma absorbs a high boron concentration (60ppm), thus the BNCT dose component is about 80% . The remaining 20% is composed of a photon component (10%) and a neutron component (10%). Even if there is a change in one of the two components, there is no appreciable modification to the total dose. More pronounced differences can be appreciated in the biological weighted doses, where the minimum dose delivered in tumour is underestimated of about 10 Gy_Eq if the parameters are obtained with KERMA. Assuming the parameters of the cell survival curve with KERMA, when the absorbed dose should be calculated in detail, the dose is overestimated in the patient. As already pointed out in previous publications, the photon iso-effective dose in tumour is lower than those obtained with the standard RBE-weighted model. Doses obtained with this model are more reliable to assess the clinical outcome of patients, as demonstrated for retrospective analysis of melanoma, brain and head and neck treatments. For this reason, in the next Chapter, only the photon isoeffective dose model will be used for in-patient dosimetry.

A clinical beam has to comply with a number of constraints as explained in subsection 3.3.1, regarding not only its capacity to treat the tumour, but also the sparing of peripheral organs and radiation protection (e.g. activation of air or room materials). In order to improve these parameters, a more collimated beam has been designed, comparing to the first version, used to simulate osteosarcoma treatment. A highly collimated neutron beam helps to minimize normal tissue dose and it is associated with increased beam penetration that can improve coverage for deep-seated tumors. On the other hand, improved collimation may affect the intensity and the spectrum of the beam. From Tables 3.7 and 3.8 it can be seen that the maximum and minimum values of dose in the tumour differ by 7%. The minimum dose to the tumour decreases of less than 3 Gy(IsoE) when the new beam is considered. This is a necessary trade-off between therapeutic potential and safety for the patients and medical staff, that must be considered when designing a clinical BNCT facility.

# Chapter 4

# BNCT of Head and Neck cancer

The head and neck tumours are a group of malignant neoplasms arising in the tissues of the upper aerodigestive tract (lips, tongue, oral cavity, throat and larynx or voice organ) or from the nasal and sinoparanasal cavities. They originate mainly from the squamous cells lining these tracts and cavities, for this reason they are called carcinomas or squamous cells [69, 70].
Tobacco and alcohol are the main factors that may increase the risk of developing head and neck cancer; they may especially affect the oral cavity, larynx, oropharynx and hypopharynx [71].
Out of the total worldwide head and neck tumors 75 % are due to these factors.
Infection with the human papilloma virus may also be a cause for the development of this type of cancer, particularly that of the oropharynx involving the tonsils and the base of the tongue [73].
Oral hygiene and exposure to radiation or certain products common in heavy industry have been recognised as possible risk factors [74].
Head and neck cancer is on average the seventh most common cancer worldwide: fifth most common among men and twelfth most common among women. In 2018, there were an estimated 888000 new cases, 70 % of which originated in developing countries, and 453000 deaths [75].
Radiotherapy, surgery and chemotherapy are the three main types of treatment that promote tumour control.
The appropriate treatment depends on the location of the tumour and the state of the lesion, as we are dealing with a complex set of diseases affecting different anatomical structures.
In general, the treatment involves both radiotherapy and surgery, while chemotherapy is used as an adjunctive or adjuvant treatment.
In the treatment of patients with squamous cell carcinoma of the head and neck, local

control of the disease is crucial since there is a high probability of recurrence at the site of the primary tumour or in regional lymph nodes. In addition, patients may develop metastatic cancer either as a consequence of the spread of the primary tumour before initial diagnosis or from recurrent or treatment-resistant locoregional disease. Both of these clinical scenarios represent extremely complex management problems [76]. Despite advances in conventional therapies, disease recurrence occurs in more than 50 % of cases, after treatment of an inoperable tumour, due to intrinsic or acquired insensitivity to radiotherapy and/or chemotherapy, or because the tumour produces metastases in distant sites [76].

If the patient has already received radiation treatment of the primary tumour, this will limit the treatment of the recurrence, as the irradiation will be limited by the dose previously received by the healthy tissues surrounding the primary lesion.

In this clinical scenario, BNCT presents itself as an alternative with a double therapeutic advantage. First, the selectivity of the borated compound ensures that dose deposition occurs mainly in tumour cells. Thus, healthy organs are not at risk of receiving high doses; thus the limitation of previous irradiation may be less stringent. The second advantage is that the tumour cells that infiltrate healthy peripheral tissue will also receive a specific high dose, thus decreasing the probability of future recurrences.

In 2001, a patient with recurrent parotid gland tumor, after standard therapies, was treated with BNCT at the Kyoto University Research Reactor Institute (KURRI). It was the first such attempt worldwide [78]. In this first case, locoregional control of the tumour was achieved for 7 years until the patient died of inter-current disease. This promising initial result prompted clinical trials of BNCT for head and neck cancer in Japan and Finland [77, 80].

In 2004, a group of Japanese scientists published the first studies on the use of BNCT for the treatment of head and neck cancers [78]. These studies involved 26 patients with very advanced tumours with no possibilities of known treatments. Out of the total cases, 12 showed complete regression, 10 showed partial regression and only 3 cases progressed without any observable effect. Median survival was 13.6 months and 24% of cases survived 6 years or more.

Between 2003 and 2012 one of the largest clinical trials of BNCT for head and neck treatment was conducted in the Central Hospital of the University of Hospital of Helsinki, using the neutron facility located in Espoo, Finland. Out of the total 117 cases treated during phase I/II clinical trials, 79 patients corresponded to cases of inoperable head and neck cancer [77]. The latter group of patients mostly received two applications of BNCT separated by an interval of 3 to 6 weeks. Each treatment application consisted of 2 hours of intravenous administration of BPA (400 mg/kg) followed by irradiation with one or two

converging neutron fields, with an average exposure to each beam of about 20 minutes. All patients were irradiated at the Finnish BNCT facility at the FiR1 reactor, in Espoo. FiR1 is a 250 kW TRIGA Mark II research reactor, modified to obtain a neutron beam whose spectral characteristics are ideal for BNCT: it is a purely epithermal beam with very low contamination of fast neutrons and photons [79].
Among the 69 treated patients, 25 complete and 22 partial remissions were recorded, while in 17 of them the disease stabilised and in 5 the disease continued to progress [79]. The most common adverse effects were oral mucositis, oral pain and fatigue, all of which were clinically controllable. Three patients lived without evidence of disease for 5.5, 7.8 and 10.3 years after treatment. The median survival was 10 months and 21% of cases lived 2 or more years [77].

This part of the thesis addresses the treatment planning of a patient affected by an adenocystic tumour of the salivary gland, to study the therapeutic potential of the beam described in the previous Chapter in this kind of tumour. Also in this case, the difference between KERMA and absorbed dose in the radiobiological experiments carried out to obtain the parameters have been explored. For this study, a radiobiological figure of merit related to the clinical outcome, namely the Tumour Control probability (TCP), was used to condense the three dimensional dose distribution into a value representing the capacity of BNCT to obtain a relevant clinical result. The effect of KERMA and dose calculation in the cell-survival curves was explored also for the TCP calculation. Finally, TCP calculated using the radiobiological experiments conducted *in vitro* in Pavia has been compared to the one calculated using radiobiological experiments *in vivo* conducted in Buenos Aires. This topic represents an important issue in BNCT clinical dosimetry, i.e. the effect of the radiobiological model chosen to convert absorbed dose into photon-equivalent units.

## 4.1 Radiobiological experimental set up

Two head and neck cancer cell lines coming from Finland patients (UT-SCC-16A and UT-SCC-2) are treated with the same protocol that had been used for rat osteosarcoma cells line. The only thing that varies is the culture medium, which consists of

- Amen high glucose 500 ml;

- FBS 50 ml (inactivated by keeping it in a 56 °C water bath for 30');

- PEN/STREP + GLUT. 5 ml (2.5 ml + 2.5 ml);

- NEAA 1x 5 ml.

This change does not have any impact in the detailed study of the particle transport described in Chapter 2.

An important difference with respect to the osteosrcoma study is that the UT-SCC are a primary cell lines.

Primary cells are isolated directly from human or animal tissue using enzymatic or mechanical methods. Once isolated, they are placed in an artificial environment in plastic or glass containers supported by a specialised medium containing essential nutrients and growth factors to support proliferation. There are two types of primary cells: adherent or suspension.

Although they usually have a limited lifespan, they can offer many advantages over immortalised cell lines, especially because they allow to study the donors and not just the cell type. However, there are various factors to be taken into account when constructing an experimental model such as age, medical history, race and gender. With a growing trend towards personalised medicine, biological model representing donor variability and tissue complexity can only be achieved with the use of primary cells. The donor characteristics are in fact difficult to replicate with cell lines that are very systematic and uniform in nature and do not capture the true diversity of a living tissue.

As mentioned in the previous chapter, an immortalised or continuous cell line has acquired the ability to proliferate indefinitely, through genetic mutations or artificial modifications. On the contrary, a finished cell line can be sub-cultured for 20-80 passages, after which it suffers senescence as those present in the living body. For this reason, immortalized cell lines are preferably used as they are easier to handle and widely published, albeit less relevant concerning the characteristics of the original tissue from which they were isolated.

## 4.2 Determination of cell survival curve

The cell survival curves are obtained using the same methodology as for the the rat osteosarcoma cell line, considering some assumptions.

In figure 4.1 the blue points represent the experimental survival data measured in Pavia for photon irradiation at the San Matteo Polyclinic, using the Best Theratronics equipment (Raycell Mk2 X-ray blood irradiator). The X-Ray irradiator is equipped with two photon beams of average energy between 60 and 80 keV. The blue curve is the fit corresponding to these data. While interesting for radiobiological reasons, these data cannot be taken as a reference radiation curve for the photon isoeffective dose calculation. In fact, the final goal is to correlate the effects of BNCT to those of a typical photon-therapy beam. In this sense, Co-60 gammas are a suiTable choice because their radiobiological effects are similar to those of a radiotherapy LINAC. Moreover, the gamma component present in BNCT

mixed field has higher average energy (around 2 MeV). Thus, it would not be adequate to use the parameters obtained with photons of 60-80 keV, to represent the biological effect of the gamma component of BNCT as had been done in section 3.2. For these reasons, we opted to use as the references the other curves shown in Figure, which are the linear quadratic fits of the survivals for the cell lines of interest, obtained in previous experiments carried at Turku University Hospital, Finland. Mentioned irradiation experiments were performed with the photon beam of 6 MV nominal energy from the Varian Clinac linear accelerator at a dose rate of 3 Gy $min^{-1}$. The three curves represent the two cell lines of head and neck cancer, irradiated in Finland and the fit of the reference radiation with the data obtained in Pavia.
The curves follow almost a linear trend, the initial shoulder is almost missing, due to the fact that the $\beta$ parameter is a hundred times smaller than the $\alpha$.
The radiobiological parameters for the reference radiation were taken from these data.

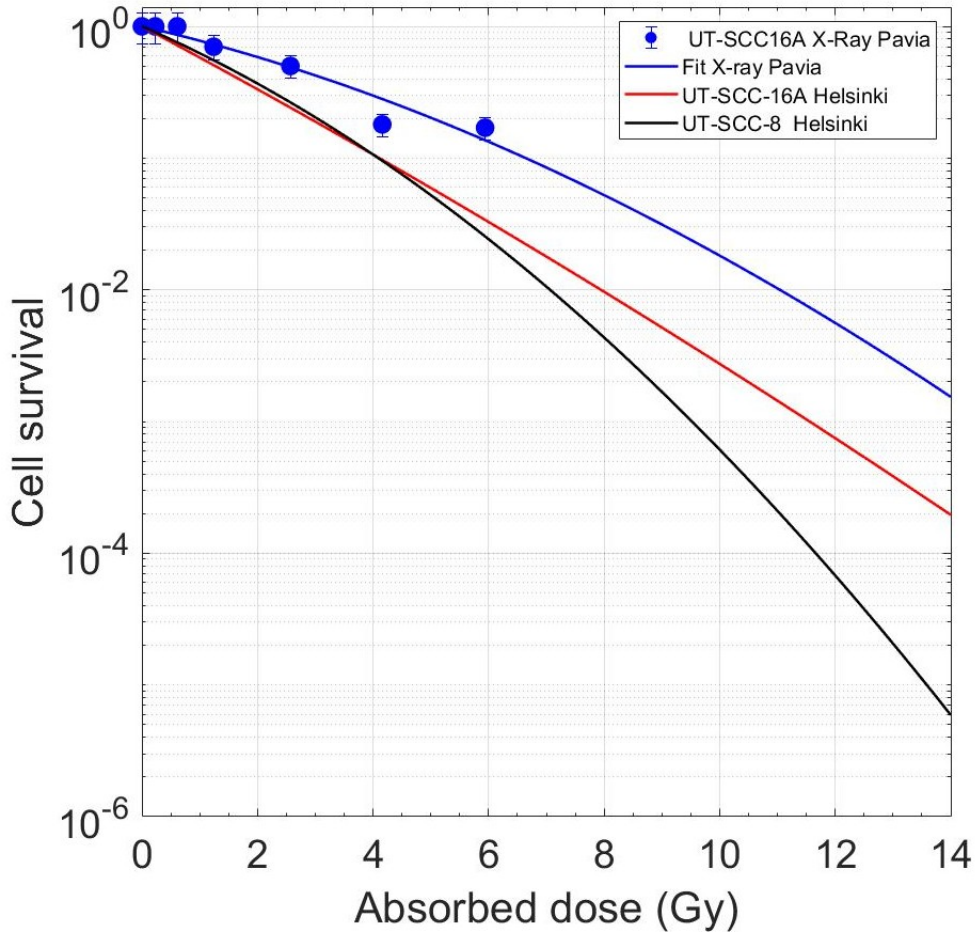


Figure 4.1: Surviving fraction for the X-Ray irradiation carried out in Pavia (X-ray irradiator) and fit of the survival curves obtained with a LINAC photon beam in Finland.

Since the $\beta$ parameter is small and photons are a low-LET radiation, i.e. radiation that

can cause lethal damage but most of the action is by combination of sublethal damage, then there will be few combinations of sublethal damage. Therefore, these type of cells when irradiated with photons behave in such a way that they die directly from lethal damage, represented in the linear quadratic model by the linear term $\alpha$.
Considering that gamma radiation has a $\beta$ parameter 100 times smaller than the $\alpha$ parameter, and charged particles generated in the interaction of neutrons in cells, are high-LET radiation, we set

$$\beta_n = \beta_B = 0.$$

Therefore, two free parameters remain to be determined instead of three as in the case of osteosarcoma:

$$\alpha_n \text{ and } \alpha_B.$$

The repair kinetic is assumed to be correctly described by a bi-exponential decay with fast and slow characteristic repair times $t_{0f}$ and $t_{0s}$, independent of the LET. The characteristic repair times fast and slow and the proportions of sublesions repaired by the two kinetics for low and high-LET radiations are given in the Table 4.1, following the results reported by Schmid et al. (2010) for a squamous carcinoma cell line.

| | | SLD repair (%) | |
|---|---|---|---|
| | Characteristic repair times | Low LET | High LET |
| $t_{0f}$ | $24/ln2\ (min)$ | 0.53 | 0.2 |
| $t_{0s}$ | $14/ln2\ (hours)$ | 0.47 | 0.8 |

Table 4.1: Parameters used for the calculation of the Lea-Catcheside time factors $G$ in the survival models.

Two cell lines have been irradiated in Pavia. Figures 4.2 show the fit of the cell survival as a function of the absorbed dose for first cell line (UT-SCC-16A), in two different situations.
The first one (left) considers all the available experimental points and the second one (right) excludes the last two points of the BNCT curve since they were obtained at a different time than the first ones. This temporal difference is important as the primary cell line has been obtained via cells of a patient. These cells behave like those of the human body and therefore the results of the experiment are influenced by the cells age and the number of passages the cells undergo. In fact, the survival values obtained for these points suggest a different radiosensitivity. Results show that a more resistant cell population had been selected. We preferred to choose a coherent set of points, corresponding to the same experiments.

The subset of chosen points plotted against absorbed dose were fitted as discussed above and the obtained parameters listed in Table 4.2.

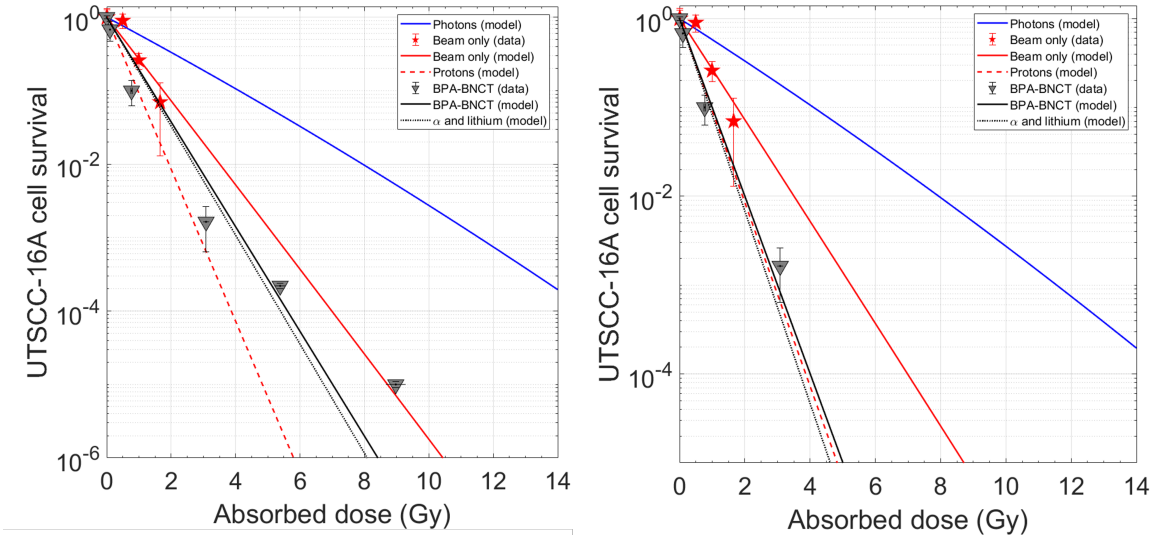


Figure 4.2: Survival curves as a function of the absorbed dose for the first line. Left: all experimental points obtained at different times, Right: selection of the set of points obtained in only one experiment.

| **Absorbed dose** | | |
|---|---|---|
| | Parameters of survival models | |
| | Alpha ($Gy^{-1}$) | Beta ($Gy^{-1}$) |
| $^{60}Co$ source Reference radiation | 0.54 | 0.005 |
| Beam gamma photon | 0.54 | 0.005 |
| Neutrons | 2.38±0.56 | 0 |
| Boron (BPA) | 2.49±0.41 | 0 |

Table 4.2: The parameters obtained from the fit of the survival curve for the first tested cell line.

The same data were plotted against the the KERMA values, the fit is shown in figure 4.3. The radiobiological parameters obtained from the fit are given in the Table 4.3.

Figure 4.4 shows the survival curve for the second cell line obtained with the same methodology as for the first cell line. It can be seen that the beam only and BNCT curves (in red and black) overlap with the reference curve (in blue). These results appear not consistent as high-LET dose due to BNCT causes higher damages to cells than low-LET photons for the same dose. We concluded that something had happened changing the conditions of the cells during the experiments: this line unfortunately cannot be used to compare photon-equivalent in-patient dosimetry. For this reason, the experiment will be

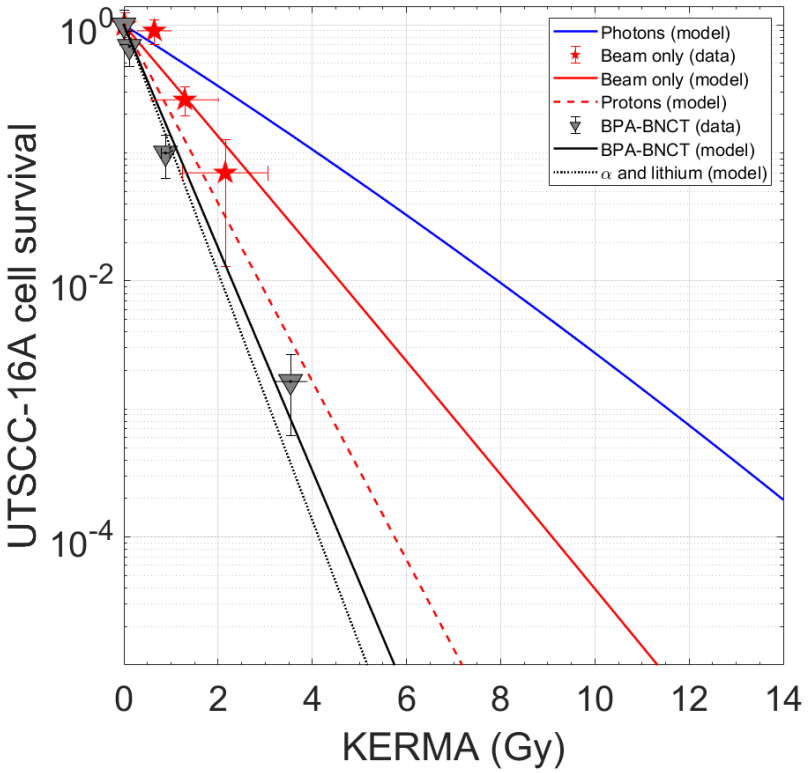


Figure 4.3: Survival curve as a function of the KERMA for the first line.

| **KERMA** | | |
|---|---|---|
| | Parameters of survival models | |
| | Alpha ($Gy^{-1}$) | Beta ($Gy^{-1}$) |
| $^{60}Co$ source<br>Reference radiation | 0.54 | 0.005 |
| Beam gamma photon | 0.54 | 0.005 |
| Neutrons | 1.6±0.4 | 0 |
| Boron (BPA) | 2.2±0.4 | 0 |

Table 4.3: The biological parameters for the survival curve obtained with KERMA calculation.

repeated as soon as possible; in this thesis the treatment plan has been calculated using the parameters of the first cell line only.

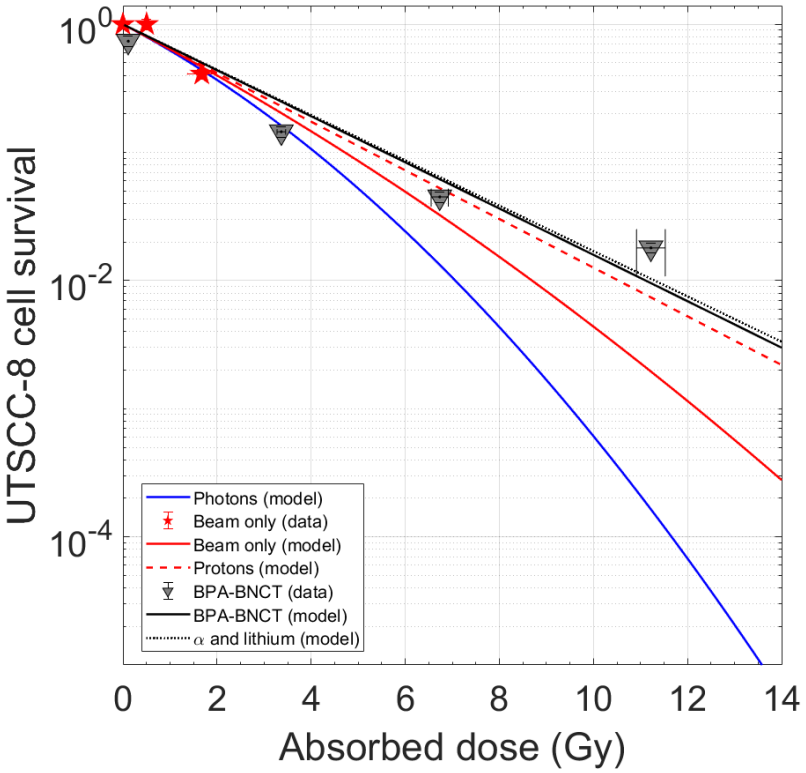


Figure 4.4: Survival curve as a function of the absorbed dose for the second line.

## 4.3 Treatment planning

The DVH for the Head and Neck case were obtained with the photon isoeffective dose model, with the parameters from *in vitro* studies (reported above) and from *in vivo* results. The latter were previously obtained in CNEA, Buenos Aires, from dose-response curves derived from irradiating exophytic tumors in the hamsters check pouch with photons and BNCT. These curves representing the rate of tumor control as a function of the dose, allow determining the parameters of the model. The *in vivo* hamster oral cheek cancer model is considered representative of human oral cancer [102, 103, 104, 105].

### 4.3.1 Tumour control probability models for the derivation of the photon isoeffective dose from *in vivo* experiments.

The treatment planning simulation gives a three-dimensional distribution of dose in the tumour and in the surrounding tissues. It is possible to use radiobiological figures of merit

which summarize this distribution into one variable, estimating the probability to control the lesions. The probability of tumour control is the probability that the tumour response is complete, i.e. that the initial volume of the lesion is reduced by 100% compared with the pre-treatment assessment by medical imaging or clinical inspection. This probability depends on two factors: tumour size and dose administered during treatment.
In 2017, a work by Gonzalez et al. [101] presented tumour control probability models for treatments with photons ($TCP_R$) and for treatments with mixed radiation fields such as BNCT (TCP). These models, valid for uniform dose distributions, take into account the repair of sublethal lesions and the synergistic interaction between the main components of the BNCT dose. The introduced models were used to fit dose-response data obtained from the *in vivo* oral cancer model in the hamsters check pouch. As explained for the case of cell survival, the parameters for photon and BNCT curves were obtained by linear minimization methods. Following the same reasoning mentioned in section 1.3, the photon isoeffective dose model was derived equating the TCP expressions for photons and for BNCT.

| | TCP | |
|---|---|---|
| | $c_1 = 22 \pm 19$ | $c_2 = 0.33 \pm 0.09$ |
| | $\alpha\,(Gy^{-1})$ | $\beta\,(Gy^{-2})$ |
| $^{60}Co$ source<br>Reference radiation | 0.029±0.008 | 0.0029±0.0008 |
| Beam gamma photon | 0.029±0.008 | 0.0029±0.0008 |
| Neutrons | 0.34±0.03 | $(1.24 \pm 2.2)10^{-5}$ |
| Boron (L-BPA-F) | 0.33±0.03 | $(1.22 \pm 3.1)10^{-5}$ |

Table 4.4: Radiobiological parameters of the TCP model based on *in-vivo* oral cancer.

As mentioned above, the oral cancer model in the hamster cheek pouch is a widely accepted model of oral cancer. Then, the photon isoeffective dose model fed with the parameters from the *in vivo* experiments were proposed to estimate photon isoeffective doses for tumours in the oral cavity or head and neck treated with BNCT. Table 4.4 reports the parameters used for the isoeffective dose calculation.

### 4.3.2 Tumour control probability model for HN cancer in humans

In conventional radiotherapy it is possible to deliver highly uniform doses to the tumour tissue. Therefore, the average absorbed dose is a representative quantity of the dose distribution in the tumour volume and thus, the majority of TCP models do not take into account inhomogeneities.
On the other hand, the dose distribution in BNCT varies considerably with the depth of

the treated tumour volume. Typically, head and neck tumours treated with BNCT are large, ranging from 20 $cm^3$ to 400 $cm^3$ [106, 108, 107]. Differences of the order of 20% between the maximum and minimum dose values are typical in these tumours. In these cases, the TCP calculated with the mean dose would not lead to a reliable result and thus, the models must be modified.
The theory developed in the equivalent subvolume model [109] can be applied to include non-homogeneous dose distributions to TCP models. Given a uniform absorbed dose $D$, and a tumour control probability ($TCP$) defined as:

$$TCP(v, D) = e^{(c_1 v^{c_2} S(D))}, \tag{4.1}$$

where $v$ is the tumour volume in $cm^3$, $c_1$ and $c_2$ are parameters modulating its effect on the probability of local control, and $S(D)$ the cell survival, the subvolume equivalent model applied to equation 4.1 gives

$$TCP_T = e^{-c_1 v^{c_2} \left(\int_T S(D(x)^{1/c_2} dx/v\right)^{c_2}}, \tag{4.2}$$

where $D(x)$ represents the dose in the subvolume centred at the x point.

A TCP model for non-uniform single-fraction photon doses was constructed based on the rate of complete responses reported by Rwigema et al. [116] for a large number of patients all with recurrent squamous cell carcinoma of the head and neck [117]. First, reported fractionated doses were converted to single fraction values using the LQ model and the alpha/beta of 10 Gy suggested in mentioned publication. Assuming that the TCP is correctly described by Eq. 4.1, the parameters of the model were obtained by non-linear minimization method. The resulting TCP model for HN in humans corresponds to single-fraction uniform photon doses. Then, applying the subvolume equivalent model [109], the final expression for non-uniform distributions was obtained.

### 4.3.3 Clinical case

The treatment planning was simulated for a patient with an adenocystic carcinoma of the salivary glands, with a volume of 57.4 $cm^3$. The position of the beams was optimized to maximize the dose to tumour while sparing the normal tissues, see Figure 4.5. The treatment was simulated using the protocol adopted by Finland group consisting in two BNCT applications, the second generally 20 days after the first, using two fields each. Boron concentration was also taken from the Finland clinical experience in Head and Neck cancer, with administration of 350 mg of BPA per kg of body weight, two hours before the irradiation. Concentration values are listed in Table 4.5.

| Tissue | $^{10}B$ concentration [ppm] |
|---|---|
| Brain, optic nerve, eye | 15 |
| skin | 22.5 |
| mucosa | 30 |
| tumor | 52.5 |

Table 4.5: $^{10}B$ concentration values assumed in tissues.

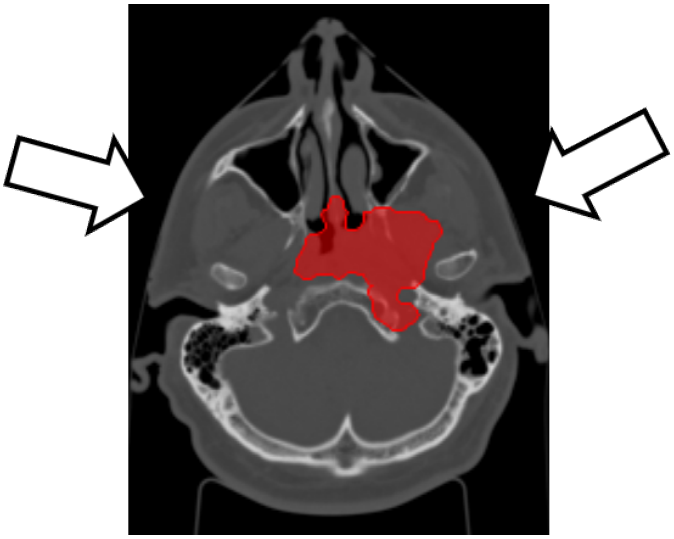

Figure 4.5: Neutron beam-port positions for the two BNCT applications.

In this case the dose-limiting organ is the mucosa. It is the organ most at risk since it absorbs twice the concentration of boron than other tissues. As mentioned in the section 4.3.1, the limiting adverse effect is oral mucositis of grade 3 or higher. According to the clinical experience en Finland, the dose prescription was assessed limiting the maximum dose in the mucosa to 6 Gy.

Fugure 4.6 shows two medical images of the patient with the isoeffective dose distribution superimposed over the anatomy.

Based on the obtained irradiation time, the cumulative dose volume histogram in the tumor (GTV) was calculated. The DVHs were obtained with the isoeffective dose model and taking into account three scenarios for the radiobiological parameters used in the model: the parameters of the *in-vitro* experiments (Table 4.7 for absorbed dose and Table 4.8 for KERMA) and those derived from the *in-vivo* cancer model [101] (Table 4.9). The DVHs for these scenarios are shown in Figures 4.7, 4.8 and 4.9 respectively.

Table 4.6 lists the maximum and minimum dose delivered to patients in the three calculation scenarios. Minimum dose is 25% higher if calculated using cell survival with absorbed dose than minimum dose obtained with KERMA and animal model. Maximum

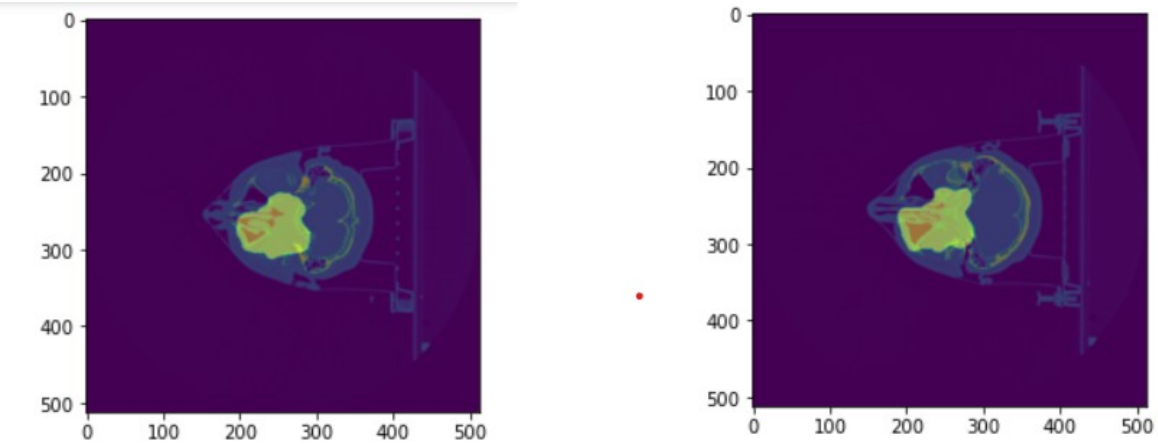


Figure 4.6: Photon isoeffective dose superimposed in two of the medical images of the patient.

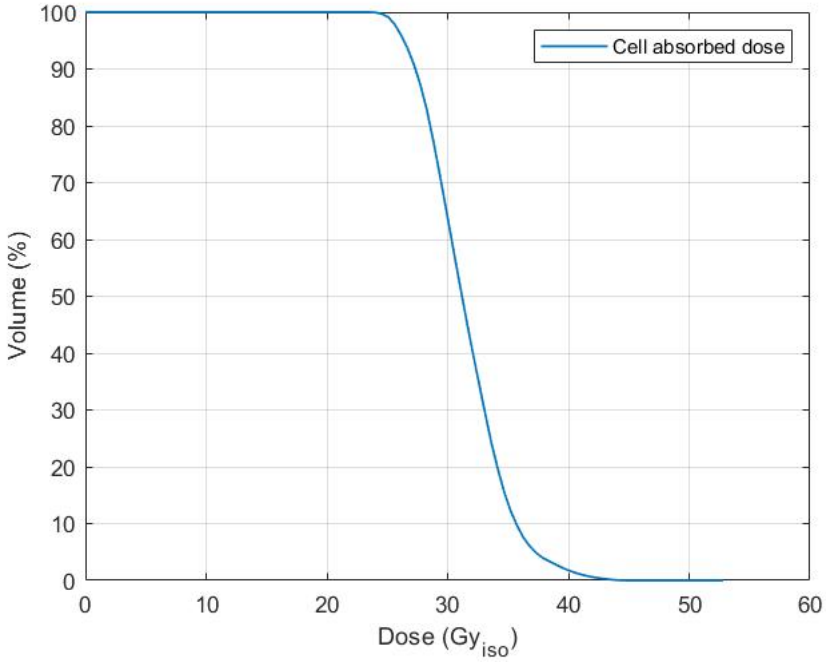


Figure 4.7: DVH of the isoeffective dose obtained from the survival curve as a function of the absorbed dose.

| | **KERMA** | **Absorbed dose** | **in vivo** |
|---|---|---|---|
| Maximum dose ($Gy_{iso}$) | 40.4 | 45.3 | 30 |
| Minimun dose ($Gy_{iso}$) | 19.4 | 24.0 | 19.4 |
| TCP | 0.46 | 0.56 | 0.49 |

Table 4.6: TCP and maximum and minimum dose values for the three proposed scenarios.

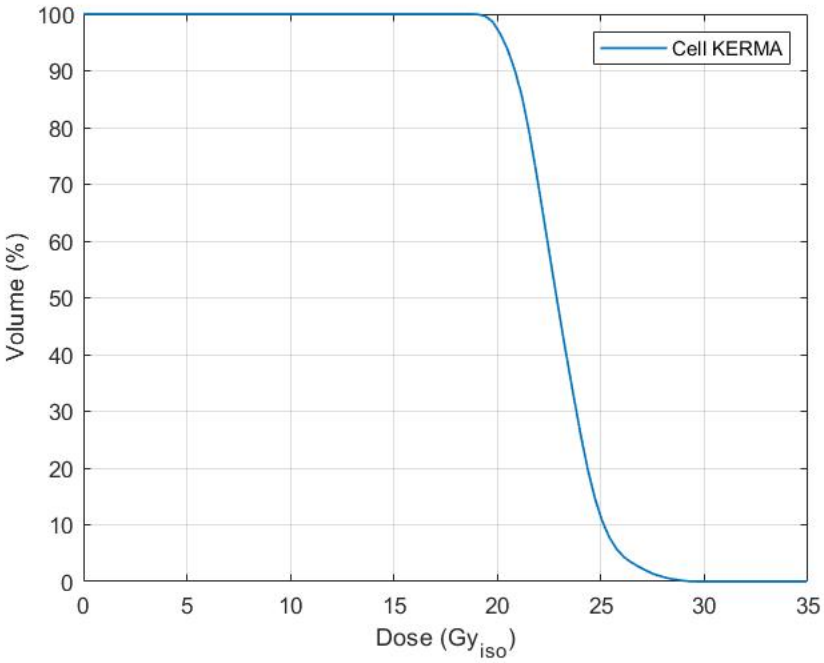


Figure 4.8: DVH of the isoeffective dose using the radiobiological parameters of the survival curves plotted against KERMA.

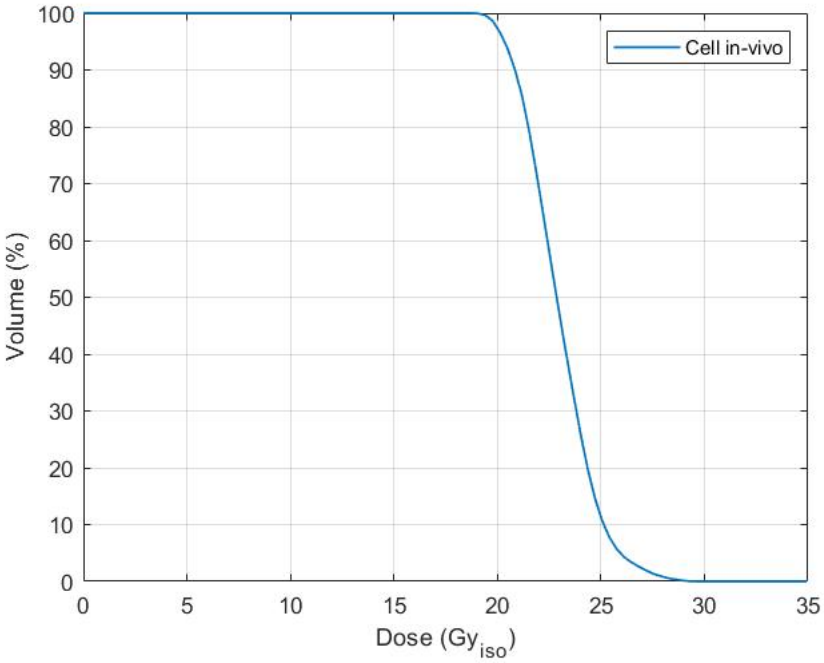


Figure 4.9: DVH of the isoeffective dose calculated with the parameters obtained from *in vivo* oral cancer model.

dose is higher if calculated with cell parameters than if calculated with animal model (30% for KERMA and almost 50% for absorbed dose). Note that the dose delivered to the patient has been calculated by treatment planning, reaching statistical convergence and relative error lower than 5% in each voxel. The uncertainty of the dose is thus linked to the precision with which boron concentration is known in tissue. This, in turn, depends on the method used to measure. In clinical practice, boron is measured in blood and the concentration in tumour and in normal tissues is assumed according to models. In this thesis, we used representative values taken from clinical practice, thus we did not propagate an experimental error to the dosimetry. However, considering than boron concentration measurements are improving and that imaging methods are currently employed, the differences between maximum and minimum doses obtained in these calculations can be considered significant. To understand whether these differences are really important in describing the clinical outcome as a function of the dose administered, a much larger study is needed, including patients who have already been treated and whose follow-up is available. However, these results point out that consistent differences in dose distribution may arise if different radiobiological models are use for the photon-equivalent dosimetry.

For the treatment planning calculated in the three scenarios, the Tumour Control Probability is also shown in Table 4.6. The relative difference between the calculation using cell survival VS absorbed dose and cell survival VS KERMA is around 17%. The difference of TCP calculated with data obtained by animal and with cell survival VS absorbed dose is about 12%. It is clear that choosing a different radiobiological model produces a difference in our ability to predict the clinical outcome of the treatment.

Two open questions remain: the first is related to the importance of establishing the best radiobiological model for the equivalence between gamma dose and BNCT dose in order to predict a clinical outcome. An answer to this can come only from a statistically relevant analysis of many patients. The second concerns the understanding the dependence of the results from the type of cells used (primary cell line and/or an immortalized line). These are topics that will defer to a necessary future investigation and study.

# Chapter 5

# Conclusions and future work

The aim of this work was to use radiobiological data to feed dosimetry models that convert the mixed field dose of BNCT in photon units. The objective is to obtain a safe and an effective patient treatment planning based on knowledge of the dose effect acquired in conventional radiotherapy. The availability of reliable dose-effect curves, both from the point of view of biological measurements and concerning dosimetry, is pivotal to reach this goal.

Two types of tumours were analyzed: osteosarcoma and head and neck tumours. In both cases, a detailed dosimetric study of *in-vitro* experiments was performed to explore the effects of some typical assumptions. BNCT is based on the boron-10 neutron capture reaction. Therefore, the $^{10}B(n,\alpha)^{7}Li$ reaction represents the most relevant component of the total absorbed dose and thus, it is essential to accurately assess the boron concentration in the cells. Cell cultures were irradiated with photons, used as reference radiation, with neutrons and with neutrons in the presence of boron inside the cells. The absorbed dose was calculated using the MCNP6 code, with a detailed model of the TRIGA Mark II reactor in Pavia, where the irradiation experiments were conducted. The complexity of the calculation derives from the coexistence of several factors: the mixed radiation field produced by neutron interactions in the tissues, the spectrum of background photons that extends over a wide energy range and the small thickness of the cell layer: 10 $\mu$m.

It has been shown that for monolayer-cultured cells, it is not adequate to assume the condition of charged particle equilibrium (CPE). Therefore, dose cannot be calculated using KERMA approximation. The secondary charged particles were then transported and the energy balance in the layer of cell studied separately. For the first time, also the dose deposited by protons set in motion by scattering of neutrons in hydrogen was evaluated, proving to be the only component for which KERMA equals the dose. In fact, hydrogen is present not only in the cells and the culture medium but also in the flasks and caps thus providing energy equilibrium in the cell layer. Electrons generated by knock-on

electrons, i.e., electrons set in motion by the interaction of another electron, and electrons generated by photons, are difficult to transport by MCNP because they require more computing resources due to the high number of interactions they undergo along their path. The default number of steps used in the transport of the condensed history was optimized.

The impact of considering detailed dose calculations for the osteosarcoma experiments was analyzed by comparing $RBE_{1\%}$ and $CBE_{1\%}$ values determined from the KERMA and dose-survival curves presented in this work. The fact that the mean $RBE1_{1\%}$ value sensibly changed highlights the importance of performing detailed dose calculations for in-vitro experiments. Since the contribution of the neutron dose is of importance particularly for the dose-limiting normal tissues, an increment of more than 30% in the biological effectiveness may lead to a different treatment prescription or to a more adequate analysis of the relationship between dose and radiotoxic effects. The radiobiological parameters obtained from the cell survival curves plotted as a function of absorbed dose and KERMA were used to calculate the dose delivered to patients. For osteosarcoma, a human parosteum of the distal femur was taken as a representative clinical case. It has been already studied in [92], where a BNCT irradiation was simulated with an accelerator-based beam, and a not-yet-optimized dosimetry. The dose was calculated using both the traditional RBE-weighted dose formalism and the isoeffective photon dose formalism. RBE-weighted dose is the traditional way to express BNCT dose in photon equivalent units, still reported in most of the literature. However, it has been demonstrated that it returns artificially high dose values in tumour, and this makes this model not suitable to draw conclusions on the effectiveness of a BNCT treatment. Photon isoeffective dose model, on the other hand, provided a more realistic assessment of dose-clinical outcome relationship in retrospective analysis of treated patient. Results showed that regardless the approximation used to derive the radiobiological parameters from the *in-vitro* experiments, photon isoeffective doses in tumour are much smaller than those from the RBE-weighted dose formalism. When comparing photon isoeffective doses using radiobiological parameters obtained from KERMA or absorbed dose, much lower differences were observed.

For osteosarcoma, the treatment planning was also carried out with a new designed beam, optimized to be suitable for a clinical BNCT facility. In this case, only the photon isoeffective dose model and the set of parameters obtained from the absorbed dose calculation were used. Results showed that the minimum dose in tumour is approximately 3 Gy lower when the new beam is used (7% of difference comparing to the old beam). This loss in dosimetry is a trade-off between the therapeutic performance of the beam and its suitability, i.e. its safety for the patient and the medical staff.

The second clinical case was a head and neck cancer patient. This type of tumour is currently the most treated target in BNCT. In this case, a human primary cell line was

used, from which the parameters for photon isoeffective dose were calculated. The results of the treatment planning were compared with the isoeffective dose obtained in the same patient using the parameters obtained from an *in-vivo* oral cancer model in Buenos Aires. The use of *in-vitro* and *in-vivo* dose-effect curves to obtain the parameters for in-patient dosimetry was explored using Dose Volume Histograms and Tumour Control Probability (TCP). The TCP allows to transform the dosimetric information into a parameter that predicts clinical success of BNCT. Results show that minimum tumour dose achieved in patient are slightly different. The difference in dose distributions calculated with the three scenarios (cell survival as a function of absorbed dose, KERMA and *in vivo* data) are reflected by different TCP values. There is in fact a difference higher than 12% between the Tumour Control Probability calculated with the three different sets of parameters. This of course impacts on the ability to predict the clinical outcome of BNCT. Figures of merit like TCP can be used as criteria to chose a treatment plan and also to evaluate the clinical performance of a neutron beam as described in [86]. A deeper insight on the influence of the radiobiological data on these figures is thus pivotal for a more precise and effective BNCT treatment.

BNCT is a promising treatment modality: there are studies and clinical trials showing that it is safe and effective for patients with advanced tumours. Nevertheless, there are fields of research which still need development. The achievement of in-patient dosimetry in units that allow for safe dose-effect assessment is one of the aspect of BNCT that needs to be optimized. To this end, it is important to enlarge the radiobiological knowledge, using suitable models to establish the parameters for photon-equivalent dose calculation. The choice of biological models, the production and analysis of data and the use of correct dosimetry models are works that must go in parallel. This thesis has addressed this topic, underlining some important questions: are immortalized cell lines and primary cell lines equivalent for isoeffective dose calculation? Do cell lines and animal models give the same results concerning dosimetry in the patient and tumour control probability? These questions still require much experimental and computational work towards a broader awareness and precision in the clinical dosimetry of BNCT.

# Bibliography


[1] Locher G. L. (1936). Biological effects and therapeutic possibilities of neutrons. Am J Roentgenol 36, 1-13.

[2] F Issa, JA Ioppolo, LM Rendina, J Reedijk, and K Poeppelmeier. Boron and Gadolinium Neutron Capture Therapy. Elsevier Amsterdam, 2013.

[3] Farr LE, Sweet WH, Locksley HB, Robertson JS. Neutron capture therapy of gliomas using boron−10. Trans Am Neurol Assoc. 1954;79:110−13.

[4] Archambeau JO. The effect of increasing exposures of the $^{1}0B(n,\alpha)^{7}Li$ reaction on the skin of man. Radiology. 1970;94:178−87.

[5] Slatkin DN. A history of boron neutron capture therapy of brain tumours. Brain. 1991;114:1609−29.

[6] Sweet WH, Soloway AH, Brownell GL. Boron-slow neutron capture therapy of gliomas. Acta Radiol Stockholm. 1963;1:114−21.

[7] Asbury AK, Ojeman RG, Nielsen SL, Sweet WH. Neuropathological study of fourteen cases of malignant brain tumor treated by boron−10 slow neutron capture radiation. J Neuropathol Exp Neurol. 1972;31(2):278−303.

[8] Hatanaka H. In: Boron- Neutron capture therapy for tumors. Niigata: Nishimura Co. Ltd.; 1986. Boron−neutron capture therapy for tumours. Preface.

[9] Hatanaka H, Sweet WH, Sano K, Ellis F. The present status of boron- neutron capture therapy for tumors. Pure Appl Chem. 1991;63(3):373−74.

[10] Mishima Y, Ichihashi M, Hatta S, Honda C, Yamamura K, Nakagawa T, et al. First human clinical trial of melanoma neutron capture. Diagnosis and therapy. Strahlenther Onkol. 1989;165(2−3):251−54.

[11] Barth R. F. et al. (2012). Current status of boron neutron capture therapy of high grade gliomas and recurrent head and neck cancer. Radiation Oncology 7, 146.

[12] Masamitsu Ichihashi, Takafumi Nakanishi, and Yutaka Mishima. Specific killing effect of 10b1−para−boronophenylalanine in thermal neutron capture therapy of malignant melanoma: In vitro radiobiological evaluation. Journal of Investigative Dermatology, 78(3):215−218, 1982.

[13] H Fukuda, J Hiratsuka, C Honda, T Kobayashi, K Yoshino,H Karashima, J Takahashi, Y Abe, K Kanda, and M Ichihashi. Boron neutron capture therapy of malignant melanoma using 10B−paraboronophenylalanine with special reference to evaluation of radiation dose and damage to the normal skin. Radiation research,138(3):435−442, 1994.

[14] Mona Zolfaghari and Mahmood Sedaghatizadeh. Design of thermal neutron beam based on an electron linear accelerator for bnct. Applied Radiation and Isotopes, 118:149−153, 2016.

[15] N Protti, S Bortolussi, Sabrina Stella, MA Gadan, A De Bari, F Ballarini, P Bruschi, C Ferrari, AM Clerici, C Zonta, et al. Calculations of dose distributions in the lungs of a rat model irradiated in the thermal column of the triga reactor in pavia. Applied Radiation and Isotopes, 67(7-8):S210−S213, 2009.

[16] Andres Juan Kreiner, Javier Bergueiro, Daniel Cartelli, Matias Baldo, Walter Castell, Javier Gomez Asoia, Javier Padulo, Juan Carlos Suárez Sandín, Marcelo Igarzabal, Julian Erhardt, et al. Present status of accelerator−based bnct. Reports of Practical Oncology & Radiotherapy, 21(2):95−101, 2016.

[17] A.J. Kreiner, J. Bergueiro, D. Cartelli, M. Baldo,W. Castell, J. Gomez Asoia, J. Padulo, J.C. Suárez Sandín, M. Igarzabal, J. Erhardt, et al. Present status ofaccelerator-based bnct. Reports of Practical Oncology & Radiotherapy,21(2):95-101, 2016.

[18] Barth RF, Soloway AH, Fairchild RG, Brugger RM. Boron neutron capture therapy for cancer, realities and prospects. Cancer. 1992;7:2995-3007.

[19] G. Gambarini, S. Agosteo, P. Marchesi, E. Nava, P. Palazzi, A. Pecci, G. Rosi, and R. Tinti. Discrimination of various contributions to the absorbed dose in BNCT: Fricke-gel imaging and intercomparison with other experimental results. Applied Radiation and Isotopes, 53(4−5):765−772, 2000.

[20] D. R. White, R. V. Griffith, and I. J. Wilson. Report 46. Journal of the International Commission on Radiation Units and Measurements, os24(1):NP−NP, 04 2016.

[21] ICRU, Report 46, Photon, Electron, Proton and Neutron Interaction Data for Body Tissues, International Commission on Radiation Units and Measurements, Vol 32, Issue 1, Bethesda (1992).

[22] Jeffrey A Coderre and Gerard M Morris. The radiation biology of boron neutron capture therapy. Radiation research, 151(1):1−18, 1999.

[23] Tatsuhiko Sato, Shin-ichiro Masunaga, Hiroaki Kumada, and Nobuyuki Hamada. Depth distributions of rbe-weighted dose and photon-isoeffective dose for boron neutron capture therapy. Radiation protection dosimetry, 183(1-2):247-250, 2019.

[24] María Pedrosa-Rivera, Javier Praena, Ignacio María José Ruiz-Magaña, and Carmen Ruiz-Ruiz. Porras, A simple approximation for the evaluation of the photon iso-effective dose in boron neutron capture therapy based on dose-independent weighting factors. Applied Radiation and Isotopes, 157:109018, 2020.

[25] Sara J González and Gustavo A Santa Cruz. The photon-isoeffective dose in boron neutron capture therapy. Radiation research, 178(6):609-621, 2012.

[26] Kellerer AM, Rossi HH. The theory of dual radiation action. Curr Top Radiat Res Q 1972; 8:85-158.

[27] Rossi HH, Zaider M. Compound dual radiation action. I. General aspects. Radiat Res 1992; 132(2):178-83.

[28] Lea DE, Catcheside DG. The mechanism of induction by radiation of chromosome aberrations in Tradescandia. J Genet 1942;44:216-45.

[29] Lea DE, action of radiation on living cells. London: Cambridge University Press; 1946.

[30] Douglas BG, Fowler JF. The effect of multiple small doses of X rays on skin reactions in the mouse and a basic interpretation. Radiat Res 1976:66:401-26.

[31] Zaider M, Rossi HH. Th synergistic effect of different radiations. Radiat Res 180;83:732-9.

[32] Railton R, Lawson RC, Porter D. Interaction of $\gamma-$rays and netron effects on the proliferative capacity of Chinese hamster cells. Int J Radiat Biol 1975;27:75-82.

[33] Barendsen GW. Parameters of linear-quadratic radiation dose-effect relationships: dependence on LET and mechanisms of reproductive cell death. Int J Radiat Biol 1997;71(6):649-55.

[34] Suzuki S.A theoretical model for simultaneus mixed iradiation with multiple types of radiation. J Radiat res 1998; 39:215-21.

[35] Schmid TE, Dollinger G, Beisker W, Hable V, Greubel C, Auer S, Mittag A, Tarnok A, Friedl AA, Molls M, Röper B. Differences in the kinetics of $\gamma$-H2AX fluorescence decay after exposure to low and high LET radiation. Int J Radiat Biol 2010, 86 (8): 682-691.

[36] T Goorley, M James, Thomas Booth, F Brown, J Bull, LJ Cox, J Durkee, J Elson, Michael Fensin, RA Forster, et al. Initial mcnp6 release overview. Nuclear Technology, 180(3):298-315, 2012.

[37] X 5 Monte Carlo Team et al. Mcnp a general monte carlo n-particle transport code version 5 volume i: Overview and theory. Los Alamos National Laboratory, Los Alamos, NM, LA-UR-03-1987, 2003.

[38] S Bortolussi, N Protti, M Ferrari, I Postuma, S Fatemi, M Prata, F Ballarini, MP Carante, R Farias, SJ González, et al. Neutron flux and gamma dose measurement in the bnct irradiation facility at the triga reactor of the university of pavia. Nuclear Instruments and Methods in Physics Research Section B: Beam Interactions with Materials and Atoms, 414:113-120, 2018.

[39] Claretta Guidi. Irradiation of reconstructed human skin cultivated in-vitro: computational dosimetry and preliminary radiobiological evaluations for BNCT studies. Università degli studi di Pavia- Facoltà di scienze MM. FF. NN., Università degli studi di Pavia-Facoltà di scienze MM. FF. NN. 2018/2019, Supervisor Silva Bortolussi, Co-supervisor Dott. Ian Postuma.

[40] Editor J.F.Briesmeister. MCNP - A General Monte Carlo N-Particle Transport Code, Version 4C, 2000 - LA-13709-M.

[41] Dennis R Schaart, Jan Th M Jansen, Johannes Zoetelief, and Piet FA de Leege. A comparison of mcnp4c electron transport with its 3.0 and experiment at incident energies between 100 keV and 20 MeV: influence of voxel size, substeps and energy indexing algorithm. Physics in Medicine & Biology, 47(9):1459, 2002.

[42] Editor C.J. Werner. MCNP User's Manual, Code Version 6.2, 2017 -LA-UR-17-29981.

[43] S. Bortolussi, N. Protti, M. Ferrari, I. Postuma, S. Fatemi, M. Prata, F. Ballarini, M.P. Carante, R. Farias, S.J. GonzÃ¡lez, M. Marrale, S. Gallo, A. Bartolotta, G. Iacoviello, D. Nigg, and S. Altieri. Neutron flux and gamma dose measurement in

the bnct irradiation facility at the triga reactor of the university of pavia. Nuclear Instruments and Methods in Physics Research Section B: Beam Interactions with Materials and Atoms, 414:113 - 120, 2018.

[44] L. Cansolino, A.M. Clerici, C. Zonta, P. Dionigi, G. Mazzini, R. Di Liberto, S. Altieri, F. Ballarini, S. Bortolussi, M.P. Carante, M. Ferrari, S.J. GonzÃ¡lez, I. Postuma, N.Protti, G.A. Santa Cruz and C. Ferrari, Comparative Study of the Radiobiological Effects Induced on Adherent vs Suspended Cells by BNCT, Neutrons and Gamma Rays Treatments, Appl Radiat Isot, 2015 106:226-32.

[45] I. Postuma, S.Bortolussi, N.Protti, F.Ballarini, P.Bruschi, L. Ciani, S.Ristori, L.Panza, C.Ferrari, L.Cansolino, S.Altieri, An improved neutron autoradiography set-up for 10B concentration measurements in biological samples, reports of practical oncology and radiotherapy, 21(2), 2016, 123-128.

[46] Bielack S, Carrle D, Casali PG, ESMO guide lines working group. Osteosarcoma: ESMO clinical recommendations for diagnosis, treatment and follow-up. Ann Oncol. 2009;20(Suppl. 4):137-9.

[47] Luetke A, Meyers PA, Lewis I, Juergens H. Osteosarcoma treatment - where do we stand? A state of the art review. Cancer Treat Rev. 2014;40:523-32.

[48] Geller DS, Gorlick R. Osteosarcoma: a review of diagnosis, management, and treatment strategies. Clin Adv Hematol Oncol. 2010;8:705-18.

[49] Bacci G, Ferrari S, Mercuri M, Bertoni F, Picci P, Manfrini M, Gasbarrini A, Forni C, Cesari M and Campanacci M, Predictive factors for local recurrence in osteosarcoma 540 patients with extremity tumors followed for minimum 2.5 years after neoadjuvant chemotherapy. Acta Orthopaedica Scandinavica, 1998;69(3):230-236.

[50] Grimer RJ, Taminiau AM, Cannon SR. Surgical outcomes in osteosarcoma. J Bone Joint Surg (Br). 2002;84-B:395-400.

[51] Yasko AW. Surgical management of primary osteosarcoma. Cancer Treat Res. 2009;152:125-45.

[52] Oya N, Kokubo M, Mizowaki T, Shibamoto Y, Nagata Y, Sasai K, Nishimura Y, Tsuboyama T, Toguchida J, Nakamura T, Hiraoka M. Definitive intraoperative very high-dose radiotherapy for localized osteosarcoma in the extremities. Int J Radiat Oncol Biol Phys. 2001;51(1):87-93.

[53] Arpornchayanon O, Leerapun T, Pruksakorn D, Panichkul P. Result of extracorporeal irradiation and re-implantation for malignant bone tumors: a review of 30 patients. Asia Pac J Clin Oncol. 2013;9(3):214-9.

[54] Chanana AD, Capala J, Chadha M, Coderre JA, Diaz AZ, Elowitz EH, et al. Boron neutron capture therapy for glioblastoma multiforme: nterim results from the phase I/II dose-escalation studies. Neurosurgery. 1999;44(6):1182-93.

[55] Busse PM, Harling OK, Palmer MR, KigerIII W S, Kaplan J, Kaplan I, et al. A critical examination of the results from the Harvard-MITNCT program phase I clinical trial of neutron capture therapy for intracranial disease. J Neurooncol. 2003;62(1-2):111-21.

[56] Sauerwein W, Zurlo A. The EORTC boron neutron capture therapy group: Achievements and future perspectives. Eur J Cancer. 2002;38(4):S31-34.

[57] Joensuu H, Kankaanranta L, Seppala T, Auterinen I, Kallio M, Kulvik M, et al. Boron neutron capture therapy of brain tumors: Clinical trials at the Finnish facility using boronophe-nylalanine. J Neurooncol. 2003;62(1-2):123-34.

[58] Capala J, Stenstam BH, Sköld K, Rosenschold PM, Giusti V, Persson C, et al. Boron neutron capture therapy for glioblastoma multiforme: Clinical studies in Sweden. J Neurooncol. 2003;62(1-2):135-44.

[59] Dbaly V, Tovarys F, Honova H, Petruzelka L, Prokes K, Burian J, et al. Contemporary state of neutron capture therapy in Czech Republic (Part 2) Cesaslov Neurol Neurochir. 2002;66-99(1):60-63.

[60] Nakagawa Y, Pooh K, Kobayashi T, Kageji T, Uyama S, Matsumura A, et al. Clinical review of the Japanese experience with boron neutron capture therapy and a proposed strategy using epithermal neutron beams. J Neurooncol. 2003;62(1-2):87-99.

[61] Ono K, Ueda S, Oda Y, Nakagawa Y, Miyatake S, Osawa M, et al. Advances in Neutron Capture Therapy. vol.I. Amsterdam: Elsevier Science; 1997. Boron neutron capture therapy for malignant glioma at Kyoto University reactor. In: Larsson B, Crawford J, Weinreich R. (Eds.) pp. 39-45.

[62] González SJ, Bonomi MR, Santa Cruz GA, Blaumann HR, Calzetta Larrieu OA, Menéndez P, et al. First BNCT treatment of a skin melanoma in Argentina: Dosimetric analysis and clinical outcome. Appl Radiat Isot. 2004;61(5):1101-05.

[63] Liu YWH, Huang TT, Jiang SH, Liu HM. Renovation of epithermal neutron beam for BNCT at THOR. Appl Radiat Isot. 2004;61:1039-43.

[64] Ana Mailén Dattoli Viegas, Ian Postuma, Silva Bortolussi, Claretta Guidi, Jessica Riback, Lucas Provenzano, Barbara Marcaccio, Silvia Thorp, Mario Gadan, Andrés Rossini, Cinzia Ferrari, Laura Casolino, Matteo Ferrari, Agustina Portu and Sara González. Detailed dosimetry calculation for in-vitro experiments and its impact on clinical BNCT.

[65] MATLAB and Statistics Toolbox Release 2020b, The MathWorks, Inc., Natick, Massachusetts, United States.

[66] Gómez-Lechón MJ, Donato MT, Castell JV, Jover R. Human hepatocytes as a tool for studying toxicity and drug metabolism. Curr Drug Metab. 2003;4:292-312. doi: 10.2174/1389200033489424.

[67] Schurr MJ, Foster KN, Centanni JM, Comer AR, Wicks A, Gibson AL, et al. Phase I/II clinical evaluation of StrataGraft: a consistent, pathogen-free human skin substitute. J Trauma. 2009;66:866-73, discussion 873-4. doi: 10.1097/TA.0b013e31819849d6.

[68] Claudia M. Hyether-Franken. The first Mother of cell culture. 03-29-2017.

[69] Stewart BW Wild CP, Weiderpass E. World Cancer Report: Cancer Research for Cancer Prevention. World Health Organization, 2020.

[70] William M Mendenhall, Anthony A Mancuso, Robert J Amdur, Scott P Stringer, Douglas B Villaret, and Nicholas J Cassisi. Squamous cell carcinoma metastatic to the neck from an unknown head and neck primary site. *American journal of otolaryngology*, 22(4):261-67, 2001.

[71] Sara Gandini, Edoardo Botteri, Simona Iodice, Mathieu Boniol, Albert B Lowenfels, Patrick Maisonneuve, and Peter Boyle. Tobacco smoking and cancer: A meta-analysis. *International journal of cancer*, 122(1):155-164, 2008.

[72] William J Blot, Joseph K McLaughlin, Deborah M Winn, Donald F Austin, Raymond S Greenberg, Susan Preston-Martin, Leslie Bernstein, Janet B Schoenberg, Annette Stemhagen, and Joseph F Fraumeni. Smoking and drinking in relation to oral and pharyngeal cancer. Cancer research, 48(11):3282-3287, 1988.

[73] Anil K Chaturvedi, Eric A Engels, Ruth M Pfeiffer, Brenda Y Hernandez, Weihong Xiao, Esther Kim, Bo Jiang, Marc T Goodman, Maria Sibug-Saber, Wendy Cozen, et al. Human papillomavirus and rising oropharyngeal cancer incidence in the united states. Journal of clinical oncology, 29(32):4294, 2011.

[74] Neela Guha, Paolo Boffetta, Victor WÃ¼nsch Filho, Jose Eluf Neto, Oxana Shangina, David Zaridze, Maria Paula Curado, Sergio Koifman, Elena Matos, Ana Menezes, et al. Oral health and risk of squamous cell carcinoma of the head and neck and esophagus: results of two multicentric case-control studies. American journal of epidemiology, 166(10):1159-1173, 2007.

[75] Freddie Bray, Jacques Ferlay, Isabelle Soerjomataram, Rebecca L Siegel, Lindsey A Torre, and Ahmedin Jemal. Global cancer statistics 2018: Globocan estimates of incidence and mortality worldwide for 36 cancers in 185 countries. CA: a cancer journal for clinicians, 68(6):394-424, 2018.

[76] Hisham M Mehanna and K Kian Ang. Head and neck cancer recurrence: Evidence-based, Multidisciplinary management. Thieme, 2012.

[77] Leena Kankaanranta, Tiina Seppälä, Hanna Koivunoro, Kauko Saarilahti, Timo Atula, Juhani Collan, Eero Salli, Mika Kortesniemi, Jouni Uusi-Simola, Petteri Välimäki, et al. Boron neutron capture therapy in the treatment of locally recurred head-and-neck cancer: final analysis of a phase i/ii trial. *International Journal of Radiation Oncology* Biology* Physics*, 82(1):e67-e75, 2012.

[78] Itsuro Kato, Koji Ono, Yoshinori Sakurai, Masatoshi Ohmae, Akira Maruhashi, Yoshio Imahori, Mitsunori Kirihata, Mitsuhiro Nakazawa, and Yoshiaki Yura. Effectiveness of bnct for recurrent head and neck malignancies. Applied Radiation and Isotopes, 61(5):1069-1073, 2004.

[79] Floyd J Wheeler, David W Nigg, Jacek Capala, Peter RD Watkins, Corine Vroegindeweij, Iiro Auterinen, Tiina Seppälä, and Darren Bleuel. Boron neutron capture therapy (bnct): implications of neutron beam and boron compound characteristics. Medical physics, 26(7):1237-1244, 1999.

[80] Aihara T, Hiratsuka J, Morita N et al. First clinical case of boron neutron capture therapy for head and neck malignancies using 18F-BPA PET. Head Neck 2006; 28:850-5.

[81] W. Muhammad et al. chapter 2 of Basic Concepts in Radiation Dosimetry.

[82] https : //physics.nist.gov/cgi − bin/Star/ap$_t$able.pl.

[83] G. van Rossum, tutorial Python, Technical Report CS-R9526, Centrum voor Wiskunde en Informatica (CWI), Amsterdam, maggio 1995.

[84] González SJ, Carando DG, Santa Cruz GA, Zamenhof RG. Voxel model in BNCT treatment planning: performance analysis and improvements. Phys Med Biol. 2005;50:441-58.

[85] Wolfgang A.G. Sauerwein, Andrea Wittig,Raymond Moss, Yoshinobu Nakagawa. Neutron Capture Therapy. Principles and Applications.

[86] Ian Postuma, Sara González, Maria S Herrera, Lucas Provenzano, Michele Ferrarini, Chiara Magni, Nicoletta Protti, Setareh Fatemi, Valerio Vercesi, Giuseppe Battistoni, Umberto Anselmi Tamburini, Yuan Hao Liu, Leena Kankaanranta, Hanna Koivunoro, Saverio Altieri, and Silva Bortolussi. A Novel Approach to Design and Evaluate BNCT Neutron Beams Combining Physical, Radiobiological and Dosimetric Figures of Merit.

[87] Suzuki, M. Boron neutron capture therapy (BNCT): a unique role in radiotherapy with a view to entering the accelerator-based BNCT era. International journal of clinical oncology 2019, pp. 1-8.

[88] Menëndez, P.; Pereira, M.; Casal, M.; Gonzälez, S.; Feld, D.; Santa Cruz, G.; Kessler, J.; Longhino, J.; Blaumann, H.; Rebagliati, R.J.; others. BNCT for skin melanoma in extremities: updated Argentine clinical results. Applied Radiation and Isotopes 2009, 67, S50-S53.

[89] Herrera, M.; Gonzälez, S.; Minsky, D.; Kreiner, A. Evaluation of performance of an accelerator-based BNCT facility for the treatment of different tumor targets. Physica Medica 2013, 29, 436-446.

[90] Capoulat, M.; Kreiner, A. A 13 C (d, n)-based epithermal neutron source for Boron Neutron Capture Therapy. Physica Medica 2016.

[91] Harris, C.R., Millman, K.J., van der Walt, S.J. et al. Array programming with NumPy. Nature 585, 357-362 (2020).

[92] Silva Bortolussi, Ian Postuma, Nicoletta Protti, Lucas Provenzano, Cinzia Ferrari, Laura Cansolino, Paolo Dionigi, Olimpio Galasso, Giorgio Gasparini, Saverio Altieri, Shin-Ichi Miyatake and Sara J. González. Understanding the potentiality of accelerator based-boron neutron capture therapy for osteosarcoma: dosimetry assessment based on the reported clinical experience. (2017) 10.1186/s13014-017-0860-6.

[93] Fukuda H, Hiratsuka J, Kobayashi T, Sakurai Y, Yoshino K, Karashima H, Turu K, Araki K, Mishima Y, Ichihashi M. Boron neutron capture therapy (BNCT) for

malignant melanoma with special reference to absorbed doses to the normal skin and tumor. Australas Phys Eng Sci Med. 2003;26:97. 35. Andoh T, Fujimoto T, Sudo T, Fujita I, Imabori M, Moritake H, Sugi.

[94] C. Ferrari, C. Zonta, L. Cansolino, A.M. Clerici, A. Gaspari, S. Altieri, S. Bortolussi, S. Stella, P. Bruschi, P. Dionigi and A. Zonta. Selective uptake of p-boronophenylalanine by ostesarcoma cells for boron neutron capture therapy. Appl. Rad. Isot. (2009) 67:341-344.

[95] C. Ferrari, J. Bakeine, F. ballarini, A. Boninella, S. Bortolussi, P Bruschi, L. Cansolino, A.M. Clerici, P. Dionigi, L. Cansolino, S. Stella, A. Zonta, C. Zonta and S. Altieri. In vitro and in vivo studies of Boron Neutron Caption Therapy: Boron Uptake/Washout and Cell Death. Rad. Res. 2011, vol, 175, 452-462.

[96] Suzuki, M. Boron neutron capture therapy (BNCT): a unique role in radiotherapy with a view to entering the accelerator-based BNCT era. International journal of clinical oncology 2019, pp. 1-8.

[97] Provenzano L, Research and development in BNCT for the treatment of new patologies, 2020, PhD Thesis, Universidad de San Martín, Buenos Aires, Argentin.

[98] Machak GN, Tkachev SI, Solovyev YN, et al. Neoadjuvant chemotherapy and local radiotherapyfor high-grade osteosarcoma of the extremities. Mayo Clin Proc. 2003;78:147-55.

[99] Calvo FA, Ortiz de Urbina D, Sierrasesumaga L, et al. Intraoperative radiotherapy in the multidisciplinary treatment of bone sarcomas in children and adolescents. Med Pediatr Oncol. 1991;19:478-85.

[100] Fujimoto T, Andoh T, Sudo T, Fujita I, Moritake H, Sugimoto T, Sakuma T, Akisue T, Kawabata S, Kirihata M, Suzuki M, Sakurai Y, Ono K, Fukumori Y, Kurosaka M, Ichikawa H. Boron neutron capture therapy (BNCT) selectively destroys human clear cell sarcoma in mouse model. Appl Radiat Isot. 2013; 73:96-100.

[101] J Gonz*ä*lez, Emiliano C*ë*sar Cayetano Pozzi, A Monti Hughes, Lucas Provenzano, H Koivunoro, Daniel Germ*ä*n Carando, Silvia In*ë*s Thorp, MR Casal, Silva Bortolussi, Ver*ö*nica Andrea Trivillin, et al. Photon iso-effective dose for cancer treatment with mixed field radiation based on dose-response assessment from human and an animal model: clinical application to boron neutron capture therapy for head and neck cancer. Physics in Medicine & Biology, 62(20):7938, 2017.

[102] Wachiraphan Supsavhad, Wessel P Dirksen, Chelsea K Martin, and Thomas J Rosol. Animal models of head and neck squamous cell carcinoma. The Veterinary Journal, 210:7-16, 2016.

[103] Yuk-Kwan Chen and Li-Min Lin. Dmba-induced hamster buccal pouch carcinoma and vx2-induced rabbit cancer as a model for human oral carcinogenesis. Expert review of anticancer therapy, 10(9):1485-1496, 2010.

[104] E Vairaktaris, S Spyridonidou, V Papakosta, A Vylliotis, A Lazaris, D Perrea, C Yapijakis, and E Patsouris. The hamster model of sequential oral oncogenesis. Oral oncology, 44(4):315-324, 2008.

[105] Erica L Kreimann, Maria E Itoiz, Juan Longhino, Herman Blaumann, Osvaldo Calzetta, and Amanda E Schwint. Boron neutron capture therapy for the treatment of oral cancer in the hamster cheek pouch model. Cancer research, 61(24):8638-8642, 2001.

[106] Itsuro Kato, Yusei Fujita, Akira Maruhashi, Hiroaki Kumada, Masatoshi Ohmae, Mitsunori Kirihata, Yoshio Imahori, Minoru Suzuki, Yoshinori Sakrai, Tetsuro Sumi, et al. Effectiveness of boron neutron capture therapy for recurrent head and neck malignancies. Applied Radiation and Isotopes, 67(7-8):S37-S42, 2009.

[107] Ling-Wei Wang, Yi-Wei Chen, Ching-Yin Ho, Yen-Wan Hsueh Liu, Fong-In Chou, Yuan-Hao Liu, Hong-Ming Liu, Jinn-Jer Peir, Shiang-Huei Jiang, Chi-Wei Chang, et al. Fractionated boron neutron capture therapy in locally recurrent head and neck cancer: a prospective phase i/ii trial. International Journal of Radiation Oncology* Biology* Physics, 95(1):396-403, 2016.

[108] Leena Kankaanranta, Tiina Seppälä, Hanna Koivunoro, Kauko Saarilahti, Timo Atula, Juhani Collan, Eero Salli, Mika Kortesniemi, Jouni Uusi-Simola, Petteri Välimäki, et al. Boron neutron capture therapy in the treatment of locally recurred head-and-neck cancer: final analysis of a phase i/ii trial. International Journal of Radiation Oncology* Biology* Physics, 82(1):e67-e75, 2012.

[109] Sara J González and Daniel G Carando. A general tumour control probability model for non-uniform dose distributions. Mathematical medicine and biology: a journal of the IMA, 25(2):171-184, 2008.

[110] Enrique Alvarez, Edward G Fey, Pascal Valax, Zachary Yim, Jeffrey D Peterson, Medhi Mesri, Michael Jeffers, Matthew Dindinger, Nancy Twomlow, Ashwini Ghatpande, et al. Preclinical characterization of cg53135 (fgf-20) in radiation and

concomitant chemotherapy/radiation-induced oral mucositis. Clinical cancer research, 9(9):3454-3461, 2003.

[111] Lidia Strigari, Piernicola Pedicini, Marco D'Andrea, Paola Pinnaró, Laura Marucci, Carolina Giordano, and Marcello Benassi. A new model for predicting acute mucosal toxicity in head-and-neck cancer patients undergoing radiotherapy with altered schedules. International Journal of Radiation Oncology* Biology* Physics, 83(5):e697-e702, 2012.

[112] Xiaoyan Wu, Peili Chen, Stephen T Sonis, Mark W Lingen, Ann Berger, and F Gary Toback. A novel peptide to treat oral mucositis blocks endothelial and epithelial cell apoptosis. International Journal of Radiation Oncology* Biology* Physics, 83(3):e409-e415, 2012.

[113] González SJ, Carando DG, Santa Cruz GA, and Zamenhof RG, Voxel model in BNCT treatment planning: performance analysis and improvements, Phys Med Biol, 2005; 50:441-458.

[114] Rorer, D.; Wambersie, G.; Whitmore, G.; Zamenhof, R.; Levin, V.; Andreo, P.; Dodd, D. Current Status of neutron capture therapy. IAEA, 2001 (8) 2001, pp. 75-77.

[115] C. Magni, I. Postuma, M. Ferrarini, N. Protti, S. Fatemi, C. Cong, U. Anselmi-Tamburini, V Vercesi, G. Battistoni, S. altieri, S. Bortolussi. Design of a BNCT irradiation room based on proton accelerator and beryllium target, Appl. Radiat. Isotop, 165,2020.

[116] Rwigema et al., Am. J. Clin. Oncol. 2011, 34(4): 372-9.

[117] Internal communication G. Perotti Bernardini, S. Bortolussi, H. Koivunoro, L. Provenzano, C. Ferrari, L. Cansolino, I. Postuma, R. Grenman, L. Kankaanranta, H. Joensuu, S.J. González, Comparison of photon isoeffective dose models based on in-vitro and in in-vivo radiobiological data for head and neck cancer (under preparation).

# Appendix A

# Comparison of dosimetry analysis tools for BNCT

In the frame of the INFN project IT_STARTS, efforts are being dedicated to build a complete and usable robust Dose Engine and Treatment Planning System, able to transform medical images of patients into computational models, and produce an input file for irradiation simulation, to perform dose distribution calculation and to analyse the results. The core of the project is to include in the dose engine more robust and validated algorithms for dose evaluation in patients. To this aim, computational work as well as experimental activity in radiobiology are being performed in this project.

IT_STARTS is carried out in close collaboration between the Pavia INFN Unit and the Argentinean Treatment Planning and Computational Dosimetry group at CNEA who developed the Photon Isoeffective Dose formalism and who already have a consistent know-how on TPS development. In fact, the TPS called MultiCell has been implemented in the last years, incorporating innovative strategies to construct voxel models from medical images, to calculate dose distribution, and to analyse results after Monte Carlo transport using a dedicated software called BNCTAr. This software consists of a set of analysis tools developed in MATLAB language arranged in a simple user interface. This work is introduced in the PhD thesis by Rubén Farias: Dosimetría y modelado computacional para irradiaciones extracorpóreas en humanos en el marco de la Terapia por Captura Neutrónica en Boro, Universidad Nacional de San Martín, Buenos Aires 2015. BnctAR: Dosimetry Tools has algorithms for calculating absorbed dose and two types of photon equivalent dose, from the results obtained with MCNP simulations. This work is described in the PhD thesis by Lucas Provenzano: Investigación y desarollo en BNCT para el tratatmiento de nuevas patologías, Universidad Nacional de San Martín, Buenos Aires 2020 and in [97]. The goal of IT_STARTS is to integrate all this knowledge into an open-access program written in Python, enlarging the pool of radiobiological data for the

translation of absorbed dose into photon-equivalent units.

A by-product of this thesis was the possibility of inter-compare the analysis of the dosimetry performed with the software BNCTAr with those obtained by the Python code set-up in Pavia. Figure A.1 shows the DVH for the skin of the osteosarcoma patient describe in Chapetr 3, obtained by RBE-weighted dose setting 22 Gy as the maximum value that can be received. The left image on the left show the DVH obtained by BNCTAr, the image on the right is the DVH previusly shown in Figure A.1 (Chapter 3).

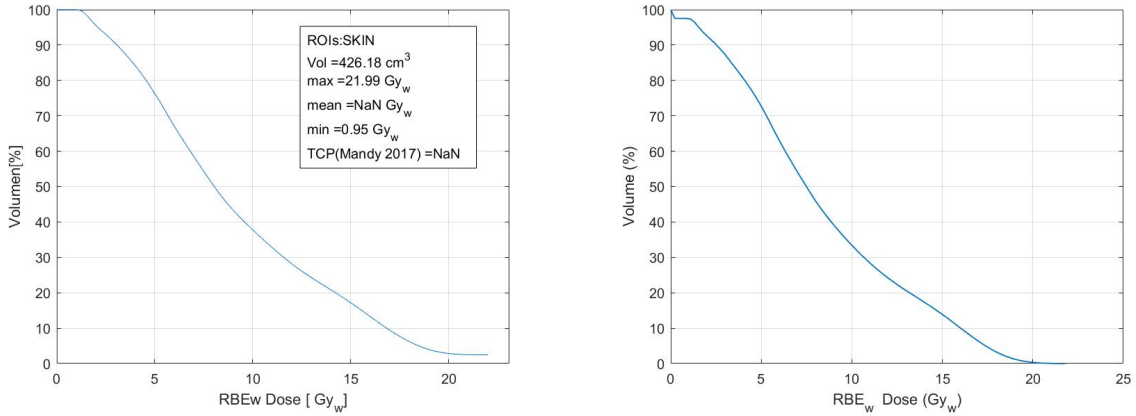


Figure A.1: Dose-volume histogram in skin calculated with RBE-weighted dose. In the left with BNCTAr and in the right with python code.

Figure A.2 shows the DVHs obtained in tumour with photon isoeffective dose model with parameters obtained by cell survival as a function of the KERMA (left), and of the absorbed dose (right). Again, for comparison, we report in Figure A.3 the same DVHs (already shown in Chapter 3) obtained with the Python code.

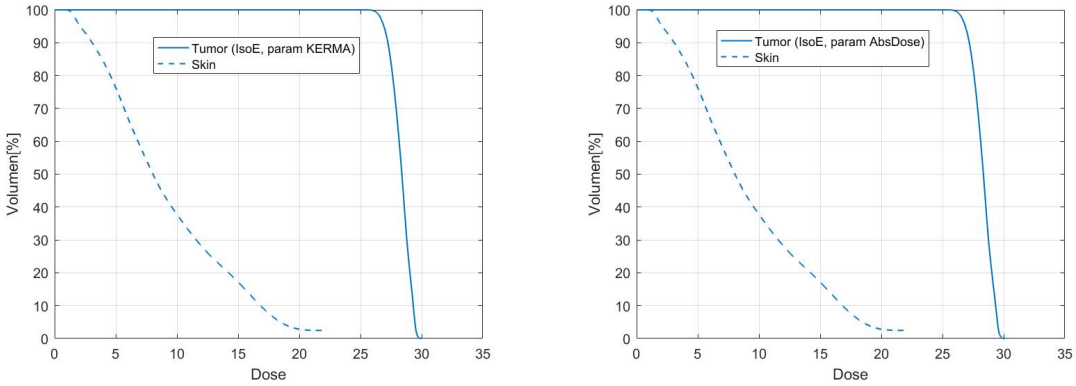


Figure A.2: Dose-volume histogram for 60 ppm in tumor. Dosimetry is calculated by photon isoeffective dose model. Left: parameters obtained by cell-survival as a function of KERMA; right: parameters obtained by cell-survival as a function of absorbed dose.

Same results in terms of consistency were obtained for the Head and Neck patient.

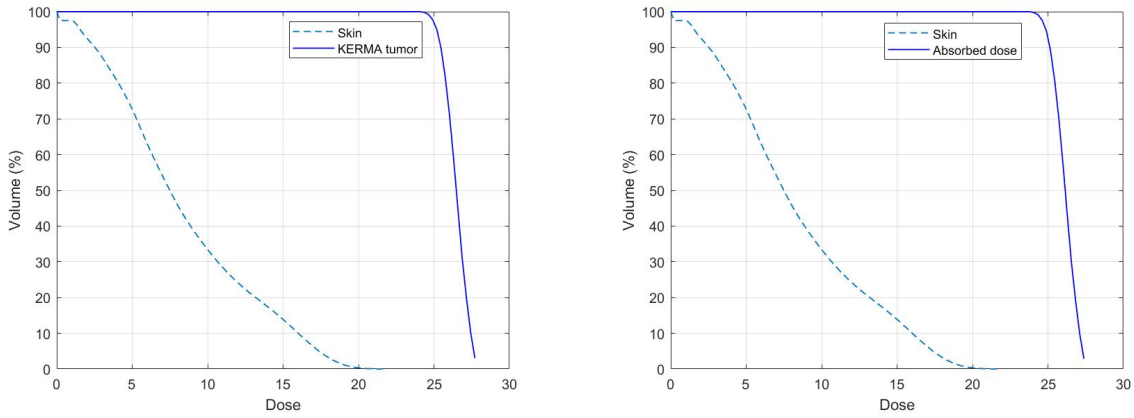


Figure A.3: Dose-volume histogram for 60 ppm in tumor and skin with the photon iso effective dose In the left the results for KERMA-based and in the right for aborbed dose.

It can be seen from the DVHs obtained that the two methods by which the results of the treatment plans were analyzed are consistent, even if the programs use different strategies for the match of dose distribution with the ROI masks. The small differences between the maximum and minimum doses are due in fact to differences in the calculation of the mask volumes. This is a work in progress toward the set-up of a inter-validated and user-friendly interface for the analysis of dose distribution in patients.